

Washington University in St. Louis

Washington University Open Scholarship

McKelvey School of Engineering Theses & Dissertations

McKelvey School of Engineering

Spring 5-15-2021

Subject-Specific Musculoskeletal Modeling of Hip Dysplasia Biomechanics

Ke Song

Washington University in St. Louis

Follow this and additional works at: https://openscholarship.wustl.edu/eng_etds



Part of the [Biomechanics Commons](#), [Mechanical Engineering Commons](#), and the [Medicine and Health Sciences Commons](#)

Recommended Citation

Song, Ke, "Subject-Specific Musculoskeletal Modeling of Hip Dysplasia Biomechanics" (2021). *McKelvey School of Engineering Theses & Dissertations*. 631.
https://openscholarship.wustl.edu/eng_etds/631

This Dissertation is brought to you for free and open access by the McKelvey School of Engineering at Washington University Open Scholarship. It has been accepted for inclusion in McKelvey School of Engineering Theses & Dissertations by an authorized administrator of Washington University Open Scholarship. For more information, please contact digital@wumail.wustl.edu.

WASHINGTON UNIVERSITY IN ST. LOUIS

McKelvey School of Engineering
Department of Mechanical Engineering and Materials Science

Dissertation Examination Committee:

Michael D. Harris, Chair

Spencer P. Lake, Co-Chair

Philip V. Bayly

Marcie Harris-Hayes

Cecilia Pascual-Garrido

Jessica E. Wagenseil

Subject-Specific Musculoskeletal Modeling of Hip Dysplasia Biomechanics

by

Ke Song

A dissertation presented to
The Graduate School
of Washington University in
partial fulfillment of the
requirements for the degree
of Doctor of Philosophy

May 2021

St. Louis, Missouri

© 2021, Ke Song

Table of Contents

List of Figures	vi
List of Tables	x
List of Abbreviations	xi
Acknowledgments.....	xii
Abstract	xv
Chapter 1: Introduction	1
1.1 Motivations.....	1
1.2 Research Aims.....	5
1.3 Summary of Chapters.....	6
1.4 References	9
Chapter 2: Background	13
2.1 Developmental Dysplasia of the Hip (DDH)	13
2.1.1 Clinical Definition.....	13
2.1.2 Significance of DDH in Premature Development of Hip OA.....	14
2.1.3 Pre-Arthritic Pathology of DDH	15
2.1.4 Diagnosis and Evaluation of DDH.....	17
2.1.5 Treatments for DDH and Clinical Outcomes.....	19
2.2 Biomechanics of the Hip Joint	21
2.2.1 Hip Biomechanics and Roles in Functionality.....	21
2.2.2 Abnormal Hip Biomechanics: Impacts and Causes in DDH	23
2.2.3 Quantifying Hip Biomechanics: In-Vitro, In-Vivo, and In-Silico	25
2.3 Musculoskeletal Model (MSM)	30
2.3.1 Standard MSM Workflow.....	31
2.3.2 Using MSMs for DDH Biomechanics	38
2.3.3 Image-Based Subject-Specific MSM.....	39
2.4 References	41
Chapter 3: Musculoskeletal Models with Generic and Subject-Specific Geometry Estimate Different Joint Biomechanics in Dysplastic Hips	56
3.1 Abstract	56
3.2 Introduction	57

3.3	Methods	59
3.3.1	Subjects	59
3.3.2	CT geometry and Gait Motion Analysis	59
3.3.3	Musculoskeletal Modeling	60
3.3.4	Biomechanical Analysis and Data Processing	63
3.3.5	Statistical Analysis	64
3.4	Results	65
3.4.1	Hip JRFs.....	65
3.4.2	Hip Muscle Forces	69
3.4.3	HJC Locations	69
3.4.4	Hip Angles and Moments	71
3.5	Discussion	71
3.6	Acknowledgments	76
3.7	Appendix 1. Sensitivity of Hip JRFs to Muscle Path in CT-Geometry Model.....	76
3.8	Appendix 2. Inter-Model Differences in Individual Hip Muscle Forces	77
3.9	Appendix 3. Inter-Model Differences in Hip Angles and Moments.....	77
3.10	References	78
Chapter 4: Dysplastic Hip Anatomy Alters Muscle Moment Arm Lengths, Lines of Action, and Contributions to Joint Reaction Forces during Gait		82
4.1	Abstract	82
4.2	Introduction	83
4.3	Methods	85
4.3.1	Subjects and Data Collection	85
4.3.2	Musculoskeletal Modeling	86
4.3.3	Model Validation	89
4.3.4	Data Analysis	89
4.4	Results	90
4.4.1	Subject Characteristics and Model Validation	90
4.4.2	Hip Muscle MALs and LoAs.....	92
4.4.3	Hip Muscle Forces and JRFs	93
4.4.4	Angles and Moments	94
4.5	Discussion	95

4.6	Acknowledgments	99
4.7	References	100
Chapter 5: Acetabular Edge Loading during Gait is Elevated by the Anatomical Deformities of Hip Dysplasia.....		104
5.1	Abstract	104
5.2	Introduction	105
5.3	Methods.....	107
5.3.1	Subjects and Data Collection	107
5.3.2	Subject-Specific Musculoskeletal Models	108
5.3.3	Estimation of Acetabular Edge Loading (AEL).....	109
5.3.4	Inter-Group Comparison and Correlations.....	111
5.4	Results	112
5.4.1	Subject Demographics and Anatomy	112
5.4.2	Hip JRFs.....	112
5.4.3	Clock-Face AEL and JRF-to-Edge Angles	113
5.4.4	Joint Angles and Moments.....	115
5.5	Discussion	115
5.6	Acknowledgments	119
5.7	References	119
Chapter 6: Hip Dysplasia Elevates Loading at the Posterior Acetabular Edge during Double-Legged Squat		123
6.1	Abstract	123
6.2	Introduction	124
6.3	Methods.....	125
6.3.1	Subjects and Experimental Data Collection.....	125
6.3.2	Image-based Musculoskeletal Models	128
6.3.3	Acetabular Edge Loading (AEL) Estimation	128
6.3.4	Data Analysis and Statistics	131
6.4	Results	131
6.4.1	Subject Demographics and Anatomy	131
6.4.2	Hip JRFs.....	133
6.4.3	Clock-Face AEL and JRF-to-Edge Angles	133

6.4.4	Joint Angles and Moments.....	135
6.5	Discussion	135
6.6	Acknowledgments.....	140
6.7	References	140
Chapter 7: Summary and Future Directions		143
7.1	Conclusions, Significance, and Novelty	143
7.2	Limitations and Future Directions.....	148
7.3	References	155

List of Figures

Figure 2.1. Representative pelvis and femur anatomy of (A) a healthy adult, and (B) a DDH patient with shallow acetabulum and reduced femoral coverage, indicated by the lateral center-edge angle (LCEA) [38].	14
Figure 2.2. Standard radiographic measures of (A) the lateral center-edge angle (LCEA) to quantify lateral femoral coverage; and the (B) acetabular inclination (AI) or Tönnis angle to quantify orientation of the weight-bearing area of the acetabulum. (Adapted from Figure 11 in Clohisy et al. J Bone Joint Surg Am. 2008 [39].)	18
Figure 2.3. Detailed acetabular anatomy have been used to analyze articular and labral contact stresses, but the specificity of results may be limited by the generic input loading conditions. (Figure 1 in Henak et al. Osteoarthritis Cartilage. 2014 [87].)	28
Figure 2.4. The anatomy of the human leg (A) is simplified to a link-segment model (B), which allows resolution of joint kinetics from kinematic data using free-body diagrams (C) and inverse dynamics. By considering forces due to body inertia (I), gravitation (m), and external contact (ground reaction force on foot (m_3), not shown), joint <i>net</i> forces (R) and moments (M) can be resolved. For example, R_{x1} and R_{y1} represent components of the <i>net</i> hip force, and M_1 represents the <i>net</i> hip moment. (Adapted from Figures 5.2 and 5.3 in Winter: Biomechanics and Motor Control of Human Movement, 4th ed. 2009 [106].)	29
Figure 2.5. The hip musculoskeletal anatomy of a baseline MSM [133], which was scaled with marker-based length measurements (pink dots) to create the generic MSMs in Chapter 3. Note that the coarse shapes of pelvis and femurs do not resemble detailed 3D hip anatomy, especially malformed bones typical of DDH patients (Figure 2.1).	32
Figure 2.6. Examples of image-based subject-specific MSM creation. (A) 3D-segmented bone and muscle anatomy (left) are added to the MSM (middle) to guide updates to joint locations and muscle paths (right). (B) Subject-specific images (left) can be used to derive precise anatomical paths for major non-linear muscles such as the iliopsoas (right). (Sub-figure A adapted from Figure 1 in Valente et al. PLoS One. 2014 [158]. Sub-figure B adapted from Figure S1 in Wesseling et al. Comput Methods Biomech Biomed Engin. 2016 [135].)	40

Figure 3.1. Flowchart showing development of models with low, moderate, and high levels of geometric specificity. (A) Top: The baseline OpenSim model. Bottom: Subject-specific pelvis geometry reconstructed from CT. (B) I: Set of experimental (blue) and virtual (pink) marker-based measurements for isotropic pelvis scaling in a Generic model. II: 3D measurements on pelvis bony geometry for anisotropic scaling in a Nonuniform model. III: Subject-specific pelvis geometry, adjusted HJC and hip muscle attachment locations in a CT-Geometry model. (C) Subsequent biomechanical analysis to estimate hip JRFs and muscle forces during gait.....	62
Figure 3.2. Average resultant hip JRFs and components during gait for DDH subjects, expressed in pelvis frame (i.e. acting on acetabulum). Shaded area represents ± 1 standard deviation; highlighted vertical bands indicate time of JRF1 and JRF2.....	65
Figure 3.3. Average resultant hip JRFs and components during gait for CONT subjects, expressed in pelvis frame (i.e. acting on acetabulum). Shaded area represents ± 1 standard deviation; highlighted vertical bands indicate time of JRF1 and JRF2.....	68
Figure 3.4. Average hip muscle group forces during gait for DDH subjects. Shaded area represents ± 1 standard deviation; highlighted vertical bands indicate time of JRF1 and JRF2.	68
Figure 3.5. Average hip muscle group forces during gait for CONT subjects. Shaded area represents ± 1 standard deviation; highlighted vertical bands indicate time of JRF1 and JRF2.	70
Figure 4.1. (A) Example model with subject-specific pelvis and femur geometries, HJC locations, and muscle paths. (B) Example hip muscle MAL (anterior gluteus medius, “GMedAnt”, red arrow). Hip flexion, abduction, and rotation MALs were extracted across an entire gait cycle. (C) Example hip muscle LoAs. The AP, SI, and ML components of each muscle’s LoA represent the percentage of its net force in a certain direction within the pelvis frame.	87
Figure 4.2. Average muscle MALs (left and center) and LoAs (right) for major hip abductors, flexors, and external rotators. Shades represent ± 1 SD. Vertical highlighted areas indicate the times of JRF peaks in early stance (JRF1) and late stance (JRF2). “*” indicates statistical inter-group significance. GMedAnt, anterior gluteus medius; TFL, tensor fasciae latae; RF, rectus femoris; IL, iliacus; GMaxAnt, anterior gluteus maximus.....	92

- Figure 4.3. Average hip JRF components overlaid with abductor and external rotator muscle forces. Internal rotator forces (not shown) followed similar patterns to abductors. Shades represent ± 1 SD. Vertical highlighted areas indicate the times of hip JRF peaks. “*” indicates statistical inter-group significance.94
- Figure 4.4. Average forces for the gluteus medius (GMed) and tensor fasciae latae (TFL) muscles. Three individual muscles had force differences between DDH and Healthy: gluteus medius, tensor fasciae latae (resultant and superior only), and gluteus minimus (similar patterns to gluteus medius). Shades represent ± 1 SD. Vertical highlighted areas indicate the times of hip JRF peaks. “*” indicates statistical inter-group significance.95
- Figure 5.1. LCEA and AI measurement methods. (A) LCEA was measured as the angle between a first line (thick white) through the femoral head center and perpendicular to the inferior aspect of ischial tuberosities (light blue) and a second line connecting the femoral head center to the lateral aspect of acetabular sourcil (red). (B) AI was measured as the angle between a first line parallel to the inferior aspect of ischial tuberosities and a second line connecting the medial and lateral aspects of acetabular sourcils (thin white).108
- Figure 5.2. Estimation of acetabular edge loading (AEL). (A) The acetabular rim of each subject was delineated using a principal curvature heat map. (B) Nine clock-face points were designated on the anterior (“A”), superior (“S”), and posterior (“P”) quadrants of the rim. (C) AEL magnitudes were estimated via trigonometric projection of the hip JRF (black arrow) along the directions from HJC towards each clock-face point on the rim (red/green arrows). The JRF-to-edge angle was calculated as the angle between the JRF and the AEL directions (i.e. between black and red/green arrows). Note zero posterior AEL when JRF is directed anteriorly. (D) An ‘acetabular edge plane (AEP)’ was fit to the rim to measure the distance between the approximated acetabular border and the HJC.110
- Figure 5.3. Average JRF-to-edge angles (top) and AEL (bottom) in (A) anterior (2-4 o’clock), (B) superior (11-1 o’clock), and (C) posterior (8-10 o’clock) regions throughout gait. Red/black shades = ± 1 SD. Vertical yellow bars indicate time of JRF peaks (JRF1 and JRF2). Blue shades illustrate accumulative impulses. Statistical significance: ‘*’ instantaneous, ‘#’ accumulative.114

Figure 6.1. LCEA and AI measurements. LCEA was measured as the angle between a first line (black) through the femoral head center and perpendicular to the inferior aspect of ischial tuberosities (blue) and a second line connecting the femoral head center to the lateral aspect of acetabular sourcil (red). AI was measured as the angle between a first line parallel to the inferior aspect of ischial tuberosities and a second line connecting the medial and lateral aspects of acetabular sourcils (purple).	126
Figure 6.2. Example of a squatting sequence. Ground reaction forces (green arrows) on each foot were recorded by an in-ground force platform. The start, end, and lowest point of a squatting trial (MaxSq) were determined using the maximum and minimum vertical positions of a skin marker placed above the top of sacrum (red dot).....	127
Figure 6.3. Estimation of acetabular edge loading (AEL) during squat. (A) The acetabular rim of each hip was delineated using a principal curvature heat map. (B) Nine clock-face points were designated on the anterior (“A”), superior (“S”), and posterior (“P”) quadrants of the rim. (C) AEL magnitudes were estimated via trigonometric projection of the hip JRF (black arrow) along the directions from HJC towards each clock-face point on the rim (e.g. green arrow for 11 o’clock). The JRF-to-edge angle was defined as the angle between the JRF and the AEL directions (e.g. between black and green arrows). Diagram depicts hip JRF near the lowest point of squat, which was in the posterior direction while AEL was projected to the posterior and superior acetabulum. (D) An ‘acetabular edge plane (AEP)’ was fit to the rim to measure the distance between the approximated acetabular border and the HJC (yellow line).....	130
Figure 6.4. Hip JRF resultant and antero-posterior, supero-inferior, medio-lateral components throughout a squatting trial, averaged among DDH and control subjects. Red/black shades = ± 1 SD. Vertical yellow bars indicate time of lowest point of squat (MaxSq). ‘*’ Indicates inter-group statistical significance.....	132
Figure 6.5. Average JRF-to-edge angles (top) and AEL (bottom) in (A) superior (11-1 o’clock) and (B) posterior (8-10 o’clock) regions throughout a squatting trial. Note AEL in the anterior region (2-4 o’clock) was minimal, where no inter-group differences were found, thus were not shown. Red/black shades = ± 1 SD. Vertical yellow bars indicate time of MaxSq. Blue shades illustrate accumulative impulses over the duration of a whole squatting trial. Inter-group statistical significance: ‘*’ instantaneous, ‘#’ accumulative.	134

List of Tables

Table 3.1.	Differences among Generic, Nonuniform, and CT-Geometry model types.	63
Table 3.2.	Hip JRFs and muscle forces (mean \pm 1 standard deviation) at JRF1 and JRF2 for DDH subjects, normalized by body weight (xBW).....	66
Table 3.3.	Hip JRFs and muscle forces (mean \pm 1 standard deviation) at JRF1 and JRF2 for CONT subjects, normalized by body weight (xBW).....	67
Table 3.4	HJC locations (cm) relative to pelvis origin for DDH and CONT groups (mean \pm 1 standard deviation).	70
Table 4.1	Demographics, gait speed, and normalized HJC ML location (mean \pm SD) for Healthy and DDH subjects.	86
Table 4.2	Hip muscle functional group definitions.	88
Table 4.3	Dynamic MALs and LoAs (mean \pm SD) for major force-generating hip muscles with significant differences (shaded) between DDH and Healthy groups. LoA expressed as percentage (%) of net muscle force.....	91
Table 5.1	Demographics, gait speed, radiographic measures, and the HJC-to-AEP distance (mean \pm SD) of DDH and control subjects.	112
Table 6.1	Demographics, radiographic measures, and the HJC-to-AEP distance (mean \pm SD) of DDH and control subjects.....	132

List of Abbreviations

2D	Two-dimensional	IL	Iliacus
3D	Three-dimensional	JRF	Joint reaction force
AEL	Acetabular edge loading	LCEA	Lateral center-edge angle
AEP	Acetabular edge plane	LoA	Line of action
AI	Acetabular inclination	MAL	Moment arm length
ANOVA	Analysis of variance	MaxSq	Maximum of squat
AP	Antero-posterior	ML	Medio-lateral
ASIS	Anterior superior iliac spine	MR	Magnetic resonance
BMI	Body mass index	MSM	Musculoskeletal model
BW	Body weight	OA	Osteoarthritis
CONT	Control	PAO	Periacetabular osteotomy
CT	Computed tomography	PRO	Patient-reported outcome
DDH	Developmental dysplasia of the hip	PSIS	Posterior superior iliac spine
DE	Discrete element	RF	Rectus femoris
EMG	Electromyography	RMSE	Root mean square error
FE	Finite element	SD	Standard deviation
GMaxAnt	Anterior gluteus maximus	SI	Supero-inferior
GMed	Gluteus medius	TFL	Tensor fasciae latae
GMedAnt	Anterior gluteus medius	y/o	Years old
HJC	Hip joint center		

Acknowledgments

It is an easy decision to first and foremost thank my research advisor, Dr. Michael Harris. Oddly enough, back in my first semester, Mike has not started his faculty position yet. I am grateful he welcomed me to the new lab as his first trainee, and gave me the opportunity to do this important and very cool new research. The journey has not been easy, and we had shared moments of smooth sails and rough stretches. Sometimes I did not feel it right away, but through the years, I recognized with increasing certainty how he has provided countless valuable feedback to my work, given me unwavering support on career success, and when I needed help, he has always been there. Thank you, Mike, for all you have done to lead me up to here. This dissertation would never be possible without your mentorship, and looking back, I would not have chosen a better lab to stay.

I want to next thank my dissertation committee for their help in so many aspects that each became essential pieces of my training experience. Dr. Spencer Lake has been helpful since my orientation days, always reminded me to think about big pictures, and has been a nice connection for me with the engineering labs. Dr. Philip Bayly welcomed me back to St. Louis to pursue this degree in the first place, and his advice has always been thought-provoking. Dr. Marcie Harris-Hayes gave me useful clinical perspectives on the projects, and has been a side mentor who always listened to my words and made my day better. Those had been so important. Dr. Cecilia Pascual-Garrido made time out of her busy schedule to discuss many valuable ideas with me, which became integral to multiple projects in this dissertation. Dr. Jessica Wagenseil kindly agreed to serve as an extra member on my committee, and before that, she has helped me with many drop-in questions as the departmental advisor. It has been a great pleasure to have each of you on my board.

Many people in the past six years have supported me over this experience, and I may never exhaustively express my gratitude to everyone that helped along the way. Dr. Brecca Gaffney

always shared her thoughts and advice despite my obnoxiously numerous questions, while it was also fun having a drink after work once in a bit. Molly Shepherd has been a delightful presence around – best of luck on your doctoral training. Outside of Harris lab, many other faculty and peers have also been supportive in and outside of work. Dr. Michael Mueller, Dr. Linda Van Dillen, Dr. Ruth Clark, and Dr. Catherine Lang have been especially helpful. Also special thanks to my fellow doctoral students from both campuses – Chris Sorensen, Alex Reiter, and everyone in the Movement Science Program – you have all made this experience much more memorable.

I will save the final acknowledgment for my family 10,000 miles away. My mom has cared about every part of my life like no one else, given all the time I could ask for to listen to me, and dedicated so much to help me with her wise words. Yet when we are stressed over the phone call, my dad has always stepped in to soothe our minds and let me know everything will be okay. Their support has been irreplaceable to keep me going especially amidst the global pandemic. I am also grateful to the other family members, especially my late grandfather who I am dedicating this dissertation to, for their love and belief in me. They meant everything to me not just as a student in school, but as the person I am. Mom and Dad – I am excited to come home after this long separation, and I will tell you all about this journey when we finally get together again.

Ke Song

Washington University in St. Louis

May 2021

Dedicated to my grandfather – you will forever be my inspiration.

ABSTRACT OF THE DISSERTATION

Subject-Specific Musculoskeletal Modeling of Hip Dysplasia Biomechanics

by

Ke Song

Doctor of Philosophy in Mechanical Engineering

Washington University in St. Louis, 2021

Professor Michael D. Harris, Chair

Professor Spencer P. Lake, Co-Chair

Developmental dysplasia of the hip (DDH) is characterized by abnormal bony anatomy, causes pain and functional limitations, and is a prominent risk factor for premature hip osteoarthritis. Although the pathology of DDH is believed to be mechanically-induced, little is known about how DDH anatomy alters hip biomechanics during activities of daily living, partly due to the difficulties with measuring hip muscle and joint forces. Musculoskeletal models (MSMs) are useful for dynamic simulations of joint mechanics, but the reliability of MSMs for DDH research is limited by an accurate model representation of the unique hip anatomy. To address such challenges, this research used subject-specific MSMs to identify how DDH hip biomechanics are influenced by the abnormal bony anatomy. First, to determine the importance of model specificity, personalized MSMs using image-based bony anatomy and muscle paths were compared against MSMs with generic anatomy. MSMs with subject-specific anatomy estimated significantly different hip muscle and joint forces compared to generic models, thus are necessary for delineating DDH-specific pathomechanics. Next, image-based MSMs were used to calculate hip muscle moment arm lengths and lines of action during gait, to determine how DDH alters dynamic muscle force production. Hips with DDH had reduced abductor moment arms, which

elevated muscle and joint forces in the medial direction. Results confirmed hip muscles' contributions to joint overloading, which could in turn interact with the abnormal anatomy to induce pathomechanics at the articular level. To verify this phenomenon, hip loading estimated from MSMs was projected to the pelvis anatomy to predict acetabular edge loading during two movement tasks, gait and double-legged squat. Results showed that edge loading was elevated by the shallow acetabulum of DDH, and was highly dependent on the kinetics and muscle demand of task-specific movements. These findings could help explain the prevalence of region-specific labral tears in DDH. Overall, this research provided new insights into the relationships among bony anatomy, muscle function, and joint biomechanics in hips with DDH. The outcomes can refine our understanding of mechanically-induced DDH pathology, and inform patient-specific clinical assessments and treatments to improve long-term hip joint health.

Chapter 1: Introduction

1.1 Motivations

The human hip serves essential biomechanical functions during daily living, supporting the body weight while allowing routine ambulation and task-specific movements. A healthy hip is maintained by balanced joint mechanical and biological environments. When such balance is disrupted due to abnormal joint mechanics, damage to biological tissues may occur, which often induces pain and limits joint mobility. Chronically, abnormal hip biomechanics cause detrimental biological responses and irreversible changes to the articular tissues, and have been considered the primary etiological factor that leads to joint degeneration and osteoarthritis (OA) [1-3].

Hip OA is among the most prevalent forms of chronic hip diseases, which affects over 20 million people in the United States aged 65 or older and may increase to over 40 million by year 2030 [4,5]. Hip OA causes significant disease burdens, including debilitating symptoms and large financial costs for treatments including total hip arthroplasty [4,6]. Such burdens especially impact those who develop hip OA prematurely, as functional limitations (including with hip prosthetics) and costs affect the patients' quality of life for a long time [4]. Significant needs thus exist to better understand the mechanistic factors that lead to OA development, and improve interventions at an early stage to delay the onset of OA and lessen the burdens it take on at-risk populations.

Premature development of hip OA is often secondary to existing structural abnormalities in the hip [1]. Developmental dysplasia of the hip (DDH), also known as hip dysplasia, is one of the most common structural diseases that predispose the hip to heightened early OA risks [1,7,8]. Despite often routinely screened in infancy as a pediatric disease, DDH is estimated to affect 1

out of 1000 adults in the United States [7,9]. Evidences of DDH is found in up to 40% of patients with hip OA, with 25% to 50% of untreated DDH patients showing radiographic OA signs by the age of 50 and requiring a total hip arthroplasty [7,10]. Because abnormal joint biomechanics play an integral role in the arthritic etiology, it is likely a key contributor to the high risks of premature OA in hips with DDH.

DDH is characterized by abnormal hip bony anatomy, including a shallow acetabulum that does not adequately cover the femoral head during movements [7,11,12]. Severe forms of DDH bony deformity can be manifested since infancy, thus diagnosed and treated in early childhood [13]. However, a significant portion of moderate or less severe DDH cases often goes undetected, and pre-arthritic symptoms such as hip pain only onset in early adulthood, when pathology often becomes further aggravated by high levels of physical activity at this age [14]. In adults, DDH is typically diagnosed with radiographic signs of hip bony deformity [12,15,16], and accordingly treated by surgeries such as the periacetabular osteotomy (PAO) to correct such anatomical abnormalities [7,17,18]. However, it has been reported that the presentation of symptoms in young adult DDH patients did not always correspond to the radiographic extent of deformity, which often delays a definitive diagnosis of the disease [14]. Furthermore, although anatomical corrections via PAO surgery can relieve symptoms and improve short-term functions [19,20], long-term surgical outcomes have been less than ideal, as a majority of patients still advanced to end-stage hip OA or underwent total hip arthroplasty 30 years post-op [21]. These evidences suggest that even as a disease defined by anatomical abnormalities, assessing anatomy alone may not be enough to predict the chronic pathology secondary to DDH, nor the long-term efficacy of surgical treatments. Quantifying the hip joint biomechanical environment in DDH, and its relationships with the known

abnormal anatomy, could be the missing link to explain how DDH bony deformity causes detrimental joint mechanics, which in turn induce symptoms, tissue damage, and degeneration.

Despite the needs to understand such relationships among DDH anatomy, biomechanics, and pathology, direct quantification of hip mechanics is difficult due to methodological limitations. It is currently not possible to directly and non-invasively measure hip joint contact loading or muscle forces during activities of daily living. In fact, only a few benchmark experimental datasets are available on in-vivo hip joint reaction forces (JRFs) [22,23], recorded with instrumented hip prosthetics installed in a small number of older arthritic subjects. Such method cannot be used to measure loading in pre-arthritic native hips due to its invasiveness. Computational models can be valuable for estimating joint mechanical quantities that are unmeasurable, and many modeling studies have demonstrated mechanical behaviors unique to DDH hip anatomy [24,25]. However, most of past DDH models are limited by a lack of subject-specific joint loading input, thus may not truly represent the hip mechanical profiles unique to the movements of DDH patients [26].

Musculoskeletal model (MSM) is a useful computational tool capable of estimating joint mechanics specific to individual dynamic movements. MSMs digitize the neuromusculoskeletal system elements by detailed representations of body segment, joint and muscle properties, which allows dynamic simulations of movements [27]. Conventionally, “generic” MSMs are created using cadaveric or imaging benchmark experimental data, which are then “scaled” to each subject and used to estimate muscle forces and JRFs using subject-specific optical motion capture data. MSM-based simulations have made valuable contributions to a variety of human biomechanics research, both on healthy populations and pathological movements of neurological diseases [27]. Yet, MSMs have not been widely used to study biomechanics in joint anatomical diseases such as DDH. A key reason for this scarcity may be that the unique anatomy of dysplastic hips has not

been available in the MSMs, and even for generic MSMs representative of healthy individuals, bony anatomy has been coarse. Because generic MSMs do not closely depict the unique bony deformity of DDH, hip mechanics estimated from such models might not be accurate and reliable enough for DDH research. For this reason, improved anatomical details may be required for MSMs to delineate the pathomechanics of DDH and their relationships with the abnormal anatomy.

A reliable source to acquire patient-specific anatomical data is three-dimensional (3D) medical images, including computed tomography (CT) and magnetic resonance (MR) imaging. CT and MR data provide an opportunity to create subject-specific MSMs with detailed joint anatomy, including abnormal features. Image-based MSMs with personalized bone and muscle anatomy could more accurately represent the mechanical properties around the joint, therefore may improve the reliability of the model estimates. Specifically, hip-focused studies have demonstrated that subject-specific MSMs with detailed 3D anatomy were able to improve hip contact force estimates [28], suggesting image-based approach as a promising direction for MSM simulations of DDH biomechanics [29]. Considering the importance of quantitative hip biomechanics for improved understanding of DDH-related pathology, great scientific values exist to establish and standardize image-based, subject-specific MSMs, use such models to estimate hip biomechanics in DDH, identify how they deviate from healthy hips, and analyze how they relate to the anatomical abnormalities. Such research also has potentials to yield new quantitative information that benefits future clinical evaluation and intervention of DDH, as surgeries and rehabilitation can use targeted restoration of the hip biomechanical environment to refine and personalize treatment decisions and plans, thereby ultimately improve long-term hip joint health for more patients.

1.2 Research Aims

Driven by the aforementioned motivations, the aims of this research were to (1) establish and standardize the creation of image-based MSMs for estimation of hip biomechanics in DDH, and then to (2) use subject-specific MSMs to estimate hip biomechanics in DDH compared to healthy controls, and analyze their relationships with the hip anatomical abnormalities of DDH.

The aim to establish and standardize subject-specific MSM for DDH focused on determining an appropriate level of anatomical details for the models to reliably quantify DDH hip biomechanics, while can be feasibly applied in large-scale future research of DDH. On the same groups of DDH and control subjects, MSMs with various levels of specificity and complexity were created, and hip biomechanical estimates were compared across the MSMs (for both subject groups) to determine the influences of using anatomical details, fully or partially. The appropriate level of details would be determined by considering both the mechanical influences and the time and computational demands of model creation. An optimized and standardized MSM workflow would enable reliable investigations of DDH biomechanics in the subsequent research aim.

In the aim to estimate and analyze hip joint biomechanics in DDH and its relationships to abnormal anatomy, a range of factors that can contribute to joint and articular-level mechanics were studied. First, the hip JRFs, which are primarily contributed from muscles surrounding the hip [30], were analyzed in context with muscle moment arm lengths and lines of action that are directly dependent on the DDH bony anatomy and muscle paths. Then, the mechanical effects due to DDH bony deformity and muscle-induced JRFs were further specified on an articular level. Specifically, MSM-estimated hip JRFs were mathematically projected to subject-specific pelvis anatomy to estimate dynamic loading at the acetabular edge, and analyze its relationships with the anatomical deformity, with implications to DDH-related labral tears and chondral lesions. The

MSM-based acetabular edge loading analyses were applied to multiple tasks, including routine gait and high hip flexion double-legged squat, to identify the effects of patient-specific movements and lifestyles on the pathomechanics.

1.3 Summary of Chapters

This dissertation contains 7 chapters, including the current Chapter 1 that provides an overview of the motivations and objectives of the whole research, and an outline of the dissertation.

Chapter 2, the Background, provides introduction to relevant concepts and literature on the current scientific and clinical knowledge of DDH, biomechanics of the hip, and MSMs with an emphasis on subject-specific methods and hip-related research. On DDH, backgrounds include definition of the clinical problem, its relevance and presentation, current knowledge on etiology, risk factors, secondary pathology, evaluation, and treatments. On hip biomechanics, backgrounds include functions of normal hips, causes and effects of abnormal hip biomechanics in DDH, and current in-vitro, in-vivo, and in-silico methods to quantify hip biomechanics. Then on MSMs, fundamental concepts and workflow are introduced, followed by a summary of the limited past MSMs for DDH research. An overview of image-based subject-specific MSMs is then described with a focus on hip-related studies. Chapter 2 does not necessarily cover all backgrounds relevant to DDH, hip biomechanics or subject-specific MSMs, but should provide sufficient contexts to support the motivations, aims, and methods used in the subsequent chapters for specific studies.

Chapters 3 through 6 describes the individual studies within the dissertation research conducted according to the overall aims (Section 1.2), each having been or is being reported in biomechanics and orthopaedics academic journals. Chapter 3 and Chapter 4 are reprinted from published manuscripts that the dissertation author contributed as the primary author, along with

other co-authors including the Dissertation Chair (research advisor). Both of these chapters were reprinted with rights granted from the publisher (see footnotes under the titles of Chapters 3 and 4). Chapters 5 and 6 are currently unpublished work under peer review or in preparation. Detailed overview of each Chapter is summarized in the following paragraphs.

Chapter 3 describes a project that addressed the first aim of this research, to establish and standardize subject-specific MSMs that can reliably and feasibly estimate DDH hip biomechanics. For both DDH and healthy control subjects, MSMs with three types of anatomical details were created, with the most subject-specific MSMs including CT-based pelvis bony geometry, hip joint center locations, and muscle paths. A second type of moderately-specific MSMs using CT-based pelvis scaling, but not the full 3D anatomy, was also created for comparison against the third type, generic marker-scaled MSMs. Each model was used to estimate hip JRFs and muscle forces during gait, and estimates were compared across the MSMs to determine the mechanical influences of model anatomical details. With such comparisons, an appropriate complexity level for the MSMs can be decided to facilitate future research of DDH hip biomechanics, for feasible discovery of meaningful findings. The study reported in Chapter 3 was published in the *Computer Methods in Biomechanics and Biomedical Engineering* journal.

With an established workflow to create subject-specific MSMs in Chapter 3, Chapters 4 through 6 addressed the second research aim to estimate hip bone-muscle mechanics and analyze their relationships with DDH anatomy. Chapter 4 describes a study to determine the influences of DDH anatomy on hip muscle force production and contributions to JRFs. The hip anatomy-force relationships are likely dependent on muscle parameters such as the moment arm lengths (MALs) and lines of action (LoAs). Using MSMs that incorporated MR images (distinct from CT-based MSMs in Chapter 3), which allowed refined personalization of muscle paths, hip muscle MALs

and LoAs were compared between DDH and control subjects along with hip muscle force and JRF estimates [29]. Results from these parallel comparisons can help explain how bony abnormalities alter muscle force production in hips with DDH and result in potentially detrimental hip joint loading. The study in Chapter 4 was published in the *Journal of Biomechanics*.

When overall hip joint loading is altered, as represented by the muscle-induced JRFs, the next question was how such altered loading leads to mechanically-induced articular damages. Joint damages associated with DDH, specifically the acetabular labral tears, may be related to abnormal mechanics near the labrum at the edge of the shallow acetabulum, which could be induced by aberrant hip JRFs. The studies in Chapters 5 and 6 thus investigated how the abnormal acetabular anatomy and dynamic joint loading in hips with DDH contribute to region-specific loading around the acetabular edge. MR-based MSMs with detailed acetabular anatomy, aligned with muscle-induced hip JRF estimates from Chapter 4, allowed mathematical projections to predict how acetabular edge loading (AEL) during gait may be different between DDH and healthy hips, and associated with the anatomical characteristics of the DDH acetabula. Chapter 5 introduces a novel MSM-based AEL analysis, and demonstrated its ability to delineate subject-specific edge loading mechanical traits in acetabula with DDH during routine gait motion. The study in Chapter 5 is currently in a manuscript under peer review in the *Frontiers in Sports and Active Living* journal.

As an extension of Chapter 5, Chapter 6 further investigated how acetabular edge loading (AEL) in hips with DDH can be influenced by the interactions of anatomical, movement, and time factors during a lifestyle-specific movement task. Other than the acetabular deformity, risks for DDH-related labral tears could also depend on subject-specific lifestyles and movement demands. Particularly, instead of the antero-superior acetabulum where most labral tears tend to occur [31], posterior labral tears may be more common in those who often perform high hip flexion tasks such

as squatting [32], indicating the roles of task-specific motion and loading in region-specific tissue damage. Thus, the study in Chapter 6 estimated AEL during double-legged squat using MR-based MSMs and similar analytical methods to Chapter 5, with DDH-to-control comparisons and associations with hip anatomical measures. Findings of Chapter 6 can help clarify the importance of task-specific movement patterns, including their acute and chronic effects, on region-specific articular-level mechanics. Chapters 5 and 6 may together improve the current understandings of DDH labral and chondral pathomechanics, thus potentially inform patient-specific clinical risk assessments and personalized treatment decision making (via correction of anatomy or movement) to mitigate labral tears and chondral lesions secondary to DDH. The study in Chapter 6 is currently in manuscript preparation for submission to the *Journal of Orthopaedic Research*.

The final Chapter 7 provides a summary of the conclusions from specific studies towards the overall research aims, as well as their significance and novelty regarding contributions to the knowledge and research methods of DDH hip biomechanics. The general limitations of this dissertation are then discussed, along with potential future directions that can extend from this research to further improve our understanding of DDH biomechanics and pathology, as well as the efficacy of clinical interventions, in a patient-specific manner.

1.4 References

1. Felson DT. Osteoarthritis as a disease of mechanics. *Osteoarthritis Cartilage*. 2013 Jan;21(1):10-5.
2. Carter DR, Beaupré GS, Wong M, Smith RL, Andriacchi TP, Schurman DJ. The mechanobiology of articular cartilage development and degeneration. *Clin Orthop Relat Res*. 2004 Oct;427 Suppl:S69-77.
3. Guilak F, Fermor B, Keefe FJ, Kraus VB, Olson SA, Pisetsky DS, Setton LA, Weinberg JB. The role of biomechanics and inflammation in cartilage injury and repair. *Clin Orthop Relat Res*. 2004 Jun;423:17-26.

4. Nho SJ, Kymes SM, Callaghan JJ, Felson DT. The burden of hip osteoarthritis in the United States: epidemiologic and economic considerations. *J Am Acad Orthop Surg.* 2013;21 Suppl 1:S1-6.
5. Leveille SG. Musculoskeletal aging. *Curr Opin Rheumatol.* 2004 Mar;16(2):114-8.
6. Murphy L, Helmick CG. The impact of osteoarthritis in the United States: a population-health perspective. *Am J Nurs.* 2012 Mar;112(3 Suppl 1):S13-9.
7. Gala L, Clohisy JC, Beaulé PE. Hip dysplasia in the young adult. *J Bone Joint Surg Am.* 2016 Jan 6;98(1):63-73.
8. Wyles CC, Heidenreich MJ, Jeng J, Larson DR, Trousdale RT, Sierra RJ. The John Charnley Award: Redefining the natural history of osteoarthritis in patients with hip dysplasia and impingement. *Clin Orthop Relat Res.* 2017 Feb;475(2):336-50.
9. Manaster BJ. From the RSNA Refresher Courses. Radiological Society of North America. Adult chronic hip pain: radiographic evaluation. *Radiographics.* 2000 Oct;20 Spec No:S3-25.
10. Michaeli DA, Murphy SB, Hipp JA. Comparison of predicted and measured contact pressures in normal and dysplastic hips. *Med Eng Phys.* 1997 Mar;19(2):180-6.
11. Cooperman DR, Wallensten R, Stulberg SD. Acetabular dysplasia in the adult. *Clin Orthop Relat Res.* 1983 May;175:79-85.
12. Wiberg G. Studies on dysplastic acetabula and congenital subluxation of the hip joint with special reference to the complication of osteoarthritis. *Acta Chir Scand.* 1939;83 Suppl 58:7-135.
13. Dezateux C, Rosendahl K. Developmental dysplasia of the hip. *Lancet.* 2007 May 5;369(9572):1541-52.
14. Nunley RM, Prather H, Hunt D, Schoenecker PL, Clohisy JC. Clinical presentation of symptomatic acetabular dysplasia in skeletally mature patients. *J Bone Joint Surg Am.* 2011 May;93 Suppl 2:17-21.
15. Tönnis D. Congenital Dysplasia and Dislocation of the Hip in Children and Adults. Berlin and Heidelberg, Germany: Springer-Verlag; 1990.
16. Clohisy JC, Carlisle JC, Beaulé PE, Kim YJ, Trousdale RT, Sierra RJ, Leunig M, Schoenecker PL, Millis MB. A systematic approach to the plain radiographic evaluation of the young adult hip. *J Bone Joint Surg Am.* 2008 Nov;90 Suppl 4:47-66.

17. Ganz R, Klaue K, Vinh TS, Mast JW. A new periacetabular osteotomy for the treatment of hip dysplasias. Technique and preliminary results. Clin Orthop Relat Res. 1988 Jul;(232):26-36.
18. Clohisy JC, Schutz AL, St John L, Schoenecker PL, Wright RW. Periacetabular osteotomy: a systematic literature review. Clin Orthop Relat Res. 2009 Aug;467(8):2041-52.
19. Boje J, Caspersen CK, Jakobsen SS, Søballe K, Mechlenburg I. Are changes in pain associated with changes in quality of life and hip function 2 years after periacetabular osteotomy? A follow-up study of 321 patients. J Hip Preserv Surg. 2019 Mar 14;6(1):69-76.
20. Novais EN, Heyworth B, Murray K, Johnson VM, Kim YJ, Millis MB. Physical activity level improves after periacetabular osteotomy for the treatment of symptomatic hip dysplasia. Clin Orthop Relat Res. 2013 Mar;471(3):981-8.
21. Lerch TD, Steppacher SD, Liechti EF, Tannast M, Siebenrock KA. One-third of hips after periacetabular osteotomy survive 30 years with good clinical results, no progression of arthritis, or conversion to THA. Clin Orthop Relat Res. 2017 Apr;475(4):1154-68.
22. Bergmann G, Deuretzbacher G, Heller M, Graichen F, Rohlmann A, Strauss J, Duda GN. Hip contact forces and gait patterns from routine activities. J Biomech. 2001 Jul;34(7):859-71.
23. Bergmann G, Bender A, Dymke J, Duda G, Damm P. Standardized loads acting in hip implants. PLoS One. 2016 May 19;11(5):e0155612.
24. Henak CR, Abraham CL, Anderson AE, Maas SA, Ellis BJ, Peters CL, Weiss JA. Patient-specific analysis of cartilage and labrum mechanics in human hips with acetabular dysplasia. Osteoarthritis Cartilage. 2014 Feb;22(2):210-7.
25. Abraham CL, Knight SJ, Peters CL, Weiss JA, Anderson AE. Patient-specific chondrolabral contact mechanics in patients with acetabular dysplasia following treatment with peri-acetabular osteotomy. Osteoarthritis Cartilage. 2017 May;25(5):676-84.
26. Thomas-Aitken HD, Willey MC, Goetz JE. Joint contact stresses calculated for acetabular dysplasia patients using discrete element analysis are significantly influenced by the applied gait pattern. J Biomech. 2018 Oct 5;79:45-53.
27. Delp SL, Anderson FC, Arnold AS, Loan P, Habib A, John CT, Guendelman E, Thelen DG. OpenSim: open-source software to create and analyze dynamic simulations of movement. IEEE Trans Biomed Eng. 2007 Nov;54(11):1940-50.

28. Wesseling M, De Groote F, Bosmans L, Bartels W, Meyer C, Desloovere K, Jonkers I. Subject-specific geometrical detail rather than cost function formulation affects hip loading calculation. *Comput Methods Biomech Biomed Engin*. 2016 Nov;19(14):1475-88.
29. Harris MD, MacWilliams BA, Bo Foreman K, Peters CL, Weiss JA, Anderson AE. Higher medially-directed joint reaction forces are a characteristic of dysplastic hips: A comparative study using subject-specific musculoskeletal models. *J Biomech*. 2017 Mar 21;54:80-7.
30. Correa TA, Crossley KM, Kim HJ, Pandy MG. Contributions of individual muscles to hip joint contact force in normal walking. *J Biomech*. 2010 May 28;43(8):1618-22.
31. Hartig-Andreasen C, Søballe K, Troelsen A. The role of the acetabular labrum in hip dysplasia. A literature overview. *Acta Orthop*. 2013 Feb;84(1):60-4.
32. Hase T, Ueo T. Acetabular labral tear: arthroscopic diagnosis and treatment. *Arthroscopy*. 1999 Mar;15(2):138-41.

Chapter 2: Background

2.1 Developmental Dysplasia of the Hip (DDH)

2.1.1 Clinical Definition

Developmental dysplasia of the hip (DDH), also known as hip dysplasia, is a joint structural disease that includes abnormal development of the hips that are unstable, malformed, or dislocated [1-3]. The malformation can range from mild, subtle to severe, and includes abnormalities on both acetabular and femoral side of the hip [1,3,4]. The presentation of DDH may start during infancy and be treated in early childhood, especially in the severe cases, but also often evade childhood screening and become clinically apparent only near early adulthood [2,5,6]. Some other congenital or demographic traits, including childbirth position, family history, and female sex, are also known risk factors of DDH [2,6]. Hips with DDH, including those not exhibiting dislocation or subluxation, typically presents a shallow acetabulum that is deficient in both shape and orientation, causing insufficient coverage of the femoral head and lateralization of the hip joint center of rotation (HJC) (**Figure 2.1**) [2,6-8]. Such anatomical abnormalities lead to altered contact areas between the shallow acetabulum and the femoral head, which could also exhibit lack of sphericity and other shape abnormalities [4,6,9], resulting in abnormal contact forces located around the hip joint, including near the acetabular rim and the labrum [9-11]. Such abnormal contact mechanics are thought to in turn cause symptoms and secondary damages to the articular cartilages, which advance the developments of osteoarthritis (OA) in the hip [6,10,12-14].

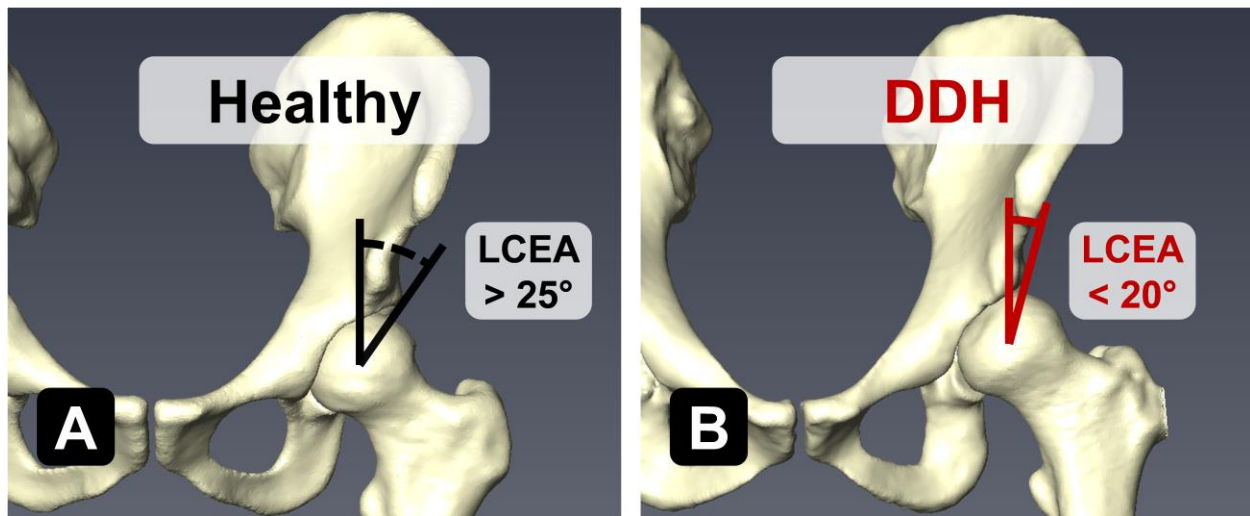


Figure 2.1. Representative pelvis and femur anatomy of (A) a healthy adult, and (B) a DDH patient with shallow acetabulum and reduced femoral coverage, indicated by the lateral center-edge angle (LCEA) [38].

2.1.2 Significance of DDH in Premature Development of Hip OA

DDH is known as one of the most prominent structural risk factors contributing to hip OA [7,12,13,15]. It has been reported that in people who developed advanced hip OA or underwent total hip arthroplasty prematurely (under 50 years old), almost half were associated with DDH abnormalities [6,16]. Vice versa, hips with DDH are at high risks of developing OA early, as longitudinal reports found that in hips with untreated DDH, 25%-50% showed radiographic signs of OA by the age of 50 [1,6,7,17]. It was estimated that hips with DDH had a likelihood of OA over 4-fold compared to structurally normal hips [18]. Because of chronic joint pain and functional limitations, early hip OA affects the patients' quality of life over a long time. Even with total hip arthroplasty, the significant costs of treatments and maintenance of prosthetic hips are undesirable for the younger patients due to the longer life expectancy and higher mobility demands [16,19]. For such reasons, to prevent the long-lasting disease burdens due to premature hip OA, it is important to detect and treat DDH at an early stage, before secondary joint failure onsets.

2.1.3 Pre-Arthritic Pathology of DDH

Despite the needs for early detection and treatments, joint lesions that precede OA development are difficult to clinically identify before degenerative changes to the articular cartilage have progressed [7]. However, hips with DDH structural deformity often present a range of pre-arthritic pathology that already affects the mobility and quality of life of the patients, which are potential initiators of more advanced joint damage and degeneration.

Commonly reported clinical presentation associated with DDH include, but are not limited to: hip pain, joint stiffness, abnormal movement patterns including limping, muscle pain and weakness, and torn acetabular labrum [6,10,20,21]. Pain is the most common symptom in hips with DDH, mostly located in the groin or lateral aspect of hip but can also simultaneously occur elsewhere such as in buttock and anterior thigh [10,20]. Such pain is usually insidious and aggravated by movements, but may not always correspond to clinical signs of anatomical abnormality [20]. The gradual and variable nature of DDH-related pain indicates that the sources of pain may be complex.

Pain and patient adaptation can result in abnormal movements and functional limitations. Limping during gait is common in most subjects with DDH, with many showing the Trendelenburg sign where the pelvis drops to contralateral [20,22,23]. Some studies also reported reduced hip extension during gait for DDH patients [22,24]. Movement deficiencies could also be directly contributed by abnormal articulation contacts, with “popping” and “clicking” common in a majority of dysplastic hips [20]. Abnormal movements could then limit mobility during tasks that demand hip functions such as stair navigation [20], which can be debilitating for young adult patients with high activity levels.

Despite being characterized by bony deformity, muscle deficiency has been increasingly reported in patients with DDH. Muscle soreness is a frequent complaint by DDH patients after activities, which may be a primary source of DDH-related hip pain. Recent studies have found muscle-related pain reproducible in these patients during clinical tests, and associated with muscle weakness as well as imaging signs of tendinopathy, in the hip flexors and abductors [21,25,26]. Muscle weakness has also been observed in chronic hip pain patient cohorts that included individuals with DDH [27]. Due to the importance of these muscles in actuating hip joint motions and stabilization [28], their deficiency could be a contributor to faulty movements (such as the Trendelenburg gait) and functional deficits, although their relationships with structural deformity or the secondary joint damages in DDH are less clear.

Lastly, before degenerative changes to the articular cartilage begin, tissue damage could occur in pre-arthritic hips with DDH deformity. The most common form of DDH-related hip joint damage is acetabular labral tears. Labral frank tears, fraying or hypertrophy can be present in more than 90% of symptomatic hips with DDH [29-31], and is a known source of hip pain. In hips with DDH, a hypertrophied labrum is often detached from the bony acetabular rim, sometimes together with bony fragments [10,29]. Similar to DDH-related pain, the onset of labral tears in dysplastic hips is usually insidious and often not linked to a known traumatic event [31-33], which could complicate the definitive clinical diagnosis [20]. Labral tears are thought to be associated with expedited development of hip OA. It has been reported that a majority of hips with torn labrum developed chondral lesions in the same acetabular regions, and such incidences increase with patient age [31,33,34]. Because labral tears potentially play a major role towards early hip joint degeneration, mitigation of labral damage risks can be an important consideration for clinical evaluation and treatments of DDH.

2.1.4 Diagnosis and Evaluation of DDH

Corresponding to the clinical definitions in Section 2.1.1, DDH is typically diagnosed and evaluated using a combination of physical examinations of symptoms and imaging examinations of anatomy [2,6]. In the pediatric cases with palpable hip instability or subluxation, physical tests are commonly used for diagnostic screening, but the reliability of such exams has been questioned [2,35]. For pre-arthritic adults with DDH, symptoms reported by the patients can be clinically verified using observation of abnormal gait motion [20,23] and range-of-motion tests including a combination of hip flexion, adduction and internal rotation [36]. Such physical tests are also used to detect DDH-related labral tears along with direct observation via arthroscopy [29,32,33].

For hips without extreme instability, imaging of the joint structure is usually needed for a definitive diagnosis of DDH [2], including ultrasonic methods for pediatric cases [37]. For skeletally mature individuals, such as those in young adulthood with symptoms onset, radiographic evaluation of hip anatomy is required. The most standard clinical measure that identifies dysplastic hip anatomy is the Wiberg lateral center-edge angle (LCEA) [38], obtained on antero-posterior radiographs and quantifies the superolateral coverage of the femoral head by the acetabulum (**Figure 2.2A**) [39]. An LCEA $<25^{\circ}$ indicates inadequate lateral coverage of the femoral head, LCEA $<20^{\circ}$ considered consistent with DDH, and between 20° and 25° as transitional or borderline (**Figure 2.1**) [6,38-40]. A second commonly used measure is the acetabular inclination or index (AI), also known as the Tönnis angle [41], on antero-posterior radiographs and depicts the orientation of the weight-bearing portion of the acetabulum (**Figure 2.2B**) [39]. An AI $>10^{\circ}$ is considered indicative of structural instability in line with DDH [39]. Other metrics used to quantify coverage include the acetabular depth-to-width ratio [39,42]. Because DDH acetabular deficiency is region-specific, measures that are on other radiographic views or more qualitative are also in

clinical use, such as the anterior center-edge angle to evaluate anterior acetabular deficiency [39,43], and the crossover and posterior wall signs to assess acetabular orientation and posterior deficiency [39,44]. Also, as DDH may involve abnormal femoral anatomy, measures such as the femoral neck-shaft angle [45], head sphericity and medio-lateral position have also been used by clinicians [39]. A unique trait for DDH is that the femoral head center is usually *lateralized* and shifted away from the pelvis due to the under-coverage [6,7,39,46]. Lastly, radiographs are used to evaluate and classify the degenerative signs indicative of hip OA, with the Tönnis grading system among the most common [41].

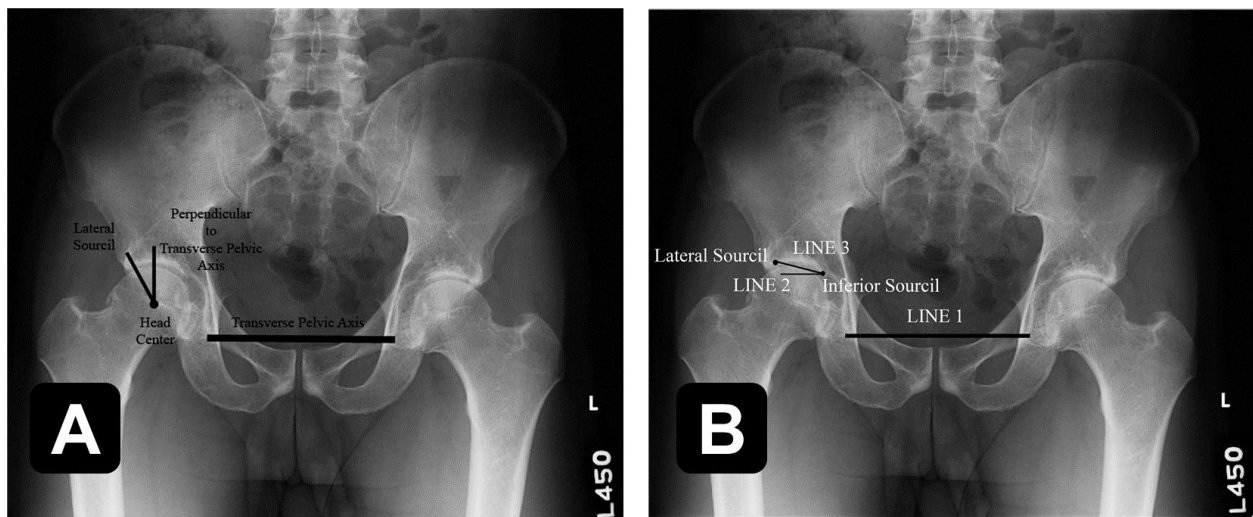


Figure 2.2. Standard radiographic measures of (A) the lateral center-edge angle (LCEA) to quantify lateral femoral coverage; and the (B) acetabular inclination (AI) or Tönnis angle to quantify orientation of the weight-bearing area of the acetabulum. (Adapted from Figure 11 in Clohisy et al. J Bone Joint Surg Am. 2008 [39].)

It should be noted that despite such a variety of physical and radiographic tools available for the evaluation of DDH, their use is at the discretion of the clinicians, thus subjectivity exists regarding diagnosis, classification and treatment decision making. Especially, it has been found that the radiographic extents of anatomical deformity do not fully correspond to the severity of DDH-related symptoms, which may have contributed to delayed diagnosis for many young adult patients, thus could risk compromising their long-term hip joint health [20]. Standard evaluations

may also miss evidences of DDH-related joint damage such as labral tears, which can be difficult to confirm without direct arthroscopy or advanced imaging such as the magnetic resonance arthrography [29,33,34,47]. These findings suggest that the current standard evaluation methods have not been optimal for the early diagnosis of DDH that would allow timely interventions. More research is thus needed to identify the clinical metrics that most reliably indicate the risks for symptoms and joint damage associated with DDH.

2.1.5 Treatments for DDH and Clinical Outcomes

Various surgical and non-surgical treatments of DDH have been used to reduce pain, restore mobility, and improve patients' quality of life. Although DDH patients with mild symptoms are sometimes treated conservatively with pain management and avoidance of pain-provoking activities, for intervention at its source, direct correction of the abnormal hip anatomy is needed. While pediatric DDH in infancy may be treated non-surgically using splint or harness [48], for symptomatic cases in adulthood after skeletal maturity, surgeries are often required. On the other end, older DDH patients who already present signs of irreversible joint damage often undergo total hip arthroplasty, which can achieve favorable outcomes as recipients live with prosthetic hips [6,49]. However, long-term complications such as instability, loosening, and need for revision surgeries are undesirable for younger patients who has higher mobility demands [49,50].

For better long-term outcomes in young adult hips with DDH and to delay the progression of OA or total hip arthroplasty, hip preservation surgeries are often performed, such as osteotomy to correct pelvis and femur deformities [6,51,52]. Due to the characteristic acetabular deformity, the most common modern surgery for young adults with DDH is the Bernese periacetabular osteotomy (PAO), which cuts loose, re-orientes and re-fixes the acetabulum to the rest of pelvic bones to restore sufficient coverage of the femoral head [53,54]. By modifying the acetabular

anatomy to resemble normal femoral coverage, PAO aims to restore functionality of the hip and thereby reduce the likelihood of secondary damage. Short-term clinical outcomes of PAO have been favorable, as patients report symptom relief, improved functionality, and better quality of life [55-58]. Yet, some patients still experience functional limitations 5 years after PAO, and self-reported healthy status is lower than controls [58,59]. Furthermore, the limited longer-term follow-up reports have shown less-than-ideal outcomes, as 71% of hips undergoing PAO eventually converted to total hip replacements at up to 30 years [60]. Suboptimal post-PAO outcomes and limited evidences both demand further research to refine the rationales for hip preservation surgery to improve clinical outcomes.

Labral repairs or debridement can be performed during preservation surgeries, or made via concurrent hip arthroscopy [30,61]. Symptoms can be effectively relieved by the repair, and patients have improved self-reported outcomes in short terms [61,62]. Yet, recent study found that in patients with recurrent pain 3 years after PAO, labral tear was present in over 80% of the hips under arthroscopy, a higher incidence rate than at the time of PAO [63]. The increased occurrence suggest labral tears may persist or develop even after bony deformity is surgically corrected, thus the effectiveness for PAO to mitigate labral damage may have been limited. Quantitative evidences are needed to understand how DDH-related labral tear risks are affected by both native dysplastic and surgically-altered hip anatomy, in order to reduce such risks during future surgical planning.

Physical therapy and rehabilitation are often involved in the management of DDH to complement surgery, or if surgeries are not recommended. Rehabilitation typically involves hip muscle strengthening, improving range of motion, activity modification and movement training, which are likewise used to treat patients with other hip disorders, unspecified labral tears, or chronic hip pain [33,64-66] Yet to date, the rationales of non-surgical managements have not been

clearly defined or validated, nor are they designed specifically for hips with DDH, especially in context with the joint deformity and the corresponding surgical treatments. As a result, the efficacy for rehabilitation to treat DDH and reduce risks of secondary damage and OA remains unclear.

2.2 Biomechanics of the Hip Joint

2.2.1 Hip Biomechanics and Roles in Functionality

A healthy hip serves essential mobility functions, as it supports body weight and facilitates movements through daily living. The hip is a ball-and-socket joint that principally allows 3 rotational degrees of freedom: flexion-extension, abduction-adduction, and internal-external rotation [67]. Relative translations of the femoral head (ball) inside the acetabulum (socket) are constrained by the labrum, hip capsule and surrounding muscles, such that the lower extremities are stabilized during motions [33,67-69]. The articulation surface at the hip joint can bear 4 times of body weight, as inertia, external contact, and muscle forces collectively contribute to movement [70,71]. Despite high repetitive forces, interface between the healthy acetabulum and femoral head is congruent, covered by smooth articular cartilages and surrounded by synovial fluids, which allows recoverable viscoelastic responses to loading, with strong support yet minimal friction [67,72,73]. Such unique structure provides the hip with stability and mobility at the same time.

Desired hip motions are primarily driven by forces generated from muscles surrounding the joint [70,71]. Depending on their primary roles in movement directions, hip muscles can be categorized in six functional groups: flexors, extensors, abductors, adductors, internal rotators, and external rotators [28,67]. Outside their primary function, many muscles also serve secondary roles to assist 3D hip motions. Mechanically, hip muscle forces can collectively produce over 3 times body weight and are the main contributors to articular loading, accounting for 80% to 95% of the total joint contact forces [70,71]. During routine movements such as walking, muscle groups that

contribute the highest forces toward hip joint loading are the major flexors (iliopsoas), extensors (gluteus maximus, hamstrings), and abductors (gluteus medius). While hip flexors and extensors are directly responsible for hip sagittal rotations required for ambulation, the abductors such as gluteus medius and minimus serve essential roles to maintain frontal-plane stability when hip joint is loaded, and make significant contributions to compressional joint contact forces [28,70,71].

Many factors influence force from muscles surrounding the hip, including their anatomy and architecture, volume and strength, tissue composition, fiber and tendon physiology, and neurological control [67,74-80]. Many past studies have investigated the influences of each factor to hip muscle forces. At the joint and whole-body level, the mechanical impacts of muscle strength, activation and anatomical structure have been the focuses, as they influence coordination among the whole hip musculature and contributions to joint loading. For example, the anatomical paths of hip muscles affect their mechanical moment arms [81] and lines of action [67], which determine the muscles' ability to produce forces in specific directions when actuating a desired joint rotation, thus collectively contribute to joint compression and shear forces [82].

A clinically important topic unique to the hip is the mechanics of the acetabular labrum. The labrum is a horseshoe-shaped fibrocartilage structure located at the rim of the acetabulum, covering the anterior, superior, and posterior parts of the rim, with an inferior opening connected by ligament [29,33,68,83]. It extends from the bony edge of the acetabulum and thus increases its depth, providing additional coverage and stabilization of the femoral head inside the acetabulum [29,33], as well as sealing and distribution of synovial fluids between the articulation surfaces [68,84]. The labral surface articulating with the femoral head is avascular and therefore incapable of self-healing [85], yet has nerve endings that could sense pain [86]. The geometrical and synovial constraints provide mechanical aids to the acetabular cartilage, by increasing contact area, securing

the synovial fluid buffer against direct contact [85], and thereby reducing mechanical stress at the articulation [87]. During walking, the load-bearing area in normally-shaped hips is deep near the center of the acetabulum, thus loading borne by the labrum at the acetabular edge should typically be minimal [29,87]. However, local regions of the labrum may be subject to higher loads during more dynamic movement tasks such as in sports [31].

2.2.2 Abnormal Hip Biomechanics: Impacts and Causes in DDH

A disrupted hip biomechanical environment, either due to traumatic injuries or chronic abnormalities, may lead to mechanically-induced articular tissue damage and symptoms that affect mobility and quality of life. In a long term, abnormal hip joint mechanics could prompt detrimental biological responses by the load-bearing articular cartilage and labrum, and lead to degenerative arthritic changes [15,72,88]. Damaged tissues may further interact with altered biomechanics and worsen joint degeneration to the point of irreversible disease [15]. Thus, abnormal biomechanics have been recognized as the primary reasons for hip OA development [15]. Considering the onset of OA is difficult to detect clinically, early identification and correction of abnormal hip joint mechanics may be the key to mitigate risks of joint damage before advanced OA progression.

Abnormal hip biomechanics may be contributed by many acute and chronic risk factors. Demographic and intrinsic factors, including age, occupation, and overweight, can directly lead to excessive or irregular joint loading [15,89]. Abnormal loading also often occurs in injuries during intensive tasks such as sports, especially if faulty movements are involved. The mechanical sources of injuries may be acute and traumatic, but can also be insidious when abnormal joint structure leads to increased articular focal stress [15], such as in hips with damaged acetabular labrum [84]. Also, because hip muscles directly contribute to articular loading [70,71], any muscle geometrical or physiological abnormalities could cause joint pathomechanics. Yet, excessive overall joint

loading is not the only contributor to articular pathomechanics such as tissue stress. An important risk factor for pathomechanics at the hip is the joint anatomical structure, which include DDH and femoroacetabular impingement bony deformities. Specifically, pathological anatomy around the hip is thought to alter the weight-bearing contact and thereby increase focal stresses [13,15]. The following paragraphs thus focus on the current concepts and theories of pathological biomechanics in hips with DDH, and their relationships with the abnormal hip anatomy.

The causes of hip joint pathology and eventual OA due to DDH are widely believed to be mechanical. A commonly presented conceptual framework is that the shallow acetabulum and poor femoral coverage in hips with DDH decreases contact area between the acetabulum and the femoral head, which results in abnormally high focal stresses or shears that exceed the healthy tolerance level of the articular cartilage and labrum [9-14]. Especially, a disproportionally high amount of stress on the acetabular rim could contribute to high incidences of labral tears or rim cartilage lesions [10,11,85]. It has also been theorized that altered hip muscle moment arms and lines of action may contribute to higher joint contact forces at the acetabular edge [11]. Labral overloading is thought to induce tears through both acute trauma and accumulative micro-damage, especially the latter [31-33,90]. Once torn, compromised labral seal leads to increased femoral instability [31,68] and disrupted articular contact that could advance chondral lesions [84,91].

Apart from labral tears, abnormal hip mechanics can also contribute to other pre-arthritis pathology of DDH. For example, aggravated hip pain during activities [20] indicate such symptom is mechanically-induced. Movement alterations can be resulted from mechanical symptoms, as well as active adaptations to avoid mechanically-induced pain. Muscle-related pain and weakness found in recent studies [21,25] can be a source (and also a result) of abnormal muscle force production, but their relationships with other DDH-related pathology are less clear.

Although these mechanical theories are widely agreed upon, and used as rationales to support surgical treatments of DDH such as the Bernese PAO [52-54], few studies have explicitly quantified hip joint biomechanics in DDH (more details in Sections 2.2.3 and 2.3.2). The hip biomechanics of DDH during dynamic movements, potential contributions from hip muscles, and their interactions with the abnormal anatomy are largely understudied. Instead, most studies of DDH focused on clinical radiographic measures (Section 2.1.4), and more recently 3D characterization of the bony anatomy [92,93], and their associations with evidences of damage or OA. Although such studies support the concept that DDH anatomy contributes to OA [12], without quantitative knowledge of hip biomechanics, the mechanistic connections between bony anatomy and joint damage remain unclear, which could continue to hinder accurate diagnosis and timely treatments for patients whose symptoms does not match bony deformity [20].

2.2.3 Quantifying Hip Biomechanics: In-Vitro, In-Vivo, and In-Silico

Even as substantial needs exist to quantify hip joint and muscle mechanics in DDH, reliable quantification of such parameters remain a major challenge. Especially, with current techniques, hip joint contact loading and muscle forces during dynamic movements are difficult to measure experimentally. To address such challenges, past research has used a variety of in-vitro, in-vivo, and in-silico methods to assess the biomechanics of human hips.

In-vitro studies of hip biomechanics use cadaveric specimens to measure and test hip joint mobility, muscle structure, and soft tissue functions. For example, several studies demonstrated the roles of hip capsule and acetabular labrum in joint stability in cadaveric hips [68,94], as well as the effects of surgical modifications [95]. Other studies quantified hip muscle anatomical paths and architecture, and speculated their roles in joint function and loading [28,74,75,96-98]. In-vitro hip joint force measurements used pressure films or sensors placed between articular surfaces to

acquire contact stresses when the specimens were given known external forces [99,100]. Although in-vitro studies can be useful for determining the mechanical behaviors of hip joint under specific structural and loading conditions, they are intrinsically limited by dependence to the experimental setups, which do not necessarily resemble the in-vivo joint mechanical environment during human movements. Moreover, in-vitro studies have rarely been conducted specifically on dysplastic hips, possibly due to a scarcity of young pre-arthritic cadaveric specimens.

Some mechanical factors that directly contribute to joint forces, such as muscle strength and anatomical paths, may be quantified non-invasively. Hip muscle strength can be tested with manual or machine-operated dynamometers, and strength tests on patient cohorts including DDH have detected weakness in the hip flexors, abductors, and external rotators [25,27]. Hip muscle lengths and moment arms can be measured from 3D medical images [101,102], which may be advantageous over in-vitro methods as they can be made on live subjects. One computed tomography study of older subjects with DDH found reduced gluteus medius moment arms compared to controls [103], which could be a source of DDH patients' weakness in hip abduction [25]. Yet, although image-based analyses may better describe specific live individuals, measures under standard testing or scan positions may not fully represent the muscles in dynamic actions.

To assess biomechanics true to dynamic hip functions of daily living, in-vivo experimental data is needed. Although 2D camera-based analyses were used historically and sometimes as a low-cost alternative to quantify in-vivo human motion [104,105], in modern research and clinical movement analysis, the most common technique is optical 3D motion capture, which uses multiple near-infrared cameras to track the position of retro-reflective markers placed on the skin surface [106,107]. Using 3 or more markers nonlinearly located on a rigid body segment [106], and relative positions between 2 adjacent bodies, 3D segment positions, joint angles, speeds, and accelerations

at a specific time can be determined via inverse kinematics algorithm (details in Section 2.3.1). For example, the relative 3D positions between pelvis and femur can be used to resolve the hip flexion-extension, abduction-adduction, and internal-external rotation angles. Compared to motion analyses with bone-mounted pins or dynamic radiographs to directly track bone movements [104,108], skin marker motion capture holds advantages in its ability to assess subject-specific kinematics non-invasively, although its accuracy for hip motion may be influenced by soft tissue artifacts [109]. Regardless, several studies have used the standard skin marker-infrared camera system to quantify kinematics in hips with DDH during a variety of movement tasks, including routine walking [22,110,111] and the more dynamic running activity that young patients with DDH often participate [24]. Several studies also reported hip kinematics in DDH patients after surgical treatments [112-115]. While some common traits were reported in hips with DDH, such as a lower-than-control hip extension during gait stance, 3D kinematic findings outside the sagittal plane were in less consensus [22,24,110,111]. The limited evidences meant more research is needed to determine whether patients with DDH exhibit abnormal hip movement patterns.

Direct measurement of in-vivo hip joint and muscle forces is difficult. To date, the only experimental data of in-vivo hip contact forces was acquired using prosthetic femurs instrumented with force sensors, then implanted to a few elderly patients who underwent joint replacement after traumatic injury or end-stage hip OA [116-118]. These very limited data directly recorded hip joint contact loading specific to common movements ranging from routine gait to dynamic jogging and cycling [118], thus is highly valued as the “gold standard” reference in hip biomechanics studies. However, the subjects’ older age and the small sample size could both limit the utility of these data for reference in a younger patient population, such as pre-arthritic adults with DDH. Furthermore, no studies to date have reported in-vivo forces in hip muscles during dynamic activities. Because

it is not possible to experimentally measure dynamic in-vivo joint and muscle forces in native human hips, predictive methods are needed to estimate such quantities, so that their roles in the pathological development of DDH can be investigated.

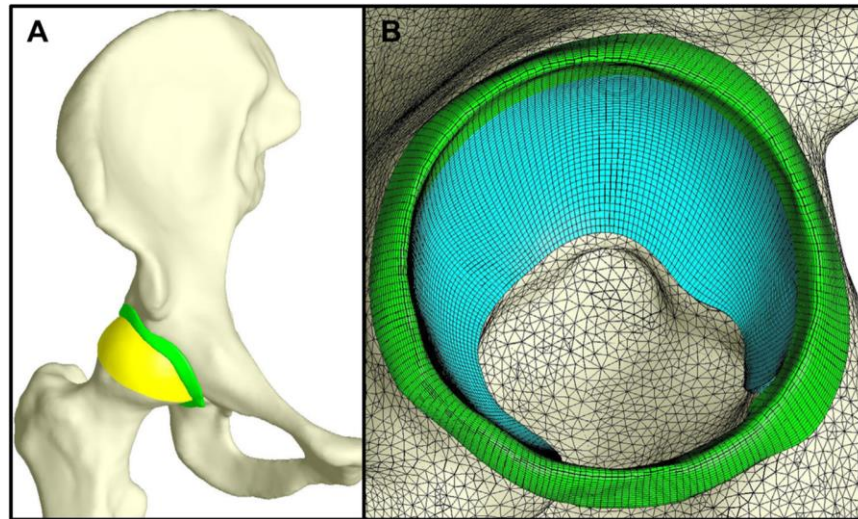


Figure 2.3. Detailed acetabular anatomy have been used to analyze articular and labral contact stresses, but the specificity of results may be limited by the generic input loading conditions. (Figure 1 in Henak et al. Osteoarthritis Cartilage. 2014 [87].)

In-silico computational models provide the opportunity to estimate hip joint mechanical quantities that cannot be measured in-vivo. Common state-of-the-art models to quantify hip biomechanics include finite element (FE) [119] and discrete element (DE) models [120] that use 3D hip anatomy reconstructed from medical imaging. These image-based FE and DE models incorporate detailed hip anatomy and mechanical properties, and have demonstrated their ability to predict joint contact stresses comparable to in-vitro measures [119]. FE and DE methods have thus been used to model joint contact mechanics in hips with DDH, and have delineated unique traits including articular cartilage and labral stresses around either native malformed or surgically-corrected acetabula [87,121,122] (**Figure 2.3**). These findings yielded new knowledge on the mechanical behaviors of dysplastic hips true to the patient-specific joint anatomy. Yet, a limitation of most FE or DE models was that they were usually driven by *generic* dynamic hip loading input

from instrumented prosthetics [117] or model estimates from other studies [71,111]. As such, the specificity of predicted hip joint stresses to the dynamic movement patterns of DDH patients, which possibly differ from healthy individuals [22,24,110,111], may be limited.

Movement-specific hip biomechanics may be estimated from optical motion capture using whole-body model based inverse dynamics [106,107]. The link-segment model [106] is a standard method that uses 3D kinematic data to resolve joint kinetics. Link-segment model considers the human body as a linked chain of rigid bodies, each with fixed mass and length while allowed to rotate relative to each other (**Figure 2.4**). The inverse dynamics algorithm (details in Section 2.3.1) then considers the forces due to body inertia, gravitation, and external contact to resolve the *net* forces, moments, impulses, and powers at the joints [106,107].

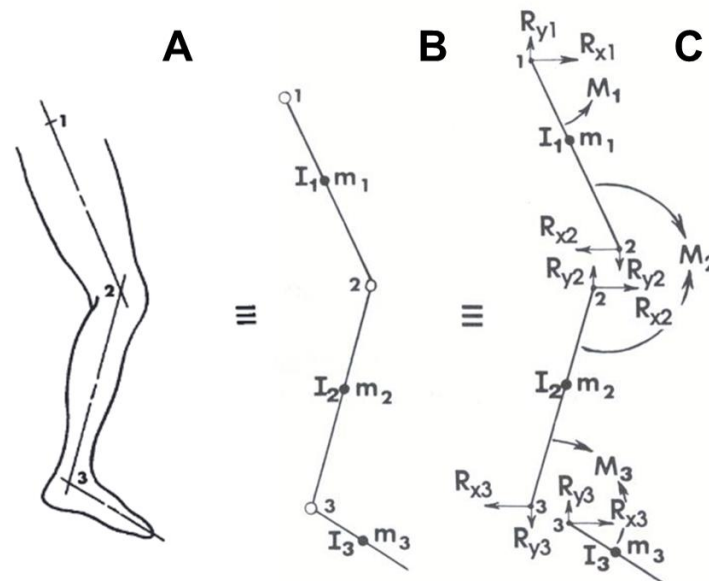


Figure 2.4. The anatomy of the human leg (A) is simplified to a link-segment model (B), which allows resolution of joint kinetics from kinematic data using free-body diagrams (C) and inverse dynamics. By considering forces due to body inertia (I), gravitation (m), and external contact (ground reaction force on foot (m_3), not shown), joint *net* forces (R) and moments (M) can be resolved. For example, R_{x1} and R_{y1} represent components of the *net* hip force, and M_1 represents the *net* hip moment. (Adapted from Figures 5.2 and 5.3 in Winter: Biomechanics and Motor Control of Human Movement, 4th ed. 2009 [106].)

Most aforementioned kinematic studies of DDH [22,24,110-115] also performed kinetic analyses, and findings included lower hip flexion moment generated in hips with DDH in the sagittal plane, although findings in frontal and transverse planes were again mixed [22,24,110,111]. These studies provided quantitative evidences on hip kinetics specific to patient's movement patterns, which added to our knowledge on how the dynamic hip biomechanical environment may differ due to DDH. Still, the clinical interpretation of such *net* joint forces remains challenging, because they do not differentiate the contributions from active muscle force production and passive joint contact (or ligament tension) [106,107]. For this reason, link-segment model-based biomechanics still fell short of identifying hip joint contact forces during patient-specific dynamic movements that may directly lead to mechanically-induced tissue damage. To delineate such clinically important mechanical quantities, a computational model that incorporates both in-vivo joint motions and muscle actions is needed.

2.3 Musculoskeletal Model (MSM)

Dynamic joint biomechanics during coordinated movements are collective outcomes from the human neuromusculoskeletal system, including bony anatomy, muscle physiology, joint motion, and neural control [123]. Because subject-specific 3D motion can be captured non-invasively using optical systems, while numerous experimental datasets are available on the neuromuscular elements (Section 2.2.3), opportunities exist to synthesize these data for in-silico simulations of dynamic movements with muscle activities incorporated, to more precisely quantify the subject-specific biomechanics in each active and passive human body component as well as their interrelationships. Musculoskeletal models (MSMs) provide such an opportunity.

MSMs hold unique values in human biomechanics research, as the muscle-driven simulations can specify muscle and joint contact forces during dynamic movements, which can be

biomechanical quantities of significant clinical importance. The assembly of modifiable neuromusculoskeletal components also facilitate investigations of cause-effect relationships, and a vast potential to explore “what if” questions that may not be feasible experimentally [123]. In recent decades, many MSM software platforms have been developed for dynamic simulation of human movements, including proprietary SIMM [124] and AnyBody [125], and the freeware OpenSim [123]. Especially, since its launch, OpenSim has provided a platform for open-source MSM and algorithm sharing as well as community-based peer support (SimTK, <https://simtk.org>), which enhanced MSM development and customization for specific research questions. For this reason, OpenSim was the chosen software for modeling DDH hip biomechanics in this dissertation. To provide technical background for the specific studies herein, the following Section 2.3.1 describes a standard MSM workflow for simulations using OpenSim, followed by focused summaries of MSMs for DDH research and image-based model personalization.

2.3.1 Standard MSM Workflow

Baseline MSM and Scaling

Creation of a MSM starts from a baseline model composed of linked rigid body segments, joints with anatomy-based coordinate system and idealized degrees of freedom, and muscle-tendon units with physiological properties derived from cadaveric experimental data [124-127]. More recently, newer baseline models have been developed with updated muscle properties derived from imaging data of live, younger subjects [101,128]. Still, the anatomy of bones in most baseline models are based on digitized geometric data from cadaveric samples, while muscle paths are represented by straight, reflected, or curved line segments (**Figure 2.5**) [124]. Many baseline MSMs have been shared among the research community [123,124,128-130], which are often further adjusted to create more baseline models specialized for movements or joints of research interest, including the hip [131-133].

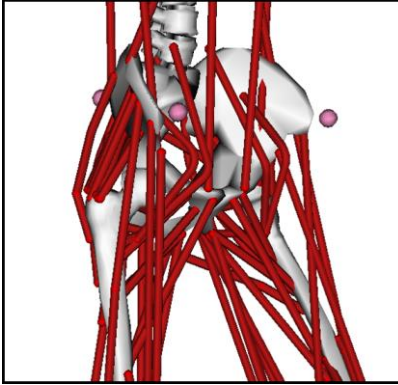


Figure 2.5. The hip musculoskeletal anatomy of a baseline MSM [133], which was scaled with marker-based length measurements (pink dots) to create the generic MSMs in Chapter 3. Note that the coarse shapes of pelvis and femurs do not resemble detailed 3D hip anatomy, especially malformed bones typical of DDH patients (Figure 2.1).

To calibrate the dimensions of a MSM so it better represents the size of a specific subject, each body segment is scaled based on the ratio of experimental-to-baseline model segment size [123,134]. The anthropometric measurements of physical dimensions [106] used in the *generic* MSM scaling method is typically derived from distances between skin-mounted markers, of which the locations on specific subjects are known from optical experimental data captured while subjects stood in a standard “static pose” [123]. Likewise, the distances can be measured between “virtual markers” placed on the baseline model (**Figure 2.5**), which determines the “virtual size” of the model segments. The experimental-to-virtual size ratio can be calculated separately in each of the 3 dimensions, and used for *nonuniform* scaling of the model segments to match a subject’s segment size. A single measured distance, or average of a set of distances on the same segment, can also be used for *uniform* scaling, which is common in studies that use generic MSMs. Because the joint (e.g. HJC), muscle origin and insertion locations are defined at specific locations within a body’s coordinate system [124], they are moved along with the scaled segment. Segment mass and inertia are usually scaled with a uniform factor to match the subject’s body mass, while relative weights between segments are preserved [123]. As muscle paths are updated after the origins and insertions are moved, in a generic workflow, the muscle architectural parameters including optimal fiber

length and tendon slack length are scaled proportionally to the length of the muscle-tendon path [123,135]. Muscle's maximum isometric force (i.e. strength) is matched to baseline and not scaled by default. Recent studies investigated the validity of these muscle property scaling methods and found the generic workflow to be appropriate for joint contact force estimation [136]. However, questions have been raised on whether marker-based generic scaling of anatomy can sufficiently personalize associated joint locations and muscle paths, which can be important parameters of muscle function and joint loading [135,137-140]. These questions have motivated the development of image-based subject-specific MSMs, which are overviewed later in Section 2.3.3.

Inverse Kinematics

On a scaled MSM, virtual marker locations are matched to the experimental markers in each subject's static pose. Then, by finding the best matches between the virtual markers and the same skin experimental markers while subjects perform dynamic movements [106,123,141], the kinematics of body translation and joint rotation (i.e. positions, angles, speeds, accelerations) can be determined and tracked over the duration of captured motion. The algorithm in a standard MSM workflow finds the best matches by solving a weighted least-squares sum (**Equation 2.1**) [123]:

$$\min \left[\sum_{i=1}^{markers} w_i (x_i^{subj} - x_i^{mod})^2 + \sum_{j=1}^{joint\ angles} \omega_j (\theta_j^{subj} - \theta_j^{mod})^2 \right] \quad \textbf{Equation 2.1.}$$

In this equation, the total experimental (subject) to MSM (model) squared errors for all marker positions (x_i) and all joint angles (θ_j) were minimized, so the trajectory of the MSM matches as close as possible to the experimental data. Note that the weights (w_i and ω_j) allow modelers to track markers and joints of which accurate motions are of the most importance to the research question (e.g. pelvis markers and the hip joint). The joint angles can then be decomposed into

Cardan angle sequences [106,107,142] that are consistent with clinical kinematic descriptions, such as hip flexion-extension, abduction-adduction, and internal-external rotation.

Inverse Dynamics

The kinetics (i.e. resultant or *net* forces, moments, impulses, powers) at each joint can be solved using a link-segment model (Section 2.2.3) and the inverse dynamics algorithm [106,107]. The equations for inverse dynamics [106,107] can be generalized and simplified as:

$$F_{proximal} = F_{inertial}(m, a) - [F_{distal} + G(m) + F_{external}] \quad \textbf{Equation 2.2.}$$

$$M_{proximal} = M_{inertial}(m, I, \alpha, \omega) - [M_{distal} + \tau_G(m) + \tau_{external}] \quad \textbf{Equation 2.3.}$$

Forces (**Equation 2.2**) and moments (**Equation 2.3**) include body weight and inertial effects solvable from anthropometry (m, I) and kinematics (a, α, ω), and external forces measured from sensors embedded to in-ground platforms, treadmills, etc. that are typical in motion capture facilities. By identifying these forces and moments, inverse dynamics resolve the *net* kinetics that include all active and passive contributions from a distal joint to its adjacent proximal joint, thereby through all link-segment joints of the human body [107].

Due to experimental artifacts, inconsistencies between optical motion and external force data, and model assumptions through the prior workflow steps, non-physical “residual” forces may be resulted from inverse dynamics that do not represent the kinetics of actual body motion. To address this problem, the common OpenSim MSM workflow uses a “residual reduction algorithm” [123] to slightly adjust model anthropometric parameters and kinematics, so the residual forces and moments are minimized for better dynamic consistency across experimental data, before the *net* joint kinetics are subsequently further resolved into muscle and joint contact forces [134].

Muscle Force Estimation: Static Optimization and Alternatives

Determining all muscle forces around a joint requires solving the underdetermined mechanical system equations of motion [143]. One of the most commonly used standard methods for such solution is the static optimization [143], which decomposes the *net* joint moment (**Equation 2.4**) using a simple performance criterion that minimizes the squared activation summed across all muscles (**Equation 2.5**) [144]:

$$\sum_{m=1}^{muscles} [a_m(t_i) F_m^0] r_{m,j}(t_i) = \tau_j(t_i) \quad \text{Equation 2.4.}$$

$$\min\{\sum_{m=1}^{muscles} [a_m(t_i)]^2\} \quad \text{Equation 2.5.}$$

The *net* moment around a joint (τ_j) is contributed from all muscles (m) that each generate a percentage of its maximal force (F_m^0) according to its relative activation level (a_m : from 0 (not activated) to 1 (maximal contraction)) [123,144]. Articular contact forces are assumed to act through the joint center and thus do not generate moments. The moment contributed from each muscle is the product of its force ($a_m F_m^0$) and moment arm length around that joint ($r_{m,j}$). Because static optimization considers muscle forces at each time frame (t_i) independently, it is computationally efficient, and has been found to be appropriate for gait simulation [144] as well as estimation of hip joint contact forces [145]. It is worth noting that the muscle activation (a_m) and moment arms ($r_{m,j}$) that contribute to joint moments (τ_j) are both time-dependent (t_i), therefore the in-vivo force production of the muscles is theoretically reliant upon their moment arms true to the dynamic joint positions [138-140].

The static optimization approach has several limitations, including sensitivity to kinematic error, omission of time-dependent muscle physiological behaviors, and underestimation of muscle coordination in highly dynamic movements [144]. Several alternative options exist to estimate or

derive muscle activation and forces dynamically, including computed muscle control optimization [123,146] and electromyography-driven forward dynamics simulation [147]. Since the studies in this dissertation only used static optimization, which was shown to be appropriate for estimating hip contact forces during gait and high hip flexion [145], details for the alternative muscle force estimation methods are not elaborated herein.

Muscle-Induced Joint Reaction Forces (JRFs)

JRFs (or joint contact forces), including 3D force components, can be computed by adding the contributions from all muscles to the mechanical force equation at a joint (**Equation 2.6**) [148]:

$$J_{proximal} = F_{inertial}(m, a) - [J_{distal} + G(m) + F_{external} + \sum F_{muscles}] \quad \text{Equation 2.6.}$$

By considering muscle forces ($F_{muscles}$) in the inverse dynamics algorithm (**Equation 2.2**), resolved forces at the joints (J) now only compose of passive (i.e. “reaction”) contributions from other joint structures. If passive force contributions from ligaments (e.g. hip capsule tension forces) or other soft structures can be assumed negligible (e.g. not at the end range of motion), the resolved passive forces (J) can be considered the articular contact forces (or JRFs) during motion.

Other MSM-based Analyses: Dynamic Muscle Moment Arms and Lines of Action

Due to its ability to represent a collection of human neuromusculoskeletal elements during dynamic movements, MSMs can also be used for many other adjunctive analyses related to the musculoskeletal anatomy and motion. Two of such analyses relevant to this dissertation are computations of dynamic muscle moment arms and lines of action. In OpenSim [123], muscle moment arms can be calculated in the MSMs with a generalized force method [81] that quantifies the effectiveness with which a muscle-tendon unit generates joint rotational moments, either at prescribed joint poses [96,139] or true to the joint positions during movements [138,140].

Muscle lines of action specific to joint positions can be extracted from MSMs to quantify muscles' roles in 3D dynamic joint function and stability [28,82], as well as force contributions to compression, shears, edge loading, etc. that could be beneficial or detrimental to the joint structure [82,149]. Past MSM research has established automated methods to extract dynamic muscle lines of action including its 3D components (antero-posterior, supero-inferior, medio-lateral) within a specified body segment coordinate system [149].

MSM Validation

To ensure the scientific and clinical utility of MSM simulation and their ability to translate to real-world meanings, proper validation of the models is essential [134]. Yet, validating MSMs is challenging due to the complexity and variability of the neuromusculoskeletal system [134]. For this reason, development or derivation of a baseline MSM [123,124,128-133] often involves extensive validation using data from benchmark experiments or previously validated models [134], including (but not limited to) comparing model-estimated muscle moment arms to cadaveric or imaging measurements, and joint moments to strength tests [123,124,128-133].

Then, when using MSMs to study specific research questions, validity of the workflow used to estimate biomechanics (e.g. scaling and muscle force estimation methods) should also be tested. This may include comparing MSM-estimated JRFs to experimental data measured from instrumented prosthesis [117,118,150] to validate the approach used for muscle property scaling [136] or cost functions used to resolve muscle forces [135,144,145]. Minimizing “residual forces” (see Inverse Dynamics) is also important for MSM-based force estimates to be valid [123,134]. In the cases when experimental data for direct validation is scarce (e.g. hip contact forces [117,118] or muscle forces), indirect validation methods may be used. Other than comparing estimates with past validated models, a useful data source for validation is electromyography, which can help

determine whether MSM-estimated muscle activation follows similar patterns to experimentally observed muscle activities [134]. An important cautionary note is that the validity of MSMs depends on the research question, hence a MSM validated to study one clinical population is not necessarily valid for other populations [134]. Thus, an iterative validation process is recommended for using derived MSMs in new specific research questions [134].

2.3.2 Using MSMs for DDH Biomechanics

MSMs have been applied in numerous studies to estimate hip joint biomechanics, such as JRFs and muscle forces during walking in healthy individuals [70,71,151], patients with femoral deformities [152-154], femoroacetabular impingement [155,156], among other clinical questions. However, very few studies have used MSMs to quantify the biomechanics in hips with DDH. Prior to this dissertation, only two studies have used MSMs to estimate JRFs and muscle forces in dysplastic hips during gait, and compared them to healthy subjects with anatomically typical hips [111,157]. The first study by Skalhøi et al. [111] found generally lower-than-control hip muscle forces, as well as lower and more superiorly-directed peak hip JRFs in late stance. In contrast, Harris et al. [157] found that DDH subjects had lower early-stance external rotator forces, higher late-stance internal rotator forces, and higher medially-directed JRFs at both early and late stance when JRFs peaked. Since substantial mismatches exist between the biomechanical findings from these studies, especially on hip JRFs, a consensus has not been reached on how dynamic hip joint loading during gait is altered in DDH. As such, more MSM studies are needed for clarification.

A potential key factor that may have contributed to the aforementioned mismatches is the different model anatomy these past MSMs used. Skalhøi et al. [111] adapted the generic marker-scaled MSM anatomy, while Harris et al. [157] used CT-based 3D pelvis anatomy to update HJC and hip muscle origin locations. Because the bone shapes in a baseline MSM (**Figure 2.5**) do not

resemble detailed 3D bony anatomy, especially malformed dysplastic hips (**Figure 2.1**), they could potentially affect the reliability of hip JRF estimates for the DDH population. However, direct comparison between the past publications is complicated by the different subject cohorts studied [111,157]. Separating the effects due to MSM anatomy from subject demographic factors, and thus determining which modeling methods MSMs should use to study DDH biomechanics, requires a direct comparison between the MSMs created on the same cohort of DDH subjects.

2.3.3 Image-Based Subject-Specific MSM

The musculoskeletal anatomy is known to vary greatly among individuals. For this reason, the reliability for scaled generic MSMs to represent individual subject's joint locations and muscle paths has been questioned, especially when used to study populations known to have abnormal anatomy [135,158]. Past studies found that MSM-based biomechanical estimates, including hip JRFs and muscle moment arms, are sensitive to anatomical deformity traits such as femoral version and neck-shaft angle [137-140,152,159]. Therefore, to estimate joint and muscle forces in presence of bony deformity, as in the case of DDH, using generic scaled MSMs may be insufficient, while a higher level of anatomical details in the models may be required.

A reliable source to acquire detailed bony anatomy is 3D medical images such as CT and MR. Hence, there has been increasing research to include image-based anatomical details in the MSMs (**Figure 2.6**), especially on populations with anatomical abnormalities [135,153,158,160]. Several studies have compared CT or MR-based subject-specific MSMs against generic scaled MSMs, and found the biomechanical estimates from these models to be substantially different [135,137-140]. Notably, a recent study found MR-based MSMs with precise personalization of nonlinear muscle paths (**Figure 2.6**) to estimate hip JRFs closer to experimental data than generic models [135]. Based on such evidences, MR-based subject-specific MSMs have been

recommended to study joints of which the anatomy is known to deviate substantially from generic models [134], as with the case of DDH.

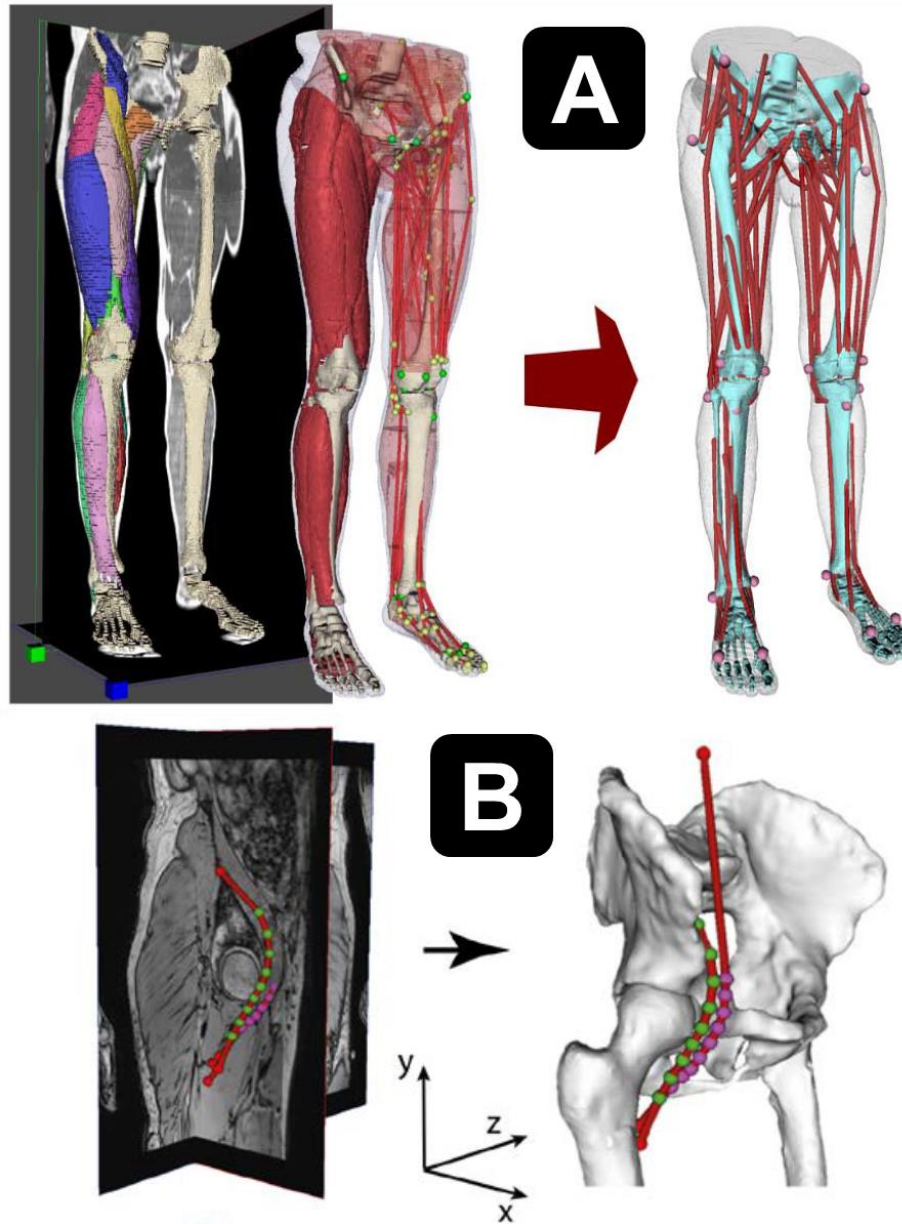


Figure 2.6. Examples of image-based subject-specific MSM creation. (A) 3D-segmented bone and muscle anatomy (left) are added to the MSM (middle) to guide updates to joint locations and muscle paths (right). (B) Subject-specific images (left) can be used to derive precise anatomical paths for major non-linear muscles such as the iliopsoas (right). (Sub-figure A adapted from Figure 1 in Valente et al. PLoS One. 2014 [158]. Sub-figure B adapted from Figure S1 in Wesseling et al. Comput Methods Biomech Biomed Engin. 2016 [135].)

Yet, the creation of image-based MSMs is known to be a complex and arduous process. The anatomical complexity of the MSMs is directly related to the time costs and computational demands on the research, as well as uncertainties inherent to model parameters, which could limit their utility in larger scales [158,160-162]. Therefore, instead of the highest level of complexity possible, MSM research may better benefit from an optimized level of anatomical specificity that depends on the research question. An inter-model comparison focused on hip biomechanical estimates [135] could help determine such an optimized model complexity level specifically for DDH, while addressing the mismatches among past MSM findings [111,157]. A standardized proper method to create MSMs for DDH can then provide a framework for reliable yet also feasible investigations of the biomechanics in dysplastic hips, including analyses of the influences and interrelationships among multiple musculoskeletal components such as bony anatomy, muscle actions, and joint motions.

2.4 References

1. Cooperman DR, Wallensten R, Stulberg SD. Acetabular dysplasia in the adult. *Clin Orthop Relat Res.* 1983 May;175:79-85.
2. Dezateux C, Rosendahl K. Developmental dysplasia of the hip. *Lancet.* 2007 May 5;369(9572):1541-52.
3. Aronsson DD, Goldberg MJ, Kling TF Jr, Roy DR. Developmental dysplasia of the hip. *Pediatrics.* 1994 Aug;94(2 Pt 1):201-8.
4. Clohisy JC, Nunley RM, Carlisle JC, Schoenecker PL. Incidence and characteristics of femoral deformities in the dysplastic hip. *Clin Orthop Relat Res.* 2009 Jan;467(1):128-34.
5. David TJ, Parris MR, Poynor MU, Hawnaur JM, Simm SA, Rigg EA, McCrae FC. Reasons for late detection of hip dislocation in childhood. *Lancet.* 1983 Jul 16;2(8342):147-9.
6. Gala L, Clohisy JC, Beaulé PE. Hip dysplasia in the young adult. *J Bone Joint Surg Am.* 2016 Jan 6;98(1):63-73.

7. Wyles CC, Heidenreich MJ, Jeng J, Larson DR, Trousdale RT, Sierra RJ. The John Charnley Award: Redefining the natural history of osteoarthritis in patients with hip dysplasia and impingement. *Clin Orthop Relat Res*. 2017 Feb;475(2):336-50.
8. van Bosse H, Wedge JH, Babyn P. How are dysplastic hips different? A three-dimensional CT study. *Clin Orthop Relat Res*. 2015 May;473(5):1712-23.
9. Michaeli DA, Murphy SB, Hipp JA. Comparison of predicted and measured contact pressures in normal and dysplastic hips. *Med Eng Phys*. 1997 Mar;19(2):180-6.
10. Klaue K, Durnin CW, Ganz R. The acetabular rim syndrome. A clinical presentation of dysplasia of the hip. *J Bone Joint Surg Br*. 1991 May;73(3):423-9.
11. Maquet P. Biomechanics of hip dysplasia. *Acta Orthop Belg*. 1999 Sep;65(3):302-14.
12. Cooperman D. What is the evidence to support acetabular dysplasia as a cause of osteoarthritis? *J Pediatr Orthop*. 2013 Jul-Aug;33 Suppl 1:S2-7.
13. Harris-Hayes M, Royer NK. Relationship of acetabular dysplasia and femoroacetabular impingement to hip osteoarthritis: a focused review. *PM R*. 2011 Nov;3(11):1055-67.e1.
14. Mavcic B, Iglic A, Kralj-Iglic V, Brand RA, Vengust R. Cumulative hip contact stress predicts osteoarthritis in DDH. *Clin Orthop Relat Res*. 2008 Apr;466(4):884-91.
15. Felson DT. Osteoarthritis as a disease of mechanics. *Osteoarthritis Cartilage*. 2013 Jan;21(1):10-5.
16. Clohisy JC, Dobson MA, Robison JF, Warth LC, Zheng J, Liu SS, Yehyawli TM, Callaghan JJ. Radiographic structural abnormalities associated with premature, natural hip-joint failure. *J Bone Joint Surg Am*. 2011 May;93 Suppl 2:3-9.
17. Murphy SB, Ganz R, Müller ME. The prognosis in untreated dysplasia of the hip. A study of radiographic factors that predict the outcome. *J Bone Joint Surg Am*. 1995 Jul;77(7):985-9.
18. Reijman M, Hazes JM, Pols HA, Koes BW, Bierma-Zeinstra SM. Acetabular dysplasia predicts incident osteoarthritis of the hip: the Rotterdam study. *Arthritis Rheum*. 2005 Mar;52(3):787-93.
19. Nho SJ, Kymes SM, Callaghan JJ, Felson DT. The burden of hip osteoarthritis in the United States: epidemiologic and economic considerations. *J Am Acad Orthop Surg*. 2013;21 Suppl 1:S1-6.

20. Nunley RM, Prather H, Hunt D, Schoenecker PL, Clohisy JC. Clinical presentation of symptomatic acetabular dysplasia in skeletally mature patients. *J Bone Joint Surg Am.* 2011 May;93 Suppl 2:17-21.
21. Jacobsen JS, Hölmich P, Thorborg K, Bolvig L, Jakobsen SS, Søballe K, Mechlenburg I. Muscle-tendon-related pain in 100 patients with hip dysplasia: prevalence and associations with self-reported hip disability and muscle strength. *J Hip Preserv Surg.* 2017 Nov 17;5(1):39-46.
22. Romanò CL, Frigo C, Randelli G, Pedotti A. Analysis of the gait of adults who had residua of congenital dysplasia of the hip. *J Bone Joint Surg Am.* 1996 Oct;78(10):1468-79.
23. Hardcastle P, Nade S. The significance of the Trendelenburg test. *J Bone Joint Surg Br.* 1985 Nov;67(5):741-6.
24. Jacobsen JS, Nielsen DB, Sørensen H, Søballe K, Mechlenburg I. Changes in walking and running in patients with hip dysplasia. *Acta Orthop.* 2013 Jun;84(3):265-70.
25. Sørensen H, Nielsen DB, Jacobsen JS, Søballe K, Mechlenburg I. Isokinetic dynamometry and gait analysis reveal different hip joint status in patients with hip dysplasia. *Hip Int.* 2019 Mar;29(2):215-21.
26. Jacobsen JS, Bolvig L, Hölmich P, Thorborg K, Jakobsen SS, Søballe K, Mechlenburg I. Muscle-tendon-related abnormalities detected by ultrasonography are common in symptomatic hip dysplasia. *Arch Orthop Trauma Surg.* 2018 Aug;138(8):1059-67.
27. Harris-Hayes M, Mueller MJ, Sahrman SA, Bloom NJ, Steger-May K, Clohisy JC, Salsich GB. Persons with chronic hip joint pain exhibit reduced hip muscle strength. *J Orthop Sports Phys Ther.* 2014 Nov;44(11):890-8.
28. Neumann DA. Kinesiology of the hip: a focus on muscular actions. *J Orthop Sports Phys Ther.* 2010 Feb;40(2):82-94.
29. Hartig-Andreasen C, Søballe K, Troelsen A. The role of the acetabular labrum in hip dysplasia. A literature overview. *Acta Orthop.* 2013 Feb;84(1):60-4.
30. Ross JR, Zaltz I, Nepple JJ, Schoenecker PL, Clohisy JC. Arthroscopic disease classification and interventions as an adjunct in the treatment of acetabular dysplasia. *Am J Sports Med.* 2011 Jul;39 Suppl:72S-8S.
31. McCarthy JC, Noble PC, Schuck MR, Wright J, Lee J. The Otto E. Aufranc Award: The role of labral lesions to development of early degenerative hip disease. *Clin Orthop Relat Res.* 2001 Dec;(393):25-37.

32. Burnett RSJ, Della Rocca GJ, Prather H, Curry M, Maloney WJ, Clohisy JC. Clinical presentation of patients with tears of the acetabular labrum. *J Bone Joint Surg Am.* 2006 Jul;88(7):1448-57.
33. Lewis CL, Sahrman SA. Acetabular labral tears. *Phys Ther.* 2006 Jan;86(1):110-21.
34. Neumann G, Mendicuti AD, Zou KH, Minas T, Coblyn J, Winalski CS, Lang P. Prevalence of labral tears and cartilage loss in patients with mechanical symptoms of the hip: evaluation using MR arthrography. *Osteoarthritis Cartilage.* 2007 Aug;15(8):909-17.
35. Barlow TG. Early diagnosis and treatment of congenital dislocation of the hip. *J Bone Joint Surg Br.* 1962 May;44(2):292-301.
36. MacDonald SJ, Garbuz D, Ganz R. Clinical evaluation of the symptomatic young adult hip. *Semin Arthroplasty.* 1997;8:3-9.
37. Graf R. The diagnosis of congenital hip-joint dislocation by the ultrasonic Compound treatment. *Arch Orthop Trauma Surg.* 1980;97(2):117-33.
38. Wiberg G. Studies on dysplastic acetabula and congenital subluxation of the hip joint with special reference to the complication of osteoarthritis. *Acta Chir Scand.* 1939;83 Suppl 58:7-135.
39. Clohisy JC, Carlisle JC, Beaulé PE, Kim YJ, Trousdale RT, Sierra RJ, Leunig M, Schoenecker PL, Millis MB. A systematic approach to the plain radiographic evaluation of the young adult hip. *J Bone Joint Surg Am.* 2008 Nov;90 Suppl 4:47-66.
40. Wyatt MC, Beck M. The management of the painful borderline dysplastic hip. *J Hip Preserv Surg.* 2018 Apr 5;5(2):105-12.
41. Tönnis D. *Congenital Dysplasia and Dislocation of the Hip in Children and Adults.* Berlin and Heidelberg, Germany: Springer-Verlag; 1990.
42. Heyman CH, Herndon CH. Legg-Perthes disease; a method for the measurement of the roentgenographic result. *J Bone Joint Surg Am.* 1950 Oct;32 A(4):767-78.
43. Lequesne M, de Seze. [False profile of the pelvis. A new radiographic incidence for the study of the hip. Its use in dysplasias and different coxopathies]. *Rev Rhum Mal Osteoartic.* 1961;28:643-52. French.
44. Reynolds D, Lucas J, Klaue K. Retroversion of the acetabulum. A cause of hip pain. *J Bone Joint Surg Br.* 1999 Mar;81(2):281-8.

45. Boese CK, Dargel J, Oppermann J, Eysel P, Scheyerer MJ, Bredow J, Lechler P. The femoral neck-shaft angle on plain radiographs: a systematic review. *Skeletal Radiol*. 2016 Jan;45(1):19-28.
46. Cheng R, Zhang H, Kernkamp WA, Zheng J, Dai K, Yao Y, Wang L, Tsai TY. Relations between the Crowe classification and the 3D femoral head displacement in patients with developmental dysplasia of the hip. *BMC Musculoskelet Disord*. 2019 Nov 11;20(1):530.
47. Petersilge CA, Haque MA, Petersilge WJ, Lewin JS, Lieberman JM, Buly R. Acetabular labral tears: evaluation with MR arthrography. *Radiology*. 1996 Jul;200(1):231-5.
48. Dezateux C, Godward S. A national survey of screening for congenital dislocation of the hip. *Arch Dis Child*. 1996 May;74(5):445-8.
49. Hartofilakidis G, Stamos K, Karachalios T, Ioannidis TT, Zacharakis N. Congenital hip disease in adults. Classification of acetabular deficiencies and operative treatment with acetabuloplasty combined with total hip arthroplasty. *J Bone Joint Surg Am*. 1996 May;78(5):683-92.
50. Papachristou G, Hatzigrigoris P, Panousis K, Plessas S, Sourlas J, Levidiotis C, Chronopoulos E. Total hip arthroplasty for developmental hip dysplasia. *Int Orthop*. 2006 Feb;30(1):21-5.
51. Millis MB, Kim YJ. Rationale of osteotomy and related procedures for hip preservation: a review. *Clin Orthop Relat Res*. 2002 Dec;(405):108-21.
52. Clohisy JC, Schutz AL, St John L, Schoenecker PL, Wright RW. Periacetabular osteotomy: a systematic literature review. *Clin Orthop Relat Res*. 2009 Aug;467(8):2041-52.
53. Ganz R, Klaue K, Vinh TS, Mast JW. A new periacetabular osteotomy for the treatment of hip dysplasias. Technique and preliminary results. *Clin Orthop Relat Res*. 1988 Jul;(232):26-36.
54. Leunig M, Siebenrock KA, Ganz R. Rationale of periacetabular osteotomy and background work. *Instr Course Lect*. 2001;50:229-38.
55. Boje J, Caspersen CK, Jakobsen SS, Søballe K, Mechlenburg I. Are changes in pain associated with changes in quality of life and hip function 2 years after periacetabular osteotomy? A follow-up study of 321 patients. *J Hip Preserv Surg*. 2019 Mar 14;6(1):69-76.
56. Novais EN, Heyworth B, Murray K, Johnson VM, Kim YJ, Millis MB. Physical activity level improves after periacetabular osteotomy for the treatment of symptomatic hip dysplasia. *Clin Orthop Relat Res*. 2013 Mar;471(3):981-8.

57. Clohisy JC, Ackerman J, Baca G, Baty J, Beaulé PE, Kim YJ, Millis MB, Podeszwa DA, Schoenecker PL, Sierra RJ, Sink EL, Sucato DJ, Trousdale RT, Zaltz I. Patient-reported outcomes of periacetabular osteotomy from the prospective ANCHOR cohort study. *J Bone Joint Surg Am*. 2017 Jan 4;99(1):33-41.
58. Bogunovic L, Hunt D, Prather H, Schoenecker PL, Clohisy JC. Activity tolerance after periacetabular osteotomy. *Am J Sports Med*. 2014 Aug;42(8):1791-5.
59. Troelsen A, Elmengaard B, Søballe K. Medium-term outcome of periacetabular osteotomy and predictors of conversion to total hip replacement. *J Bone Joint Surg Am*. 2009 Sep;91(9):2169-79.
60. Lerch TD, Steppacher SD, Liechti EF, Tannast M, Siebenrock KA. One-third of hips after periacetabular osteotomy survive 30 years with good clinical results, no progression of arthritis, or conversion to THA. *Clin Orthop Relat Res*. 2017 Apr;475(4):1154-68.
61. Kim KI, Cho YJ, Ramteke AA, Yoo MC. Peri-acetabular rotational osteotomy with concomitant hip arthroscopy for treatment of hip dysplasia. *J Bone Joint Surg Br*. 2011 Jun;93(6):732-7.
62. Domb BG, Stake CE, Lindner D, El-Bitar Y, Jackson TJ. Arthroscopic capsular plication and labral preservation in borderline hip dysplasia: two-year clinical outcomes of a surgical approach to a challenging problem. *Am J Sports Med*. 2013 Nov;41(11):2591-8.
63. Cvetanovich GL, Heyworth BE, Murray K, Yen YM, Kocher MS, Millis MB. Hip arthroscopy in patients with recurrent pain following Bernese periacetabular osteotomy for acetabular dysplasia: operative findings and clinical outcomes. *J Hip Preserv Surg*. 2015 Jun 13;2(3):295-302.
64. Adler KL, Cook PC, Geisler PR, Yen YM, Giordano BD. Current concepts in hip preservation surgery: Part II--Rehabilitation. *Sports Health*. 2016 Jan-Feb;8(1):57-64.
65. Hunt D, Prather H, Harris Hayes M, Clohisy JC. Clinical outcomes analysis of conservative and surgical treatment of patients with clinical indications of prearthritic, intra-articular hip disorders. *PM R*. 2012 Jul;4(7):479-87.
66. Harris-Hayes M, Czuppon S, Van Dillen LR, Steger-May K, Sahrman S, Schootman M, Salsich GB, Clohisy JC, Mueller MJ. Movement-pattern training to improve function in people with chronic hip joint pain: A feasibility randomized clinical trial. *J Orthop Sports Phys Ther*. 2016 Jun;46(6):452-61.
67. Neumann DA. *Kinesiology of the Musculoskeletal System: Foundations for Rehabilitation*. St. Louis, MO: Mosby; 2013.

68. Crawford MJ, Dy CJ, Alexander JW, Thompson M, Schroder SJ, Vega CE, Patel RV, Miller AR, McCarthy JC, Lowe WR, Noble PC. The 2007 Frank Stinchfield Award. The biomechanics of the hip labrum and the stability of the hip. *Clin Orthop Relat Res*. 2007 Dec;465:16-22.
69. Retchford TH, Crossley KM, Grimaldi A, Kemp JL, Cowan SM. Can local muscles augment stability in the hip? A narrative literature review. *J Musculoskelet Neuronal Interact*. 2013 Mar;13(1):1-12.
70. Lewis CL, Sahrman SA, Moran DW. Effect of hip angle on anterior hip joint force during gait. *Gait Posture*. 2010 Oct;32(4):603-7.
71. Correa TA, Crossley KM, Kim HJ, Pandy MG. Contributions of individual muscles to hip joint contact force in normal walking. *J Biomech*. 2010 May 28;43(8):1618-22.
72. Carter DR, Beaupré GS, Wong M, Smith RL, Andriacchi TP, Schurman DJ. The mechanobiology of articular cartilage development and degeneration. *Clin Orthop Relat Res*. 2004 Oct;427 Suppl:S69-77.
73. Richard F, Villars M, Thibaud S. Viscoelastic modeling and quantitative experimental characterization of normal and osteoarthritic human articular cartilage using indentation. *J Mech Behav Biomed Mater*. 2013 Aug;24:41-52.
74. Dostal WF, Soderberg GL, Andrews JG. Actions of hip muscles. *Phys Ther*. 1986 Mar;66(3):351-61.
75. Ward SR, Eng CM, Smallwood LH, Lieber RL. Are current measurements of lower extremity muscle architecture accurate? *Clin Orthop Relat Res*. 2009 Apr;467(4):1074-82.
76. Grimaldi A, Richardson C, Stanton W, Durbridge G, Donnelly W, Hides J. The association between degenerative hip joint pathology and size of the gluteus medius, gluteus minimus and piriformis muscles. *Man Ther*. 2009 Dec;14(6):605-10.
77. Grimaldi A, Richardson C, Durbridge G, Donnelly W, Darnell R, Hides J. The association between degenerative hip joint pathology and size of the gluteus maximus and tensor fascia lata muscles. *Man Ther*. 2009 Dec;14(6):611-7.
78. Arokoski MH, Arokoski JP, Haara M, Kankaanpää M, Vesterinen M, Niemitukia LH, Helminen HJ. Hip muscle strength and muscle cross sectional area in men with and without hip osteoarthritis. *J Rheumatol*. 2002 Oct;29(10):2185-95.

79. Rasch A, Byström AH, Dalen N, Berg HE. Reduced muscle radiological density, cross-sectional area, and strength of major hip and knee muscles in 22 patients with hip osteoarthritis. *Acta Orthop*. 2007 Aug;78(4):505-10.
80. Suetta C, Aagaard P, Magnusson SP, Andersen LL, Sipilä S, Rosted A, Jakobsen AK, Duus B, Kjaer M. Muscle size, neuromuscular activation, and rapid force characteristics in elderly men and women: effects of unilateral long-term disuse due to hip-osteoarthritis. *J Appl Physiol*. 2007 Mar;102(3):942-8.
81. Sherman MA, Seth A, Delp SL. What is a moment arm? Calculating muscle effectiveness in biomechanical models using generalized coordinates. *Proc ASME Des Eng Tech Conf*. 2013 Aug;2013:V07BT10A052.
82. Yanagawa T, Goodwin CJ, Shelburne KB, Giphart JE, Torry MR, Pandy MG. Contributions of the individual muscles of the shoulder to glenohumeral joint stability during abduction. *J Biomech Eng*. 2008 Apr;130(2):021024.
83. Seldes RM, Tan V, Hunt J, Katz M, Winiarsky R, Fitzgerald RH Jr. Anatomy, histologic features, and vascularity of the adult acetabular labrum. *Clin Orthop Relat Res*. 2001 Jan;(382):232-40.
84. Ferguson SJ, Bryant JT, Ganz R, Ito K. An in vitro investigation of the acetabular labral seal in hip joint mechanics. *J Biomech*. 2003 Feb;36(2):171-8.
85. Petersen W, Petersen F, Tillmann B. Structure and vascularization of the acetabular labrum with regard to the pathogenesis and healing of labral lesions. *Arch Orthop Trauma Surg*. 2003 Jul;123(6):283-8.
86. Kim YT, Azuma H. The nerve endings of the acetabular labrum. *Clin Orthop Relat Res*. 1995 Nov;(320):176-81.
87. Henak CR, Abraham CL, Anderson AE, Maas SA, Ellis BJ, Peters CL, Weiss JA. Patient-specific analysis of cartilage and labrum mechanics in human hips with acetabular dysplasia. *Osteoarthritis Cartilage*. 2014 Feb;22(2):210-7.
88. Guilak F, Fermor B, Keefe FJ, Kraus VB, Olson SA, Pisetsky DS, Setton LA, Weinberg JB. The role of biomechanics and inflammation in cartilage injury and repair. *Clin Orthop Relat Res*. 2004 Jun;423:17-26.
89. Felson DT. Obesity and vocational and avocational overload of the joint as risk factors for osteoarthritis. *J Rheumatol Suppl*. 2004 Apr;70:2-5.
90. Santori N, Villar RN. Acetabular labral tears: result of arthroscopic partial limbectomy. *Arthroscopy*. 2000 Jan-Feb;16(1):11-5.

91. Ferguson SJ, Bryant JT, Ganz R, Ito K. The influence of the acetabular labrum on hip joint cartilage consolidation: a poroelastic finite element model. *J Biomech.* 2000 Aug;33(8):953-60.
92. Nepple JJ, Wells J, Ross JR, Bedi A, Schoenecker PL, Clohisy JC. Three patterns of acetabular deficiency are common in young adult patients with acetabular dysplasia. *Clin Orthop Relat Res.* 2017 Apr;475(4):1037-44.
93. Gaffney BMM, Hillen TJ, Nepple JJ, Clohisy JC, Harris MD. Statistical shape modeling of femur shape variability in female patients with hip dysplasia. *J Orthop Res.* 2019 Mar;37(3):665-73.
94. Myers CA, Register BC, Lertwanich P, Ejnisman L, Pennington WW, Giphart JE, LaPrade RF, Philippon MJ. Role of the acetabular labrum and the iliofemoral ligament in hip stability: an in vitro biplane fluoroscopy study. *Am J Sports Med.* 2011 Jul;39 Suppl:85S-91S.
95. Abrams GD, Hart MA, Takami K, Bayne CO, Kelly BT, Espinoza Orías AA, Nho SJ. Biomechanical evaluation of capsulotomy, capsulectomy, and capsular repair on hip rotation. *Arthroscopy.* 2015 Aug;31(8):1511-7.
96. Delp SL, Hess WE, Hungerford DS, Jones LC. Variation of rotation moment arms with hip flexion. *J Biomech.* 1999 May;32(5):493-501.
97. Visser JJ, Hoogkamer JE, Bobbert MF, Huijing PA. Length and moment arm of human leg muscles as a function of knee and hip-joint angles. *Eur J Appl Physiol Occup Physiol.* 1990;61(5-6):453-60.
98. Ward SR, Winters TM, Blemker SS. The architectural design of the gluteal muscle group: implications for movement and rehabilitation. *J Orthop Sports Phys Ther.* 2010 Feb;40(2):95-102.
99. Brown TD, Shaw DT. In vitro contact stress distributions in the natural human hip. *J Biomech.* 1983;16(6):373-84.
100. Lee S, Wuerz TH, Shewman E, McCormick FM, Salata MJ, Philippon MJ, Nho SJ. Labral reconstruction with iliotibial band autografts and semitendinosus allografts improves hip joint contact area and contact pressure: an in vitro analysis. *Am J Sports Med.* 2015 Jan;43(1):98-104.
101. Handsfield GG, Meyer CH, Hart JM, Abel MF, Blemker SS. Relationships of 35 lower limb muscles to height and body mass quantified using MRI. *J Biomech.* 2014 Feb 7;47(3):631-8.

102. Németh G, Ohlsén H. In vivo moment arm lengths for hip extensor muscles at different angles of hip flexion. *J Biomech.* 1985;18(2):129-40.
103. Liu R, Wen X, Tong Z, Wang K, Wang C. Changes of gluteus medius muscle in the adult patients with unilateral developmental dysplasia of the hip. *BMC Musculoskelet Disord.* 2012 Jun 15;13:101.
104. Eberhart HD, Inman VT. An evaluation of experimental procedures used in a fundamental study of human locomotion. *Ann N Y Acad Sci.* 1951 Jan;51(7):1213-28.
105. Ugbohue UC, Papi E, Kaliarntas KT, Kerr A, Earl L, Pomeroy VM, Rowe PJ. The evaluation of an inexpensive, 2D, video based gait assessment system for clinical use. *Gait Posture.* 2013 Jul;38(3):483-9.
106. Winter DA. *Biomechanics and Motor Control of Human Movement.* 4th ed. Hoboken, NJ: John Wiley & Sons; 2009.
107. Robertson DGE, Caldwell GE, Hamill J, Kamen G, Whittlesey SN. *Research Methods in Biomechanics.* 2nd ed. Champaign, IL: Human Kinetics; 2013.
108. Bey MJ, Zauel R, Brock SK, Tashman S. Validation of a new model-based tracking technique for measuring three-dimensional, in vivo glenohumeral joint kinematics. *J Biomech Eng.* 2006 Aug;128(4):604-9.
109. Fiorentino NM, Atkins PR, Kutschke MJ, Goebel JM, Foreman KB, Anderson AE. Soft tissue artifact causes significant errors in the calculation of joint angles and range of motion at the hip. *Gait Posture.* 2017 Jun;55:184-90.
110. Pedersen ENG, Simonsen EB, Alkjaer T, Søballe K. Walking pattern in adults with congenital hip dysplasia: 14 women examined by inverse dynamics. *Acta Orthop Scand.* 2004 Feb;75(1):2-9.
111. Skalskøi O, Iversen CH, Nielsen DB, Jacobsen J, Mechlenburg I, Søballe K, Sørensen H. Walking patterns and hip contact forces in patients with hip dysplasia. *Gait Posture.* 2015 Oct;42(4):529-33.
112. Endo H, Mitani S, Senda M, Kawai A, McCown C, Umeda M, Miyakawa T, Inoue H. Three-dimensional gait analysis of adults with hip dysplasia after rotational acetabular osteotomy. *J Orthop Sci.* 2003;8(6):762-71.
113. Pedersen EN, Alkjaer T, Søballe K, Simonsen EB. Walking pattern in 9 women with hip dysplasia 18 months after periacetabular osteotomy. *Acta Orthop.* 2006 Apr;77(2):203-8.

114. Sucato DJ, Tulchin K, Shrader MW, DeLaRocha A, Gist T, Sheu G. Gait, hip strength and functional outcomes after a Ganz periacetabular osteotomy for adolescent hip dysplasia. *J Pediatr Orthop*. 2010 Jun;30(4):344-50.
115. Jacobsen JS, Nielsen DB, Sørensen H, Søballe K, Mechlenburg I. Joint kinematics and kinetics during walking and running in 32 patients with hip dysplasia 1 year after periacetabular osteotomy. *Acta Orthop*. 2014 Dec;85(6):592-9.
116. Hodge WA, Fijan RS, Carlson KL, Burgess RG, Harris WH, Mann RW. Contact pressures in the human hip joint measured in vivo. *Proc Natl Acad Sci U S A*. 1986 May;83(9):2879-83.
117. Bergmann G, Deuretzbacher G, Heller M, Graichen F, Rohlmann A, Strauss J, Duda GN. Hip contact forces and gait patterns from routine activities. *J Biomech*. 2001 Jul;34(7):859-71.
118. Bergmann G, Bender A, Dymke J, Duda G, Damm P. Standardized loads acting in hip implants. *PLoS One*. 2016 May 19;11(5):e0155612.
119. Anderson AE, Ellis BJ, Maas SA, Peters CL, Weiss JA. Validation of finite element predictions of cartilage contact pressure in the human hip joint. *J Biomech Eng*. 2008 Oct;130(5):051008.
120. Abraham CL, Maas SA, Weiss JA, Ellis BJ, Peters CL, Anderson AE. A new discrete element analysis method for predicting hip joint contact stresses. *J Biomech*. 2013 Apr 5;46(6):1121-7.
121. Abraham CL, Knight SJ, Peters CL, Weiss JA, Anderson AE. Patient-specific chondrolabral contact mechanics in patients with acetabular dysplasia following treatment with peri-acetabular osteotomy. *Osteoarthritis Cartilage*. 2017 May;25(5):676-84.
122. Thomas-Aitken HD, Willey MC, Goetz JE. Joint contact stresses calculated for acetabular dysplasia patients using discrete element analysis are significantly influenced by the applied gait pattern. *J Biomech*. 2018 Oct 5;79:45-53.
123. Delp SL, Anderson FC, Arnold AS, Loan P, Habib A, John CT, Guendelman E, Thelen DG. OpenSim: open-source software to create and analyze dynamic simulations of movement. *IEEE Trans Biomed Eng*. 2007 Nov;54(11):1940-50.
124. Delp SL, Loan JP, Hoy MG, Zajac FE, Topp EL, Rosen JM. An interactive graphics-based model of the lower extremity to study orthopaedic surgical procedures. *IEEE Trans Biomed Eng*. 1990 Aug;37(8):757-67.

- 125.Damsgaard M, Rasmussen J, Christensen ST, Surma E, de Zee M. Analysis of musculoskeletal systems in the AnyBody Modeling System. *Simul Model Pract Theory*. 2006 Nov 1;14(8):1100-11.
- 126.Friederich JA, Brand RA. Muscle fiber architecture in the human lower limb. *J Biomech*. 1990;23(1):91-5.
- 127.Wickiewicz TL, Roy RR, Powell PL, Edgerton VR. Muscle architecture of the human lower limb. *Clin Orthop Relat Res*. 1983 Oct;(179):275-83.
- 128.Rajagopal A, Dembia CL, DeMers MS, Delp DD, Hicks JL, Delp SL. Full-body musculoskeletal model for muscle-driven simulation of human gait. *IEEE Trans Biomed Eng*. 2016 Oct;63(10):2068-79.
- 129.Arnold EM, Ward SR, Lieber RL, Delp SL. A model of the lower limb for analysis of human movement. *Ann Biomed Eng*. 2010 Feb;38(2):269-79.
- 130.Modenese L, Phillips AT, Bull AM. An open source lower limb model: Hip joint validation. *J Biomech*. 2011 Aug 11;44(12):2185-93.
- 131.Lai AKM, Arnold AS, Wakeling JM. Why are antagonist muscles co-activated in my simulation? A musculoskeletal model for analysing human locomotor tasks. *Ann Biomed Eng*. 2017 Dec;45(12):2762-74.
- 132.Catelli DS, Wesseling M, Jonkers I, Lamontagne M. A musculoskeletal model customized for squatting task. *Comput Methods Biomech Biomed Engin*. 2019 Jan;22(1):21-4.
- 133.Shelburne KB, Decker MJ, Krong J, Torry MR, Philippon MJ. Muscle forces at the hip during squatting exercise. Poster session presented at: 56th Annual Meeting of the Orthopaedic Research Society. 2010 March 6–9; New Orleans, LA.
- 134.Hicks JL, Uchida TK, Seth A, Rajagopal A, Delp SL. Is my model good enough? Best practices for verification and validation of musculoskeletal models and simulations of movement. *J Biomech Eng*. 2015 Feb 1;137(2):020905.
- 135.Wesseling M, De Groote F, Bosmans L, Bartels W, Meyer C, Desloovere K, Jonkers I. Subject-specific geometrical detail rather than cost function formulation affects hip loading calculation. *Comput Methods Biomech Biomed Engin*. 2016 Nov;19(14):1475-88.
- 136.Modenese L, Montefiori E, Wang A, Wesarg S, Viceconti M, Mazzà C. Investigation of the dependence of joint contact forces on musculotendon parameters using a codified workflow for image-based modelling. *J Biomech*. 2018 May 17;73:108-18.

137. Lenaerts G, Bartels W, Gelaude F, Mulier M, Spaepen A, Van der Perre G, Jonkers I. Subject-specific hip geometry and hip joint centre location affects calculated contact forces at the hip during gait. *J Biomech.* 2009 Jun 19;42(9):1246-51.
138. Scheys L, Van Campenhout A, Spaepen A, Suetens P, Jonkers I. Personalized MR-based musculoskeletal models compared to rescaled generic models in the presence of increased femoral anteversion: effect on hip moment arm lengths. *Gait Posture.* 2008 Oct;28(3):358-65.
139. Scheys L, Spaepen A, Suetens P, Jonkers I. Calculated moment-arm and muscle-tendon lengths during gait differ substantially using MR based versus rescaled generic lower-limb musculoskeletal models. *Gait Posture.* 2008 Nov;28(4):640-8.
140. Scheys L, Desloovere K, Suetens P, Jonkers I. Level of subject-specific detail in musculoskeletal models affects hip moment arm length calculation during gait in pediatric subjects with increased femoral anteversion. *J Biomech.* 2011 Apr 29;44(7):1346-53.
141. Lu TW, O'Connor JJ. Bone position estimation from skin marker co-ordinates using global optimisation with joint constraints. *J Biomech.* 1999 Feb;32(2):129-34.
142. Wu G, Siegler S, Allard P, Kirtley C, Leardini A, Rosenbaum D, Whittle M, D'Lima DD, Cristofolini L, Witte H, Schmid O, Stokes I; Standardization and Terminology Committee of the International Society of Biomechanics. ISB recommendation on definitions of joint coordinate system of various joints for the reporting of human joint motion--part I: ankle, hip, and spine. International Society of Biomechanics. *J Biomech.* 2002 Apr;35(4):543-8.
143. Crowninshield RD, Brand RA. A physiologically based criterion of muscle force prediction in locomotion. *J Biomech.* 1981;14(11):793-801.
144. Anderson FC, Pandy MG. Static and dynamic optimization solutions for gait are practically equivalent. *J Biomech.* 2001 Feb;34(2):153-6.
145. Wesseling M, Derikx LC, de Groote F, Bartels W, Meyer C, Verdonschot N, Jonkers I. Muscle optimization techniques impact the magnitude of calculated hip joint contact forces. *J Orthop Res.* 2015 Mar;33(3):430-8.
146. Thelen DG, Anderson FC, Delp SL. Generating dynamic simulations of movement using computed muscle control. *J Biomech.* 2003 Mar;36(3):321-8.
147. Lloyd DG, Besier TF. An EMG-driven musculoskeletal model to estimate muscle forces and knee joint moments in vivo. *J Biomech.* 2003 Jun;36(6):765-76.
148. Steele KM, Demers MS, Schwartz MH, Delp SL. 2012. Compressive tibiofemoral force during crouch gait. *Gait Posture.* 35(4):556-60.

149. van Arkel RJ, Modenese L, Phillips AT, Jeffers JR. Hip abduction can prevent posterior edge loading of hip replacements. *J Orthop Res*. 2013 Aug;31(8):1172-9.
150. Fregly BJ, Besier TF, Lloyd DG, Delp SL, Banks SA, Pandy MG, D'Lima DD. Grand challenge competition to predict in vivo knee loads. *J Orthop Res*. 2012 Apr;30(4):503-13.
151. Valente G, Taddei F, Jonkers I. Influence of weak hip abductor muscles on joint contact forces during normal walking: probabilistic modeling analysis. *J Biomech*. 2013 Sep 3;46(13):2186-93.
152. Heller MO, Bergmann G, Deuretzbacher G, Claes L, Haas NP, Duda GN. Influence of femoral anteversion on proximal femoral loading: measurement and simulation in four patients. *Clin Biomech (Bristol, Avon)*. 2001 Oct;16(8):644-9.
153. Bosmans L, Wesseling M, Desloovere K, Molenaers G, Scheys L, Jonkers I. Hip contact force in presence of aberrant bone geometry during normal and pathological gait. *J Orthop Res*. 2014 Nov;32(11):1406-15.
154. Passmore E, Graham HK, Pandy MG, Sangeux M. Hip- and patellofemoral-joint loading during gait are increased in children with idiopathic torsional deformities. *Gait Posture*. 2018 Jun;63:228-35.
155. Ng KCG, Mantovani G, Modenese L, Beaulé PE, Lamontagne M. Altered walking and muscle patterns reduce hip contact forces in individuals with symptomatic cam femoroacetabular impingement. *Am J Sports Med*. 2018 Sep;46(11):2615-23.
156. Catelli DS, Ng KCG, Wesseling M, Kowalski E, Jonkers I, Beaulé PE, Lamontagne M. Hip muscle forces and contact loading during squatting after cam-type FAI surgery. *J Bone Joint Surg Am*. 2020 Nov 4;102(Suppl 2):34-42.
157. Harris MD, MacWilliams BA, Bo Foreman K, Peters CL, Weiss JA, Anderson AE. Higher medially-directed joint reaction forces are a characteristic of dysplastic hips: A comparative study using subject-specific musculoskeletal models. *J Biomech*. 2017 Mar 21;54:80-7.
158. Valente G, Pitto L, Testi D, Seth A, Delp SL, Stagni R, Viceconti M, Taddei F. Are subject-specific musculoskeletal models robust to the uncertainties in parameter identification? *PLoS One*. 2014 Nov 12;9(11):e112625.
159. Lenaerts G, De Groote F, Demeulenaere B, Mulier M, Van der Perre G, Spaepen A, Jonkers I. Subject-specific hip geometry affects predicted hip joint contact forces during gait. *J Biomech*. 2008;41(6):1243-52.

160. Martelli S, Valente G, Viceconti M, Taddei F. Sensitivity of a subject-specific musculoskeletal model to the uncertainties on the joint axes location. *Comput Methods Biomech Biomed Engin.* 2015;18(14):1555-63.
161. Blemker SS, Asakawa DS, Gold GE, Delp SL. Image-based musculoskeletal modeling: applications, advances, and future opportunities. *J Magn Reson Imaging.* 2007 Feb;25(2):441-51.
162. Viceconti M, Testi D, Taddei F, Martelli S, Clapworthy GJ, Jan SV. Biomechanics modeling of the musculoskeletal apparatus: status and key issues. *Proc IEEE.* 2006 Apr 10;94(4):725-39.

Chapter 3: Musculoskeletal Models with Generic and Subject-Specific Geometry Estimate Different Joint Biomechanics in Dysplastic Hips¹

3.1 Abstract

Optimizing the geometric complexity of musculoskeletal models is important for reliable yet feasible estimation of joint biomechanics. This study investigated the effects of subject-specific model geometry on hip joint reaction forces (JRFs) and muscle forces in patients with developmental dysplasia of the hip (DDH) and healthy controls. For nine DDH and nine control subjects, three models were created with increasingly subject-specific pelvis geometry, hip joint center locations and muscle attachments. Hip JRFs and muscle forces during a gait cycle were compared among the models. For DDH subjects, resultant JRFs from highly specific models including subject-specific pelvis geometry, joint locations and muscle attachments were not significantly different compared to models using generic geometry in early stance, but were significantly higher in late stance ($p = 0.03$). Estimates from moderately specific models using CT-informed scaling of generic pelvis geometry were not significantly different from low specificity models using generic geometry scaled with skin markers. For controls, resultant JRFs in early stance from highly specific models were significantly lower than moderate and low specificity models ($p \leq 0.02$) with no significant differences in late stance. Inter-model JRF differences were larger for DDH subjects than controls. Inter-model differences for JRF

¹ Reprinted from: Song K, Anderson AE, Weiss JA, Harris MD. Musculoskeletal models with generic and subject-specific geometry estimate different joint biomechanics in dysplastic hips. *Comput Methods Biomech Biomed Engin.* 2019 Feb;22(3):259-270. *Supplemental Tables and Figures* cited throughout Chapter 3 can be found in the online version of the article, doi: 10.1080/10255842.2018.1550577. Rights granted from Taylor & Francis Group.

components and muscle forces were similar to resultant JRFs. Incorporating subject-specific pelvis geometry significantly affects JRF and muscle force estimates in both DDH and control groups, which may be especially important for reliable estimation of pathomechanics in dysplastic hips.

3.2 Introduction

Developmental dysplasia of the hip (DDH) is a structural disease characterized by a shallow acetabulum, insufficient femoral coverage, and abnormal intra-articular loading [1-3]. Abnormal hip loads may contribute to acetabular labrum and articular cartilage damage [4], which often progresses to early osteoarthritis [5,6]. Reliable quantification of hip loads, including joint reaction forces (JRFs) and muscle forces, may improve our understanding of tissue damage and the pathogenesis of osteoarthritis among patients with DDH.

Musculoskeletal models are valuable for quantifying biomechanical variables that are difficult to measure in vivo, including JRFs and muscle forces. Model accuracy depends on many factors, including kinematics and force input, joint representation, and passive and active muscle properties. One major factor that can affect model accuracy is representation of the musculoskeletal geometry, which dictates joint center and muscle attachment locations. To reliably estimate hip JRFs and muscle forces for specific populations, it is important to understand the level of model complexity needed with regard to bone and muscle geometry [7]. The majority of musculoskeletal modeling research has used generic bony geometry derived from cadavers, which are scaled to match anthropometrics of individuals [8-10]. This generic scaling approach is straightforward and may be adequate for investigating healthy adult gait [11,12]. However, for populations with structural hip disease, models with subject-specific geometry may be necessary due to the potential associations among abnormal geometry, joint biomechanics, and tissue damage [13-15]. Yet, there is a direct relationship between model pre-processing time and computational

demands with geometric complexity of the models [7,12,16]. Comparing estimates from models with varying levels of geometric detail is one method that can help researchers optimize specificity and complexity for reliable, yet feasible, estimation of joint biomechanics in a given population.

Geometric deformities relevant to DDH include lateralized hip joint centers (HJCs), abnormal pelvis bony geometry, and associated alterations in muscle paths [17-19], making this condition a microcosm for determining the sensitivity of JRF and muscle force estimates to the level of geometric detail in a model. However, previously reported biomechanical estimates from models of DDH are limited in number, and findings have not been in full agreement [20,21]. A study using generic geometry to model gait in patients with DDH [20] reported smaller hip JRFs versus controls, whereas a separate study using subject-specific pelvis geometry [21] found no difference in resultant hip JRFs, but larger medial JRFs in patients with DDH. The levels of pelvis geometry complexity may have contributed to the contrasting findings in these studies. Specifically, generic geometry may not adequately represent biomechanical differences in DDH compared to healthy hips because they omit the abnormal pelvis geometry and HJCs. Comparison between prior studies of DDH is further complicated by the use of different subject demographics and data collection protocols. By comparing generic and subject-specific models created for the same subject group, we can directly assess the effects of geometric specificity on estimation of hip biomechanics in patients with DDH.

The objective of this study was to compare JRFs and muscle forces among models with low, moderate and high levels of pelvis geometry specificity in patients with DDH and healthy controls. We hypothesized that hip JRFs and muscle forces would be significantly different for models with highly specific pelvis geometry, HJCs, and muscle paths compared to those of lower specificity. We also hypothesized that JRFs and muscle forces would be different, but to a lesser

extent, for moderately specific models with scaling informed by imaging versus low specificity models scaled with skin markers.

3.3 Methods

3.3.1 Subjects

With Institutional Review Board approval and informed consent, eighteen subjects were recruited and reported previously [21]. Nine subjects had symptomatic DDH ('DDH' group; 6 female, 3 male, 26 ± 7 years old, body mass index: 22.7 ± 3.1 kg/m²), with lateral center edge angles smaller than 20° [22] confirmed by an orthopaedic surgeon and a musculoskeletal radiologist. Six patients had radiographic evidence of bilateral DDH, but all patients had unilateral symptoms at the time of data collection. The other 9 subjects were healthy controls ('CONT' group; 6 female, 3 male, 26 ± 4 years old, body mass index: 23.8 ± 4.5 kg/m²) who had no history of DDH, hip injury or other hip diseases as confirmed by radiographic inspection.

3.3.2 CT geometry and Gait Motion Analysis

Computed tomography (CT) images of each subject's pelvis and proximal femurs were collected, segmented, and reconstructed in 3D with Amira v6.1 software (FEI, Hillsboro, OR, USA), using previously reported methods [23]. Kinematic data during gait were collected for each subject in a motion capture laboratory and previously reported [21]. Briefly, twenty-one retro-reflective markers were placed on the pelvis, thighs, shanks, feet and upper trunk and subjects walked barefoot at their self-selected speed along a 10m runway, while marker trajectories were recorded at 100 Hz and ground reaction forces were recorded at 1000 Hz. A residual analysis [24] was performed on marker and force data separately to determine appropriate cutoff frequencies and a 4th-order, zero-lag Butterworth low-pass filter was then applied to the signals with 6 Hz and

20 Hz cutoffs, respectively. Filtered data were imported to OpenSim musculoskeletal modeling software v3.3 [25].

3.3.3 Musculoskeletal Modeling

A 23 degree-of-freedom model with pelvis, lower limbs, torso, head segments and 96 muscle-tendon actuators was used as the baseline model for this study, with modifications made to the path, maximum isometric force and tendon slack length of muscles around the hip [26,27]. A virtual marker set corresponding to experimental markers was placed on the model. The baseline model (**Figure 3.1A**) was personalized for each subject in OpenSim via three different methods: (1) marker-based isotropic scaling ('Generic'), (2) imaging-informed anisotropic scaling of the pelvis ('Nonuniform'), or (3) a previous method using subject-specific pelvis geometry, HJCs, and muscle paths from CT reconstructions ('CT-Geometry') [21]. These methods represented low, moderate, and high levels of model geometric specificity, respectively (**Table 3.1**).

'Generic' Model - Marker-Based Isotropic Scaling

Generic models were created by adjusting the size and inertial properties of the baseline model with one isotropic scale factor for each segment, derived from distance ratios between experimental and corresponding virtual markers. Specifically for the pelvis, a set of distances were measured and averaged between the left and right anterior superior iliac spine (ASIS) and posterior superior iliac spine (PSIS) markers (**Figure 3.1B**). Hip joint center and muscle attachment locations were moved automatically as the generic geometry was scaled (**Table 3.1**). After scaling, a least squares optimization was used to fit the model to an experimentally captured static pose, and virtual marker positions were adjusted to match experimental marker placement specific to each subject.

'Nonuniform' Model - Imaging-Informed Anisotropic Scaling of the Pelvis

Nonuniform models were also created by scaling the generic pelvis geometry of the baseline model, but used anisotropic scale factors informed by CT-based pelvis reconstructions (termed ‘CT pelvis’) instead of skin marker measurements. First, the CT pelvis of each subject was adjusted in Amira to match the spatial orientation of the OpenSim model pelvis geometry. Then, the anteroposterior (AP, horizontal distance between ASIS and PSIS), superoinferior (SI, vertical distance from top of iliac crest to lower border of ischial tuberosity), and mediolateral (ML, distance between left and right iliac crests) dimensions of each geometry were measured (**Figure 3.1B**). Three distinct scale factors (AP, SI, and ML) for the model pelvis segment were calculated as the ratios of each CT pelvis dimension to the corresponding baseline pelvis dimension. The generic pelvis geometry was scaled using the AP, SI, and ML ratios, which again moved the HJC and muscle attachment locations automatically with the model pelvis (**Table 3.1**). The other model segments were scaled with marker-based measurements similar to the Generic method. By incorporating a CT-informed pelvis size, Nonuniform models were incrementally more subject-specific than the Generic models.

‘CT-Geometry’ Model - Subject-Specific Pelvis Geometry, HJCs, and Muscle Paths

CT-Geometry models built upon the Nonuniform models, by incorporating fully subject-specific pelvis geometry and HJC locations derived from CT. Specifically, the generic OpenSim pelvis was removed from the model and replaced by the exact CT pelvis geometry at the corresponding location and orientation in the model. HJCs for both sides were moved to subject-specific locations, determined in PreView software (<https://febio.org/preview/>) as the centroid of a sphere fit to the 3D-reconstructed femoral head geometry. Attachment locations for twenty-nine muscles crossing the hip were then updated using the subject-specific pelvis geometry (**Figure 3.1B; Table 3.1**) and anatomical descriptions [28]. A sensitivity analysis was performed to test the

robustness of model estimates against uncertainty in muscle attachment point placement (Section 3.7). The other model segments were scaled with markers, similar to the Generic and Nonuniform methods. As the most subject-specific models, CT-Geometry were considered the reference standard for inter-model analyses.

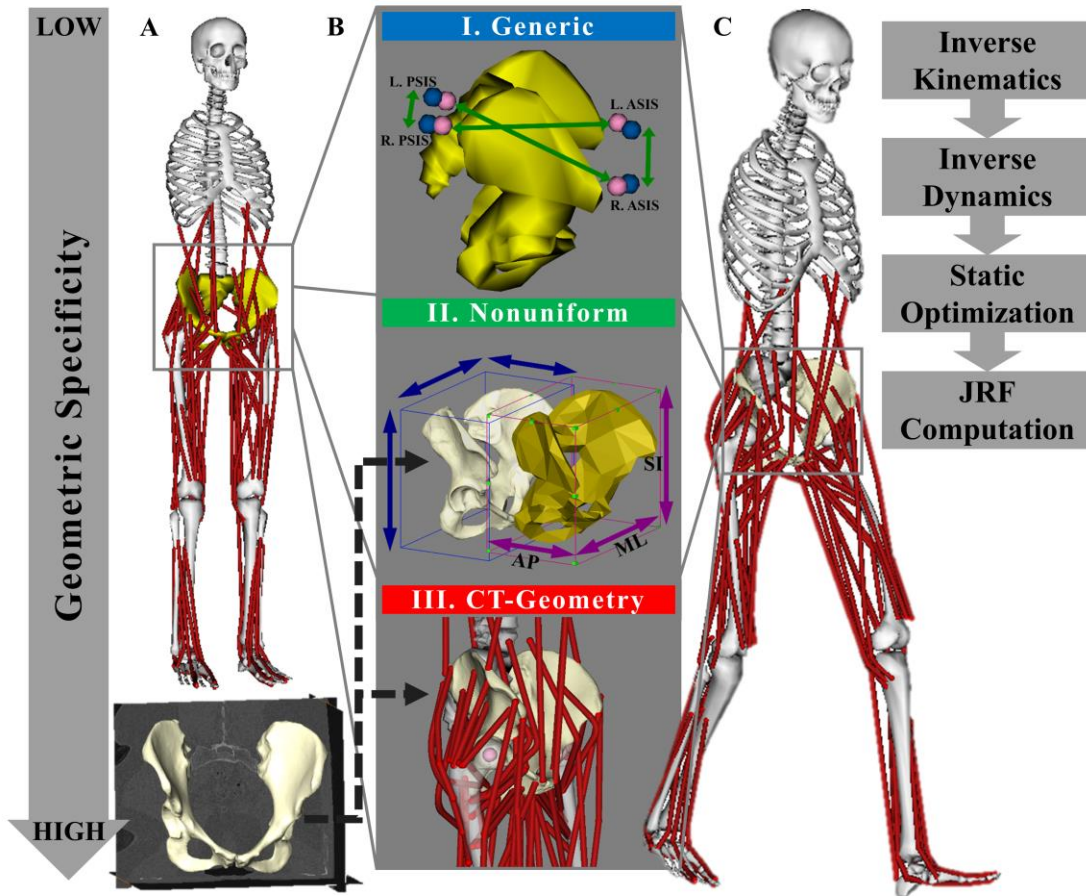


Figure 3.1. Flowchart showing development of models with low, moderate, and high levels of geometric specificity. (A) Top: The baseline OpenSim model. Bottom: Subject-specific pelvis geometry reconstructed from CT. (B) I: Set of experimental (blue) and virtual (pink) marker-based measurements for isotropic pelvis scaling in a Generic model. II: 3D measurements on pelvis bony geometry for anisotropic scaling in a Nonuniform model. III: Subject-specific pelvis geometry, adjusted HJC and hip muscle attachment locations in a CT-Geometry model. (C) Subsequent biomechanical analysis to estimate hip JRFs and muscle forces during gait.

Table 3.1. Differences among Generic, Nonuniform, and CT-Geometry model types.

	Generic	Nonuniform	CT-Geometry
Pelvis Geometry	Generic	Generic	Subject-specific from CT reconstruction
Pelvis Scaling	Uniform: 1 scale factor, derived from skin markers	Nonuniform: 3 scale factors, derived from CT dimensions (height, width, depth)	Step 1: Nonuniform Step 2: Substitute in subject-specific
HJC Locations and Hip Muscle Attachments	Automatically moved from baseline locations via uniform scaling	Automatically moved from baseline locations via nonuniform scaling	Subject-specific from CT reconstruction

3.3.4 Biomechanical Analysis and Data Processing

For the three models (Generic, Nonuniform, CT-Geometry) created for each subject, hip joint angles, moments, muscle forces and JRFs were computed in OpenSim (**Figure 3.1C**). Analyses were performed on a full gait cycle of a representative trial for each subject. Data were analyzed for the symptomatic side of DDH subjects, and a randomly chosen side of CONT subjects. Hip joint angles were calculated by inverse kinematics, using least squares optimization to minimize virtual to experimental marker differences; internal net hip joint moments were then calculated by inverse dynamics [24]. A residual reduction algorithm was used to reduce nonphysical compensatory forces in the full-body inverse dynamics solution, which may originate from marker placement errors, data filtering artifacts and model body-joint assumptions [25]. Muscle forces were estimated by static optimization using the minimized total of squared muscle activation criterion [29], which has been shown to be appropriate for estimating muscle forces during gait [30]. Lastly, hip JRF components were computed from static optimization results [31].

Hip JRFs, muscle forces, angles, and moments from each model were extracted and processed using Matlab R2016a (MathWorks, Natick, MA, USA). Data were time-normalized to

percentage of a gait cycle. JRFs and muscle forces were normalized by body weight; moments were normalized by body mass. JRF components were expressed in the pelvis frame to represent hip loads acting on the acetabulum. Individual hip muscles were grouped according to their functional roles in gait, and net muscle force magnitudes were summed algebraically for each functional group (hip flexors, extensors, abductors, adductors, internal rotators, external rotators). Variables were analyzed at the time points when resultant hip JRF peaked, first during early stance (termed 'JRF1') and again during mid-to-late stance (termed 'JRF2').

3.3.5 Statistical Analysis

Inter-model differences for each outcome variable were statistically analyzed using SPSS Statistics v24 (IBM, Armonk, NY, USA). Resultant hip JRFs and components were the primary outcome variables. Secondary outcome variables included HJC locations in each model, as well as hip angles, moments, individual and grouped muscle forces at the time of JRF1 and JRF2. Normality of data was tested using the Shapiro-Wilk test; variables with normally distributed data in all 3 models were compared using one-way ANOVA with repeated measures, while variables with any model violating data normality were compared using the Friedman test. Homogeneity of variance among inter-model differences (sphericity) was examined using Mauchly's test, with Greenhouse-Geisser corrections for data violating sphericity. Level of significance was set as $\alpha = 0.05$ for all statistical tests. For variables with significant differences among the 3 models, post hoc pairwise t-tests or Wilcoxon signed-rank tests were performed with Bonferroni corrections. Root mean square errors (RMSE) among the three model types were calculated for the resultant JRFs, JRF components, and muscle group forces at JRF1 and JRF2. All statistical tests were implemented separately for DDH and CONT subject groups.

3.4 Results

3.4.1 Hip JRFs

For DDH subjects, CT-Geometry models estimated larger resultant and superior JRFs at JRF2 versus Generic and Nonuniform models, while there were no significant inter-model differences at JRF1 (**Figure 3.2; Table 3.2**). In contrast, CT-Geometry models for CONT subjects estimated smaller medial JRFs at both JRF1 and JRF2, and slightly yet statistically different resultant, superior and posterior JRFs at JRF1 only (**Figure 3.3; Table 3.3**). Lastly, JRF estimates were not different between Nonuniform and Generic models for either group at JRF1 or JRF2. Root-mean-square error (RMSE) of hip JRFs between CT-Geometry and the other two models (¹*Supplemental Tables 6 and 7*) were generally larger for DDH compared to CONT, especially at JRF2, while much smaller between Nonuniform and Generic models.

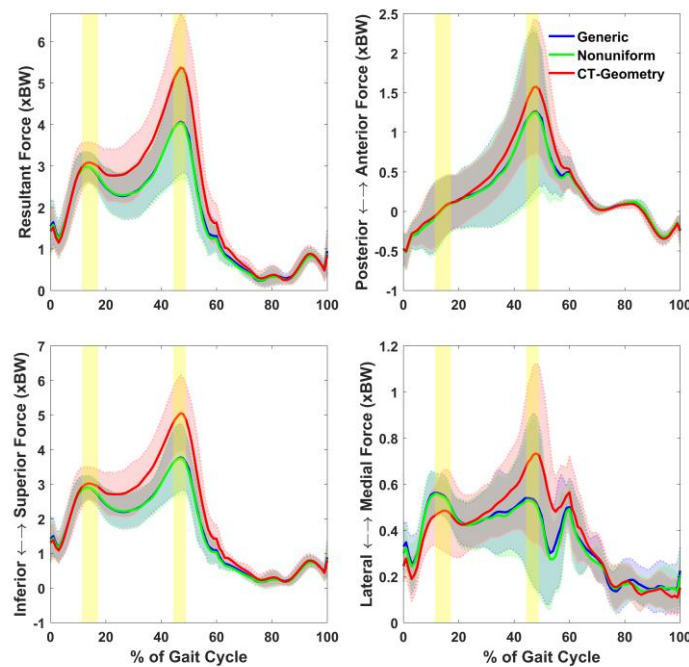


Figure 3.2. Average resultant hip JRFs and components during gait for DDH subjects, expressed in pelvis frame (i.e. acting on acetabulum). Shaded area represents ± 1 standard deviation; highlighted vertical bands indicate time of JRF1 and JRF2.

Table 3.2. Hip JRFs and muscle forces (mean \pm 1 standard deviation) at JRF1 and JRF2 for DDH subjects, normalized by body weight (xBW).

	At JRF1				At JRF2			
	Generic	Nonuniform	CT-Geometry	<i>p</i> -value	Generic	Nonuniform	CT-Geometry	<i>p</i> -value
JRF: resultant	3.05 \pm 0.40	3.05 \pm 0.42	3.19 \pm 0.55	n.s.	4.18 \pm 1.24	4.15 \pm 1.33	*† 5.47 \pm 1.27	*=.033 †=.023
JRF: (+) AP (-)	<0.01 \pm 0.41	0.01 \pm 0.42	0.07 \pm 0.39	n.s.	1.30 \pm 1.02	1.28 \pm 1.09	1.59 \pm 0.86	n.s.
JRF: (+) SI (-)	2.97 \pm 0.39	2.97 \pm 0.40	3.13 \pm 0.54	n.s.	3.87 \pm 0.94	3.85 \pm 0.99	*† 5.14 \pm 1.07	*=.001 †=.001
JRF: (+) ML (-)	0.57 \pm 0.10	0.57 \pm 0.11	0.50 \pm 0.15	n.s.	0.56 \pm 0.36	0.56 \pm 0.35	0.74 \pm 0.38	n.s.
Flexors	0.15 \pm 0.18	0.17 \pm 0.20	*† 0.48 \pm 0.44	*=.023 †=.033	2.31 \pm 1.09	2.23 \pm 1.16	*† 3.27 \pm 1.11	*=.001 †=.001
Extensors	1.05 \pm 0.31	1.00 \pm 0.27	*† 0.64 \pm 0.34	*<.001 †<.001	0.21 \pm 0.14	0.22 \pm 0.13	0.14 \pm 0.14	n.s.
Abductors	1.79 \pm 0.50	1.85 \pm 0.48	1.95 \pm 0.44	n.s.	1.40 \pm 0.34	1.46 \pm 0.38	1.85 \pm 0.49	n.s.
Adductors	0.02 \pm 0.02	0.01 \pm 0.02	0.01 \pm 0.02	n.s.	<0.01 \pm <0.01	<0.01 \pm <0.01	<0.01 \pm <0.01	n.s.
Internal rotators	0.84 \pm 0.32	0.87 \pm 0.31	*† 1.18 \pm 0.39	*=.001 †=.006	0.83 \pm 0.26	0.87 \pm 0.28	*† 1.25 \pm 0.44	*=.025 †=.026
External rotators	0.39 \pm 0.14	0.40 \pm 0.15	*† 0.23 \pm 0.08	*=.010 †=.010	0.22 \pm 0.17	0.21 \pm 0.14	0.14 \pm 0.12	n.s.

Notes: Symbols indicating statistical significance: *CT-Geometry vs. Generic; †CT-geometry vs. Nonuniform. n.s.: not significant.

Table 3.3. Hip JRFs and muscle forces (mean \pm 1 standard deviation) at JRF1 and JRF2 for CONT subjects, normalized by body weight (xBW).

	At JRF1				At JRF2			
	Generic	Nonuniform	CT-Geometry	<i>p</i> -value	Generic	Nonuniform	CT-Geometry	<i>p</i> -value
JRF: resultant	3.44 \pm 0.58	3.47 \pm 0.59	*† 3.30 \pm 0.55	* =.024 † =.009	4.32 \pm 0.81	4.32 \pm 0.77	4.71 \pm 0.67	n.s.
JRF: (+) AP (-)	-0.28 \pm 0.48	-0.28 \pm 0.49	† -0.35 \pm 0.46	† =.032	1.46 \pm 0.68	1.44 \pm 0.67	1.33 \pm 0.55	n.s.
JRF: (+) SI (-)	3.34 \pm 0.53	3.36 \pm 0.54	† 3.24 \pm 0.51	† =.023	4.01 \pm 0.63	4.02 \pm 0.61	4.49 \pm 0.62	n.s.
JRF: (+) ML (-)	0.62 \pm 0.15	0.66 \pm 0.15	*† 0.37 \pm 0.09	* =.023 † =.023	0.52 \pm 0.14	0.53 \pm 0.10	*† 0.28 \pm 0.11	* =.009 † =.002
Flexors	0.06 \pm 0.10	0.06 \pm 0.07	*† 0.16 \pm 0.16	* =.033 † =.033	2.37 \pm 0.79	2.32 \pm 0.77	*† 2.82 \pm 0.66	* =.019 † =.035
Extensors	1.31 \pm 0.48	1.33 \pm 0.48	*† 0.98 \pm 0.43	* =.033 † =.023	0.18 \pm 0.09	‡ 0.21 \pm 0.09	*† 0.07 \pm 0.06	* =.004 † =.002 ‡ =.039
Abductors	2.17 \pm 0.46	2.22 \pm 0.46	*† 2.04 \pm 0.43	* =.020 † =.003	1.49 \pm 0.22	1.55 \pm 0.20	1.34 \pm 0.36	n.s.
Adductors	0.02 \pm 0.02	0.01 \pm 0.02	*† 0.04 \pm 0.03	* =.023 † =.023	<0.01 \pm <0.01	<0.01 \pm <0.01	<0.01 \pm <0.01	n.s.
Internal rotators	0.97 \pm 0.26	0.98 \pm 0.22	*† 1.05 \pm 0.23	* =.038 † =.009	0.95 \pm 0.18	0.96 \pm 0.16	1.03 \pm 0.39	n.s.
External rotators	0.50 \pm 0.15	0.51 \pm 0.16	*† 0.23 \pm 0.09	* =.001 † =.001	0.16 \pm 0.07	‡ 0.18 \pm 0.07	*† 0.07 \pm 0.06	* =.008 † =.002 ‡ =.033

Notes: Symbols indicating statistical significance: *CT-Geometry vs. Generic; †CT-geometry vs. Nonuniform; ‡Nonuniform vs. Generic. n.s.: not significant.

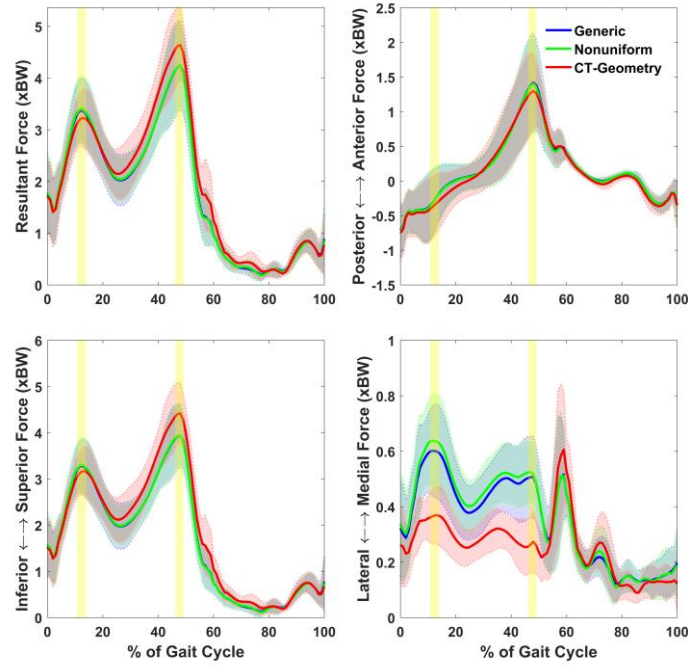


Figure 3.3. Average resultant hip JRFs and components during gait for CONT subjects, expressed in pelvis frame (i.e. acting on acetabulum). Shaded area represents ± 1 standard deviation; highlighted vertical bands indicate time of JRF1 and JRF2.

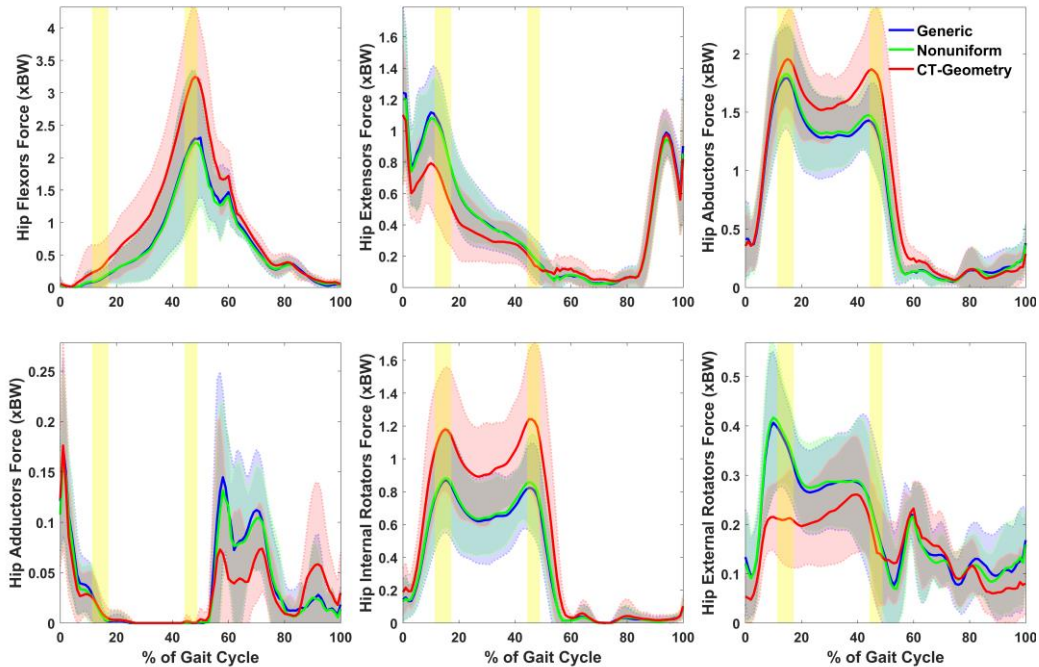


Figure 3.4. Average hip muscle group forces during gait for DDH subjects. Shaded area represents ± 1 standard deviation; highlighted vertical bands indicate time of JRF1 and JRF2.

3.4.2 Hip Muscle Forces

For DDH, CT-Geometry models estimated larger hip flexor and internal rotator forces at both JRF1 and JRF2, as well as smaller forces in the extensors and external rotators at JRF1, compared to Generic and Nonuniform models (**Figure 3.4; Table 3.2**). Similarly for CONT, CT-Geometry models estimated larger flexor forces at both JRF1 and JRF2 (**Figure 3.5; Table 3.3**). However, CT-Geometry models for CONT estimated smaller extensor and external rotator forces at both JRF1 and JRF2 compared to Generic and Nonuniform models, as well as larger internal rotator forces, larger adductor forces, and smaller abductor forces at JRF1 (**Figure 3.5; Table 3.3**). Inter-model differences were larger in DDH than CONT for hip flexor, internal rotator and early-stance extensor forces, but smaller for external rotator and mid-to-late stance extensor forces (**Tables 3.2 and 3.3**). Lastly, compared to Generic, Nonuniform models estimated marginally larger hip extensor and external rotator forces at JRF2 for CONT (**Table 3.3**), and no significant differences in hip muscle group forces for DDH. RMSE values of hip muscle group forces followed similar trends (¹*Supplemental Tables 6 and 7*). Inter-model differences for individual muscle forces are reported in Section 3.8.

3.4.3 HJC Locations

For DDH, HJC locations in CT-Geometry models were more lateral than both Generic and Nonuniform models, more anterior than Nonuniform, but not significantly different from either Generic or Nonuniform in the SI direction (**Table 3.4**). For CONT, HJCs in CT-Geometry models were more anterior and inferior than both Generic and Nonuniform, but not significantly different in the ML direction (**Table 3.4**). HJC locations were not different between Nonuniform and Generic models for either subject group.

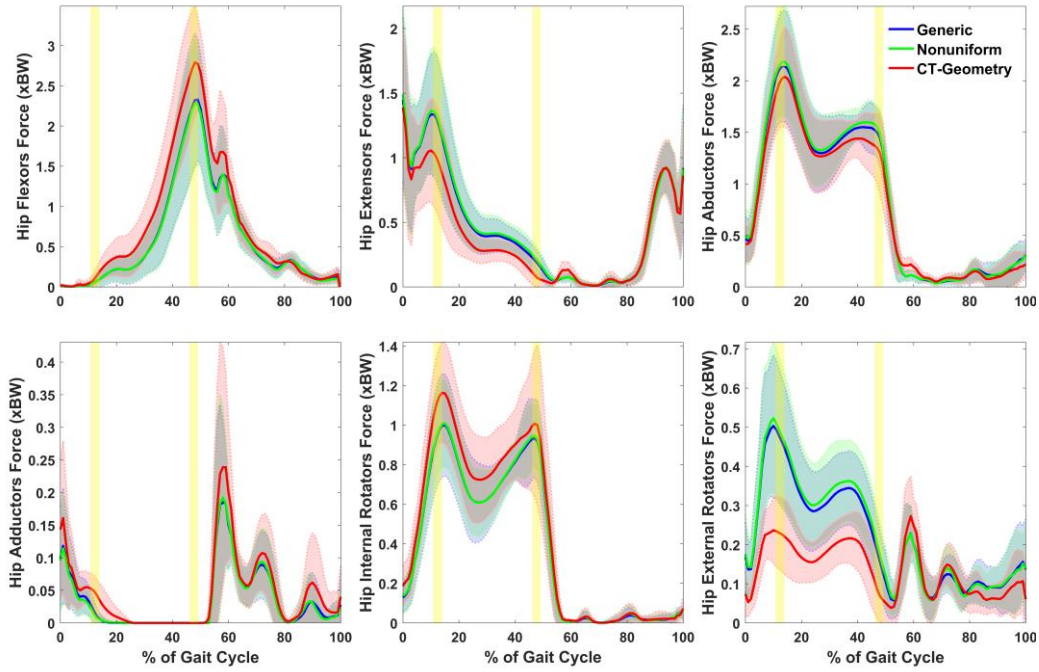


Figure 3.5. Average hip muscle group forces during gait for CONT subjects. Shaded area represents ± 1 standard deviation; highlighted vertical bands indicate time of JRF1 and JRF2.

Table 3.4. HJC locations (cm) relative to pelvis origin for DDH and CONT groups (mean ± 1 standard deviation).

		Generic	Nonuniform	CT-Geometry	<i>p</i> -value
DDH	(+) AP (-)	-6.7 ± 0.4	-7.3 ± 0.7	$\dagger -5.9 \pm 0.9$	$\dagger <.001$
	(+) SI (-)	-6.3 ± 0.3	-6.5 ± 0.4	-6.9 ± 0.6	n.s.
	(-) ML (+)	8.0 ± 0.4	8.2 ± 0.6	$*\dagger 9.1 \pm 0.4$	$* <.001$ $\dagger =.008$
CONT	(+) AP (-)	-7.3 ± 0.5	-7.3 ± 0.4	$*\dagger -5.9 \pm 0.6$	$* =.001$ $\dagger <.001$
	(+) SI (-)	-6.8 ± 0.5	-6.6 ± 0.5	$*\dagger -7.3 \pm 0.6$	$* =.028$ $\dagger =.001$
	(-) ML (+)	8.6 ± 0.6	8.7 ± 0.5	8.9 ± 0.5	n.s.

Notes: Symbols indicating statistical significance: *CT-Geometry vs. Generic; \dagger CT-geometry vs. Nonuniform. n.s.: not significant.

3.4.4 Hip Angles and Moments

Inter-model differences in hip angles and moments were found for both DDH and CONT groups at JRF1 and/or JRF2 (Section 3.9). Briefly, CT-Geometry models had larger hip adduction at JRF1 and a larger flexion moment throughout stance for both groups, but a larger abduction moment for DDH only and not for CONT (Section 3.9). Hip angles and moments were not significantly different between Nonuniform and Generic models.

3.5 Discussion

Optimizing the level of geometric detail needed for musculoskeletal models to reliably estimate biomechanics can be challenging, especially when studying hips with structural diseases such as DDH. The objective of this study was to compare hip JRFs and muscle forces among models with low, moderate and high levels of geometric specificity in patients with DDH and healthy controls. Overall, models with highly subject-specific pelvis geometry, hip joint locations, and muscle paths (CT-Geometry) estimated significantly different hip JRFs and muscle forces compared to models with moderate (Nonuniform) or low specificity (Generic) during gait. Specifically, using subject-specific pelvis geometry and HJC resulted in larger resultant and medial JRFs at mid-to-late stance for patients with DDH, but smaller medial JRFs for controls. In contrast, moderately subject-specific Nonuniform models did not differ substantially from low-specificity Generic models. The larger hip JRFs and related muscle forces due to patient-specific geometry support theories of pathomechanics in DDH [19,32], and emphasize the importance of accurately representing abnormal geometry when modeling joint biomechanics in patients with DDH.

As hypothesized, a high level of subject-specific geometric detail caused significant changes in hip JRF estimates for both subject groups, but there were distinct patterns for each group. For controls, CT-Geometry models estimated a slightly smaller resultant hip JRF at its

early-stance peak and smaller medial JRFs throughout stance, which might be influenced by HJCs being more anterior and inferior than less specific models. HJC location has been reported to significantly affect hip JRF estimates [15] due to altered flexor and extensor muscle moment arm lengths (MALs) and muscle forces that contribute to joint torques [32]. Indeed, CT-Geometry models estimated reduced early-stance extensor forces and net extension moments, as the HJC moved anteriorly and away from extensor muscle lines of action. As more anterior HJCs and changed hip flexor-extensor forces were also found in CT-Geometry models for DDH subjects, we speculate these traits might have not been closely represented by the coarse geometry of the generic models, for either healthy or deformed hips.

The primary effects of subject-specific geometry on models of DDH were larger resultant and superior hip JRFs at mid-to-late stance, which were not found for controls. Also unique to DDH, CT-Geometry models had significantly more lateral HJCs, which supports radiographic studies [17]. The more lateral HJCs reduced hip abductor muscle MALs, which increased demands on the abductors to generate larger force and provide stabilizing torque prior to push-off [32]. This finding coincided with the DDH-specific trend of increased abductor muscle forces and significantly larger net abduction moments. Elevated hip abductor forces, together with increased flexor forces, then contributed to larger medial, superior, and resultant hip JRFs (**Figure 3.2**). If we consider models with high geometric specificity as the ‘reference standard’, the generic models might have underestimated potentially abnormal JRFs in DDH hips, because they could not adequately characterize the aberrant HJC locations or excessive abductor muscle demands. Therefore, it may be particularly essential to include structural details to reliably estimate hip biomechanics in the DDH population.

Significantly different muscle forces caused by subject-specific model geometry were not always reflected in changes to hip JRFs, possibly due to the changing function and coordination of individual muscles at various joint positions. For example in the DDH group, CT-Geometry models estimated larger anterior gluteus medius forces throughout stance (¹*Supplemental Table 1*) but larger resultant hip JRFs only in mid-to-late stance. While hip abductor forces increased in early stance, simultaneously decreased extensor forces might neutralize the overall effect on peak hip JRF. In contrast, during mid-to-late stance, increased hip flexor forces combined with larger abductor forces to raise the hip JRF peak. Moreover, effects from other individual muscles (¹*Supplemental Tables 1 and 2*) could account for specific changes in hip JRFs as well. As such, the effects on muscle force estimates should be interpreted cautiously with regard to their potential clinical relevance.

Joint kinematics can also affect JRF estimates. For instance, changes in hip extension angle may alter anterior JRFs during gait [33]. However, neither peak hip extension nor the AP component of hip JRF was substantially different among the models in the current study. The CT-Geometry models did have larger hip adduction during early stance (¹*Supplemental Figure 1*) especially for DDH, which could be related to the lateralized HJCs. These inter-model kinematic differences demonstrate the influence of subject-specific geometry, in particular HJC locations, on motion tracking by the models, which may affect accuracy of model estimation.

Nonuniform models were created to improve upon marker-based scaling, and represented a method that could be feasibly replicated with multi-view 2D radiographic images of the pelvis. However, the only notable differences between Nonuniform and Generic models were mid-to-late stance hip extensor and external rotator muscle forces, whose functions were minor at that time point. Even with improved scaling, the pelvis geometry in Nonuniform models was still derived

from a single generic shape, and did not incorporate important geometric traits such as unique muscle lines of action relative to HJC locations. Therefore, using 2D radiographs to scale model geometry may be inadequate for improving the accuracy of JRF and muscle force estimates.

Some limitations of this study should be recognized. First, muscle attachment points were adjusted on the pelvis using reconstructed bony geometry and canonical descriptions of muscle anatomy. As found in the sensitivity analysis, hip JRF estimates were mostly sensitive to attachment perturbations of six hip flexor and extensor muscles in ML. Since the attachment surface area of those six muscles are either small (e.g. rectus femoris) or primarily along the sagittal plane (e.g. iliacus), it was unlikely that uncertainty in muscle placement during CT-Geometry model creation meaningfully altered hip muscle force and JRF estimation. Magnetic resonance imaging could be used in future studies to improve estimation of subject-specific muscle paths [34-36]. Second, we did not acquire subject-specific muscle properties such as physiological cross-sectional areas or fiber-tendon length. It is not known how muscle properties may differ between DDH and healthy groups, but because our DDH subjects were young, capable adults, and were similar to control subjects in height, weight and BMI [21], we assumed muscle properties to be the same as controls and to the baseline model [26]. Third, full femur geometry was not available from CT. Femoral deformities in DDH have been reported in the literature [17], but their influence on DDH biomechanics is unknown. Nonetheless, we used image-based femoral head geometry to determine subject-specific HJC locations in the CT-Geometry models. Another limitation is a relatively small sample size. However, our two groups were matched demographically, inter-model comparisons were made on the same gait trials for each subject, and the comparisons demonstrated statistically significant differences in key biomechanical variables such as JRFs. As experimental hip JRF and muscle force data were not available for our subjects, direct validation

of the model estimates was not possible. While highly subject-specific models could provide more accurate estimation, results should be interpreted with caution in the absence of directly referable experimental force data. However, hip JRFs estimates and muscle activations from models similar to the CT-Geometry models have been shown to be comparable to electromyography signals and published force estimates in healthy hips [21]. Lastly, assumptions inherent to the baseline model behavior (e.g. rotation-only hip joint, muscle force objective function) affect the accuracy of any simulation [25,37]. Thus, model results should not be considered an exact representation of musculoskeletal behavior and may not elucidate all biomechanical differences between healthy and pathologic populations. Because the objective of the current study was to quantify changes due to increasingly specific model geometry, the inter-model differences could still indicate relative improvement in model accuracy.

In conclusion, models with highly subject-specific, CT-based pelvis geometry, hip joint locations and muscle paths estimated significantly different hip JRFs and muscle forces compared to models of lower specificity. Moderately specific models with improved image-informed scaling, despite being simpler to implement than highly specific models, did not estimate hip biomechanics differently than generic models. Inter-model differences due to highly specific model geometry were greater for patients with DDH compared to healthy controls. Therefore, we recommend incorporating image-based subject-specific geometric details for musculoskeletal models of dysplastic hips. Future research may focus on improving automation of image-based subject-specific musculoskeletal models, and exploring the appropriate levels of model complexity for other structural hip diseases.

3.6 Acknowledgments

No potential conflict of interest was reported by the authors. This work was supported by the National Institute of Arthritis and Musculoskeletal and Skin Diseases of the National Institutes of Health [grant numbers K01AR072072, P30AR057235, and R01AR05344] and the Lottie Caroline Hardy Charitable Trust. The content is solely the responsibility of the authors and does not necessarily represent the official views of the National Institutes of Health.

3.7 Appendix 1. Sensitivity of Hip JRFs to Muscle Path in CT-Geometry Model

An analysis was performed to test the sensitivity of hip JRF estimates to the uncertainty in muscle attachment point placement during creation of the CT-Geometry model. To demonstrate the boundary of sensitivity for both DDH and CONT groups, CT-Geometry models for one DDH and one CONT subject were chosen for the analysis, which had the largest inter-model differences in estimated resultant hip JRF (versus Generic and Nonuniform). Muscle attachment points on the CT pelvis for each of the 16 muscles generating > 0.1 xBW force during gait were perturbed by ± 5 mm in anterior, posterior, superior, inferior, medial, and lateral directions. The ± 5 mm perturbation followed a 10mm uncertainty range, which was representative of the errors when marking muscle origins and insertions with bone pins on cadaveric specimens [38,39]. Static optimization analysis was again performed for each perturbed model; hip JRF estimates were then recomputed, and compared to the unperturbed CT-Geometry model.

For the two CT-Geometry models analyzed, a ± 5 mm perturbation of muscle attachment point in AP, SI or ML direction resulted in a large change of estimated JRFs only for a few muscles or muscle portions. Specifically, hip JRF resultant or component values differed by > 0.1 xBW at JRF1 or JRF2 among original and perturbed models (¹*Supplemental Tables 1 and 2*) for six major

hip flexors and extensors: iliacus (in ML), rectus femoris (in AP, SI and ML), tensor fasciae latae (in ML), sartorius (in ML), anterior portion of gluteus medius (in SI), and semimembranosus (in SI and ML). JRF estimates at JRF1 or JRF2 were not sensitive to attachment perturbations on other hip muscles.

3.8 Appendix 2. Inter-Model Differences in Individual Hip Muscle Forces

For both DDH and CONT subjects, CT-Geometry models estimated larger forces (than Generic and/or Nonuniform) in iliacus and tensor fasciae latae, as well as smaller forces in gluteus maximus, posterior gluteus medius, and gluteus minimus, at JRF1 and/or JRF2 (¹*Supplemental Tables 3 and 4*). Additionally, CT-Geometry estimated larger forces in gluteus medius (anterior, middle, and total) and smaller force in semimembranosus for DDH only (¹*Supplemental Table 3*), as well as smaller forces in long head of biceps femoris and piriformis for CONT (¹*Supplemental Table 4*). For muscles generating large force ($> 0.5 \times \text{BW}$ at JRF1 or JRF2), including gluteus maximus, gluteus medius, and iliacus, estimates from CT-Geometry were more different from the other models in DDH than in CONT, both by value and statistically (¹*Supplemental Tables 3 and 4*). Lastly, compared to Generic, Nonuniform only estimated marginally smaller forces in the middle portion of gluteus maximus at JRF1 for DDH (¹*Supplemental Table 3*).

3.9 Appendix 3. Inter-Model Differences in Hip Angles and Moments

For DDH, CT-Geometry models had smaller hip flexion and larger adduction at JRF1, as well as larger extension at JRF2, compared to Generic and/or Nonuniform models; while for CONT, CT-Geometry only had larger hip adduction at JRF1 (¹*Supplemental Figure 1*;

Supplemental Table 5). Hip angles were not different between Nonuniform and Generic models at JRF1 or JRF2 for either DDH or CONT.

For DDH, CT-Geometry models had a smaller hip extension moment and larger abduction moment at JRF1, as well as a larger flexion moment and larger abduction moment at JRF2, compared to Generic and/or Nonuniform (¹*Supplemental Figure 2; Supplemental Table 5*). For CONT, CT-Geometry had a smaller extension moment and larger internal rotation moment at JRF1, as well as a larger flexion moment at JRF2 (¹*Supplemental Figure 2; Supplemental Table 5*). Inter-model differences in flexion moments were similar for DDH and CONT, whereas CT-Geometry models had significantly different abduction moments only for DDH and not for CONT. Hip moments were not different between Nonuniform and Generic at JRF1 or JRF2 for either group.

3.10 References

1. Leunig M, Siebenrock KA, Ganz R. Rationale of periacetabular osteotomy and background work. Instr Course Lect. 2001;50:229-38.
2. Gala L, Clohisy JC, Beaulé PE. Hip dysplasia in the young adult. J Bone Joint Surg Am. 2016 Jan 6;98(1):63-73.
3. Henak CR, Abraham CL, Anderson AE, Maas SA, Ellis BJ, Peters CL, Weiss JA. Patient-specific analysis of cartilage and labrum mechanics in human hips with acetabular dysplasia. Osteoarthritis Cartilage. 2014 Feb;22(2):210-7.
4. Cooperman D. What is the evidence to support acetabular dysplasia as a cause of osteoarthritis? J Pediatr Orthop. 2013 Jul-Aug;33 Suppl 1:S2-7.
5. Jessel RH, Zurakowski D, Zilkens C, Burstein D, Gray ML, Kim YJ. Radiographic and patient factors associated with pre-radiographic osteoarthritis in hip dysplasia. J Bone Joint Surg Am. 2009 May;91(5):1120-9.
6. Harris-Hayes M, Royer NK. Relationship of acetabular dysplasia and femoroacetabular impingement to hip osteoarthritis: a focused review. PM R. 2011 Nov;3(11):1055-67.e1.

7. Blemker SS, Asakawa DS, Gold GE, Delp SL. Image-based musculoskeletal modeling: applications, advances, and future opportunities. *J Magn Reson Imaging*. 2007 Feb;25(2):441-51.
8. Neptune RR, Kautz SA, Zajac FE. Contributions of the individual ankle plantar flexors to support, forward progression and swing initiation during walking. *J Biomech*. 2001 Nov;34(11):1387-98.
9. Hamner SR, Seth A, Delp SL. Muscle contributions to propulsion and support during running. *J Biomech*. 2010 Oct 19;43(14):2709-16.
10. Lenhart RL, Thelen DG, Wille CM, Chumanov ES, Heiderscheit BC. Increasing running step rate reduces patellofemoral joint forces. *Med Sci Sports Exerc*. 2014 Mar;46(3):557-64.
11. Correa TA, Baker R, Graham HK, Pandy MG. Accuracy of generic musculoskeletal models in predicting the functional roles of muscles in human gait. *J Biomech*. 2011 Jul 28;44(11):2096-105.
12. Valente G, Pitto L, Testi D, Seth A, Delp SL, Stagni R, Viceconti M, Taddei F. Are subject-specific musculoskeletal models robust to the uncertainties in parameter identification? *PLoS One*. 2014 Nov 12;9(11):e112625.
13. Heller MO, Bergmann G, Deuretzbacher G, Claes L, Haas NP, Duda GN. Influence of femoral anteversion on proximal femoral loading: measurement and simulation in four patients. *Clin Biomech (Bristol, Avon)*. 2001 Oct;16(8):644-9.
14. Lenaerts G, De Groote F, Demeulenaere B, Mulier M, Van der Perre G, Spaepen A, Jonkers I. Subject-specific hip geometry affects predicted hip joint contact forces during gait. *J Biomech*. 2008;41(6):1243-52.
15. Lenaerts G, Bartels W, Gelaude F, Mulier M, Spaepen A, Van der Perre G, Jonkers I. Subject-specific hip geometry and hip joint centre location affects calculated contact forces at the hip during gait. *J Biomech*. 2009 Jun 19;42(9):1246-51.
16. Viceconti M, Testi D, Taddei F, Martelli S, Clapworthy GJ, Jan SV. Biomechanics modeling of the musculoskeletal apparatus: status and key issues. *Proc IEEE*. 2006 Apr 10;94(4):725-39.
17. Wyles CC, Heidenreich MJ, Jeng J, Larson DR, Trousdale RT, Sierra RJ. The John Charnley Award: Redefining the natural history of osteoarthritis in patients with hip dysplasia and impingement. *Clin Orthop Relat Res*. 2017 Feb;475(2):336-50.

18. Clohisy JC, Dobson MA, Robison JF, Warth LC, Zheng J, Liu SS, Yehyaw TM, Callaghan JJ. Radiographic structural abnormalities associated with premature, natural hip-joint failure. *J Bone Joint Surg Am.* 2011 May;93 Suppl 2:3-9.
19. Maquet P. Biomechanics of hip dysplasia. *Acta Orthop Belg.* 1999 Sep;65(3):302-14.
20. Skalhøi O, Iversen CH, Nielsen DB, Jacobsen J, Mechlenburg I, Søballe K, Sørensen H. Walking patterns and hip contact forces in patients with hip dysplasia. *Gait Posture.* 2015 Oct;42(4):529-33.
21. Harris MD, MacWilliams BA, Bo Foreman K, Peters CL, Weiss JA, Anderson AE. Higher medially-directed joint reaction forces are a characteristic of dysplastic hips: A comparative study using subject-specific musculoskeletal models. *J Biomech.* 2017 Mar 21;54:80-7.
22. Wiberg G. Studies on dysplastic acetabula and congenital subluxation of the hip joint with special reference to the complication of osteoarthritis. *Acta Chir Scand.* 1939;83 Suppl 58:7-135.
23. Harris MD, Anderson AE, Henak CR, Ellis BJ, Peters CL, Weiss JA. Finite element prediction of cartilage contact stresses in normal human hips. *J Orthop Res.* 2012 Jul;30(7):1133-9.
24. Winter DA. *Biomechanics and Motor Control of Human Movement.* 3rd ed. Hoboken, NJ: John Wiley & Sons; 2004.
25. Delp SL, Anderson FC, Arnold AS, Loan P, Habib A, John CT, Guendelman E, Thelen DG. OpenSim: open-source software to create and analyze dynamic simulations of movement. *IEEE Trans Biomed Eng.* 2007 Nov;54(11):1940-50.
26. Delp SL, Loan JP, Hoy MG, Zajac FE, Topp EL, Rosen JM. An interactive graphics-based model of the lower extremity to study orthopaedic surgical procedures. *IEEE Trans Biomed Eng.* 1990 Aug;37(8):757-67.
27. Shelburne KB, Decker MJ, Krong J, Torrey MR, Philippon MJ. Muscle forces at the hip during squatting exercise. Poster session presented at: 56th Annual Meeting of the Orthopaedic Research Society. 2010 March 6–9; New Orleans, LA.
28. Netter FH. *Atlas of Human Anatomy.* 6th ed. Philadelphia, PA: W.B. Saunders; 2014.
29. Crowninshield RD, Brand RA. A physiologically based criterion of muscle force prediction in locomotion. *J Biomech.* 1981;14(11):793-801.

30. Anderson FC, Pandy MG. Static and dynamic optimization solutions for gait are practically equivalent. *J Biomech.* 2001 Feb;34(2):153-61.
31. Steele KM, Demers MS, Schwartz MH, Delp SL. 2012. Compressive tibiofemoral force during crouch gait. *Gait Posture.* 35(4):556-60.
32. Delp SL, Maloney W. Effects of hip center location on the moment-generating capacity of the muscles. *J Biomech.* 1993 Apr-May;26(4-5):485-99.
33. Lewis CL, Sahrman SA, Moran DW. 2010. Effect of hip angle on anterior hip joint force during gait. *Gait Posture.* 32(4):603-7.
34. Wesseling M, De Groote F, Bosmans L, Bartels W, Meyer C, Desloovere K, Jonkers I. Subject-specific geometrical detail rather than cost function formulation affects hip loading calculation. *Comput Methods Biomech Biomed Engin.* 2016 Nov;19(14):1475-88.
35. Bosmans L, Wesseling M, Desloovere K, Molenaers G, Scheys L, Jonkers I. Hip contact force in presence of aberrant bone geometry during normal and pathological gait. *J Orthop Res.* 2014 Nov;32(11):1406-15.
36. Handsfield GG, Meyer CH, Hart JM, Abel MF, Blemker SS. Relationships of 35 lower limb muscles to height and body mass quantified using MRI. *J Biomech.* 2014 Feb 7;47(3):631-8.
37. Hicks JL, Uchida TK, Seth A, Rajagopal A, Delp SL. Is my model good enough? Best practices for verification and validation of musculoskeletal models and simulations of movement. *J Biomech Eng.* 2015 Feb 1;137(2):020905.
38. Brand RA, Crowninshield RD, Wittstock CE, Pedersen DR, Clark CR, van Krieken FM. A model of lower extremity muscular anatomy. *J Biomech Eng.* 1982 Nov;104(4):304-10.
39. White SC, Yack HJ, Winter DA. 1989. A three-dimensional musculoskeletal model for gait analysis. Anatomical variability estimates. *J Biomech.* 22(8-9):885-93.

Chapter 4: Dysplastic Hip Anatomy Alters Muscle Moment Arm Lengths, Lines of Action, and Contributions to Joint Reaction Forces during Gait¹

4.1 Abstract

Developmental dysplasia of the hip (DDH) is characterized by abnormal bony anatomy, which causes detrimental hip joint loading and leads to secondary osteoarthritis. Hip joint loading depends, in part, on muscle-induced joint reaction forces (JRFs), and therefore, is influenced by hip muscle moment arm lengths (MALs) and lines of action (LoAs). The current study used subject-specific musculoskeletal models and in-vivo motion analysis to quantify the effects of DDH bony anatomy on dynamic muscle MALs, LoAs, and their contributions to JRF peaks during early (~17%) and late-stance (~52%) of gait. Compared to healthy hips (N = 15, 16-39 y/o), the abductor muscles in patients with untreated DDH (N = 15, 16-39 y/o) had smaller abduction MALs (e.g. anterior gluteus medius, 35.3 vs. 41.6 mm in early stance, 45.4 vs. 52.6 mm late stance, $p \leq 0.01$) and more medially-directed LoAs. Abduction-adduction and rotation MALs also differed for major hip flexors such as rectus femoris and iliacus. The altered MALs in DDH corresponded to higher hip abductor forces, medial JRFs (1.26 vs. $0.87 \times \text{BW}$ early stance, $p = 0.03$), and resultant JRFs (5.71 vs. $4.97 \times \text{BW}$ late stance, $p = 0.05$). DDH anatomy not only affected hip muscle force generation in the primary plane of function, but also their out-of-plane mechanics, which collectively elevated JRFs. Overall, hip muscle MALs and their contributions to JRFs were

¹ Reprinted from: Song K, Gaffney BMM, Shelburne KB, Pascual-Garrido C, Clohisy JC, Harris MD. Dysplastic hip anatomy alters muscle moment arm lengths, lines of action, and contributions to joint reaction forces during gait. J Biomech. 2020 Sep 18;110:109968. *Supplementary data* to Chapter 4 can be found in the online version of the article, doi: 10.1016/j.jbiomech.2020.109968. Rights granted from Elsevier B.V.

significantly altered by DDH bony anatomy. Therefore, to better understand the mechanisms of joint degeneration and improve the efficacy of treatments for DDH, the dynamic anatomy-force relationships and multi-planar functions of the whole hip musculature must be collectively considered.

4.2 Introduction

Developmental dysplasia of the hip (DDH) is characterized by abnormal acetabular and femoral anatomy [1]. When untreated, these abnormalities alter hip intra-articular loading, cause tissue damage, and increase the risk of early secondary osteoarthritis [2,3]. Muscle forces and joint reaction forces (JRFs) are major mechanical contributors to hip joint loading [4], and are found to be altered in patients with untreated DDH [5,6]. It has been speculated that the abnormal bony features of DDH, such as lateralized hip joint centers (HJCs), are the sources of altered muscle-induced loading [7,8], but the relationships that explain how bony anatomy alters muscle and joint forces have not been explicitly established.

Among factors influencing muscle mechanics, the ability of muscles to generate forces and moments around a joint is directly affected by their anatomical paths. Two key mechanical parameters that describe the anatomy-force relationships of muscles are their moment arm lengths (MALs) and lines of action (LoA). MALs, defined as the perpendicular distance from the joint center to the muscle LoA, represent the effectiveness of muscles at generating moments to rotate the joint [9,10]. If a muscle MAL is reduced, higher force from that muscle is needed to generate the same joint moment. LoAs dictate the direction of muscle forces, which affects muscle contributions to loading within the joint [11]. The MALs and LoAs of multiple muscles collectively influence compressive and shear forces borne by the joint [11]. A few radiographic reports and theoretical models have suggested that abnormal bony anatomy in untreated DDH

reduces hip abductor MALs and alters their medio-lateral LoAs in a way that may increase hip articular pressure [8,12]. These studies provided preliminary insight into the links between DDH bony anatomy and muscle-induced joint loading, but were limited to the abductor muscles in a static position. Because muscle paths vary with joint positions, their dynamic force-generating abilities induce variable joint loading during an activity, and therefore lead to motion-specific risks for tissue damage. However, no study has reported MALs and LoAs in patients with untreated DDH during dynamic motions, and how they collectively contribute to hip JRFs.

Because muscle forces cannot be measured directly during motion, musculoskeletal models have been used to quantify dynamic hip muscle MALs and LoAs [13-15] and their contributions to JRFs [16-18]. The default generic geometry in most musculoskeletal models represents healthy bony anatomy, which makes such models less reliable for estimating muscle mechanics in populations with anatomical deformities [16]. Therefore, including subject-specific anatomy is important for estimating hip mechanics in DDH [19], and has helped elucidate significant hip JRF differences compared to healthy controls [6]. However, these recent models of DDH fell short of establishing the underlying relationships between the muscle-induced hip joint loading (e.g. JRFs) of DDH and the bony deformity. As such, the potentially vital roles of muscle anatomy-force parameters (MALs, LoAs) in the patho-mechanics of DDH also remain unclear.

The objective of this study was to quantify how hip muscle MALs, LoAs, and their contributions to hip JRFs during gait are altered in patients with untreated DDH compared to healthy controls. We hypothesized that patients with DDH would have smaller hip abductor MALs and more medially-directed LoAs due to lateralized HJCs [7], which would result in higher medially-directed hip muscle forces and JRFs [6].

4.3 Methods

4.3.1 Subjects and Data Collection

With Institutional Review Board approval and informed consent, 15 female patients with untreated DDH (age: 16-39 y/o) and 15 female healthy controls (age: 16-39 y/o) were included (**Table 4.1**). An a priori power analysis [20] based on prior hip JRF findings [6] indicated 15 subjects per group could detect inter-group differences with power of 0.8. Patients were diagnosed by a single orthopaedic surgeon, had hip pain lasting at least 3 months, and radiographic evidence of DDH determined by a lateral center edge angle $<20^\circ$ [21]. For each DDH patient, the symptomatic hip was chosen for analysis. Healthy controls had no self-reported history of hip pathology, and no pain or discomfort during a flexion-adduction-internal-rotation clinical screening exam [22]. A random side was chosen for comparison with DDH patients. Both groups had no previous hip surgeries, other lower extremity diseases, or pain that limited functional activities. Magnetic resonance (MR) images were collected from the psoas major muscle origin to the knees using a 3T scanner (VIDA, Siemens AG; Munich, Germany) with T1-weighted VIBE gradient-echo sequences and SPAIR fat suppression ($1 \times 1 \times 1$ mm voxels). During imaging, subjects were prone with the hip positioned at approximately zero degrees flexion, adduction, and rotation. From the MR images, 3D geometries of the pelvis and femurs for each subject were reconstructed using Amira software (Thermo Fisher Scientific, Houston, TX).

Full-body gait data were collected using 70 retro-reflective markers while subjects walked at a self-selected speed on an instrumented treadmill (Bertec; Columbus, OH), with a 5-minute warm-up [23]. Marker trajectories were collected at 100 Hz using 10 infrared cameras (Vicon; Centennial, CO). Ground reaction forces were collected at 2000 Hz by the treadmill. Fourth-order Butterworth low-pass filters were applied to marker data using an 8 Hz cutoff determined with

residual analysis [24], and a 6 Hz cutoff for force data to reduce analog noise on instrumented treadmills [25].

Table 4.1. Demographics, gait speed, and normalized HJC ML location (mean \pm SD) for Healthy and DDH subjects.

Demographics	Healthy (N = 15)	DDH (N = 15)	<i>p</i> -value
Age (years)	24.6 \pm 6.3	26.5 \pm 7.9	0.62
Height (m)	1.67 \pm 0.06	1.66 \pm 0.07	0.85
Mass (kg)	61.9 \pm 7.8	62.7 \pm 9.3	0.79
BMI (kg/m ²)	22.3 \pm 2.3	22.7 \pm 2.4	0.64
Walking speed (m/s)	1.39 \pm 0.15	1.37 \pm 0.15	0.59
Normalized HJC ML location (%)	77.2% \pm 8.6%	88.4% \pm 10.2%	< 0.01

Note: Normalized HJC ML location = ML location of HJC / ML distance between anterior superior iliac spine and mid-sagittal plane.

4.3.2 Musculoskeletal Modeling

Subject-specific musculoskeletal models were created from an existing OpenSim model [26], similar to procedures recently described [19]. The generic model was modified by adding torso and hip external rotator muscles (**Table 4.2**) with experimental-based paths and strengths [27,28], yielding 98 muscle-tendon actuators. Then, MR-based 3D pelvis and femur geometries were substituted into the model for each subject (**Figure 4.1A**). HJCs were moved to subject-specific locations, determined as the centroid of a sphere fit to the 3D-reconstructed femoral head [6]. Each MR femur was then rotated about the subject-specific HJC until the femoral shaft axis and the distal trans-epicondyle axis were both aligned to the generic geometries.

Origin and insertion sites of the hip muscles were then updated on the subject-specific pelvis and femurs based on reconstructed bone-muscle geometries, MR images, and anatomical guidelines [29] (**Figure 4.1A**). Via points approximating nonlinear muscle paths (e.g. tensor fasciae latae) and wrapping objects for the iliacus and psoas major muscles were also updated,

using the MR images as a guide [30]. The remaining model segments were non-uniformly scaled in antero-posterior (AP), supero-inferior (SI), and medio-lateral (ML) dimensions using experimental marker data. Muscle optimal fiber lengths and tendon slack lengths were linearly scaled from the generic model according to the total length of updated muscle paths in each subject-specific model [30], which assumed no muscle architecture adaptations (e.g. sarcomere loss) had occurred due to the DDH anatomy.

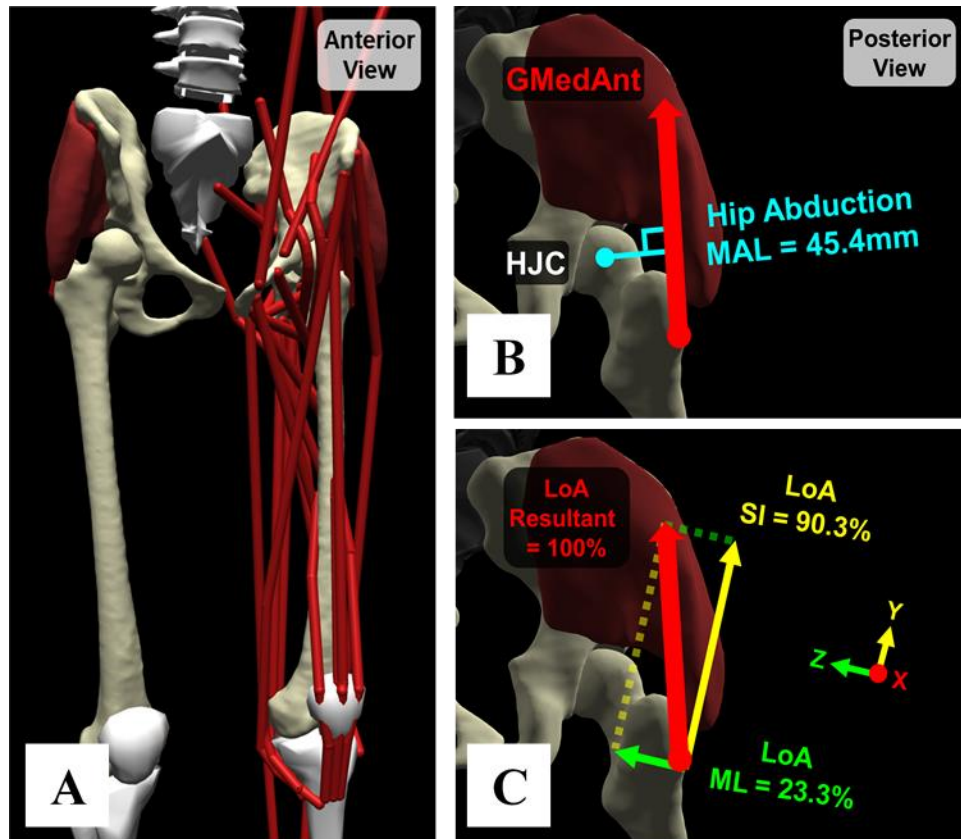


Figure 4.1. (A) Example model with subject-specific pelvis and femur geometries, HJC locations, and muscle paths. (B) Example hip muscle MAL (anterior gluteus medius, “GMedAnt”, red arrow). Hip flexion, abduction, and rotation MALs were extracted across an entire gait cycle. (C) Example hip muscle LoAs. The AP, SI, and ML components of each muscle’s LoA represent the percentage of its net force in a certain direction within the pelvis frame.

Hip and pelvis angles were calculated via inverse kinematics, and internal hip moments were calculated via inverse dynamics [24], for each subject across a representative gait cycle. Residual reduction was applied to minimize the nonphysical residual forces and moments and

maintain dynamic consistency within inverse dynamics results [31]. Muscle forces were estimated using static optimization that minimized the sum-square of muscle activations [32]. The forces of individual hip muscles were then summed by functional groups [26,27] (**Table 4.2**). Lastly, resultant hip JRFs and AP, SI, ML directional components were calculated from muscle forces [33] and expressed in the pelvis frame to represent loading on the acetabulum.

Table 4.2. Hip muscle functional group definitions.

Hip Muscle Group	Individual muscles included (alphabetic order)
Hip Flexors	adductor brevis, adductor longus, gluteus minimus (anterior), gracillis, iliacus, *pectineus, psoas major, rectus femoris, sartorius, tensor fasciae latae
Hip Extensors	adductor magnus (distal and ischial), biceps femoris long head, gluteus maximus, gluteus medius (middle and posterior), gluteus minimus (posterior), semimembranosus, semitendinosus
Hip Abductors	gluteus maximus (anterior), gluteus medius, gluteus minimus, piriformis, sartorius, tensor fasciae latae
Hip Adductors	adductor brevis, adductor longus, adductor magnus, gluteus maximus (posterior), gracillis, obturator externus, *pectineus, quadratus femoris
Hip Internal Rotators	adductor brevis, adductor longus, adductor magnus (ischial), gluteus medius (anterior), gluteus minimus (anterior), *pectineus, tensor fasciae latae
Hip External Rotators	*gemelli, gluteus maximus, gluteus medius (posterior), gluteus minimus (posterior), *obturator externus, *obturator internus, piriformis, *quadratus femoris

*Hip muscles added to the generic OpenSim musculoskeletal model. Torso muscles were also added to the model, including erector spinae, external oblique, internal oblique, and rectus abdominis [27].

Subject-specific MALs and LoAs for all hip muscles were extracted across the entire gait cycle. Dynamic muscle MALs (**Figure 4.1B**) were computed within OpenSim using a generalized force approach [10]. Hip muscle LoAs were extracted using an established method [17] and expressed as unit vectors with AP, SI, and ML components in the pelvis frame (**Figure 4.1C**). Individual muscle forces were decomposed along each LoA component to determine the

proportion of that muscle's net force in the AP, SI, ML directions. These three muscle force components were also each summed by functional groups.

4.3.3 Model Validation

The subject-specific models were validated using established methods [34]. First, model-estimated muscle activations were compared to surface electromyography (EMG) signals. EMG during gait was collected from bilateral gluteus maximus, gluteus medius, rectus femoris, tensor fasciae latae, biceps femoris long head, vastus lateralis, medial gastrocnemius, and erector spinae, following SENIAM guidelines [35]. Signals were recorded at 2000 Hz using a 16-channel system (MA300-XVI, Motion Lab Systems Inc.; Baton Rouge, LA), shifted by 1.2 ms to offset wireless latency, band-pass filtered with 10-350 Hz cutoffs, rectified, and smoothed with a 10 Hz fourth-order Butterworth low-pass filter [36]. Model-estimated muscle activations from static optimization were reported on a scale of 0 (none) to 1 (maximum). For comparison, EMG signals in each trial were also normalized to a 0-to-1 scale relative to the maximum within that trial [33]. Second, model errors and residuals were ensured to be within limits recommended for gait simulations [34], for both motion tracking (root-mean-square marker error < 2 cm) and static optimization (residual force < 5% \times BW, moment < 0.5 Nm/kg). Finally, estimated hip JRFs and muscle forces were qualitatively compared to recent subject-specific modeling studies to ensure they are within 2 standard deviations of previously reported values [6,18,19,30,34].

4.3.4 Data Analysis

Hip muscle LoAs, MALs, individual and grouped muscle forces, hip JRFs, as well as joint angles and moments were time-normalized to the gait cycle. JRFs and muscle forces were normalized by body weight (\times BW), while joint moments were normalized by body mass (Nm/kg) [37]. Peak resultant hip JRFs in early stance (~17% of gait cycle, termed 'JRF1') and late stance

(~52% of gait cycle, termed ‘JRF2’) were determined, as well as joint angles and moments at these two time points. LoAs, MALs and forces for all muscles crossing the analyzed hip (**Table 4.2**) were extracted at JRF1 and JRF2. Within each functional group, the muscles that produced the maximum force at JRF1 or JRF2 were categorized as the primary dependent variables for statistical comparisons. The other individual muscles were categorized as secondary variables.

All variables were examined with the Shapiro-Wilk test for normality and Levene’s test for homogeneity of variance. Normally distributed variables were compared between Healthy and DDH groups using independent *t*-tests, with corrections for unequal variances. Other variables were compared non-parametrically using Mann-Whitney *U* tests. Statistical significance for each test was $\alpha = 0.05$. Effect sizes for inter-group differences were determined with Cohen’s *d* [38] and classified as small ($0.2 \leq d < 0.5$), medium ($0.5 \leq d < 0.8$), or large ($d \geq 0.8$). Primary variables compared between DDH and Healthy were LoAs, MALs, and forces of muscles selected from each functional group, and hip JRFs. Secondary variables were LoAs, MALs, and forces of other individual muscles, as well as joint angles and moments. To further quantify the bony features of untreated DDH that may directly influence muscle anatomy-force relationships, especially the relative lateralization of HJCs [7], the ML location of HJC was normalized by the ML distance between the anterior superior iliac spine and the mid-sagittal plane, then compared between groups. The depth, height, and width of the pelvises were also compared between the DDH and Healthy subjects.

4.4 Results

4.4.1 Subject Characteristics and Model Validation

There were no significant differences between DDH and Healthy groups in age, height, mass, body-mass index, walking speed (**Table 4.1**), and pelvis dimensions. Compared to Healthy

subjects, HJCs were significantly lateralized in DDH. Model-estimated muscle activation qualitatively agreed with EMG timings (¹*Supplemental Figure 1*). Model motion tracking errors, residual forces and moments were under 2 cm, $0.025 \times \text{BW}$ and 0.4 Nm/kg, respectively (¹*Supplemental Figure 2*). Hip muscle forces and JRFs were in ranges similar to recent subject-specific modeling studies.

Table 4.3. Dynamic MALs and LoAs (mean \pm SD) for major force-generating hip muscles with significant differences (shaded) between DDH and Healthy groups. LoA expressed as percentage (%) of net muscle force.

		At JRF1				At JRF2			
Hip MAL (mm)		Healthy	DDH	<i>p</i> -value	Cohen's <i>d</i>	Healthy	DDH	<i>p</i> -value	Cohen's <i>d</i>
Gluteus Medius (anterior section)	Flexion	6.3 \pm 6.4	6.1 \pm 7.6	0.94	0.03	-7.0 \pm 7.2	-6.3 \pm 9.1	0.82	0.08
	Adduction	-41.6 \pm 5.9	-35.3 \pm 6.4	0.01	1.02	-52.6 \pm 4.0	-45.4 \pm 4.8	< 0.01	1.63
	Rotation	24.5 \pm 5.7	21.9 \pm 4.8	0.19	0.49	0.1 \pm 3.9	0.2 \pm 6.4	0.51	0.03
Rectus Femoris	Flexion	40.6 \pm 5.7	40.6 \pm 4.8	1.00	0.00	29.4 \pm 2.1	29.9 \pm 2.5	0.58	0.20
	Adduction	-4.4 \pm 4.4	1.9 \pm 4.6	< 0.01	1.41	-7.9 \pm 4.5	-0.4 \pm 4.9	< 0.01	1.60
	Rotation	-0.5 \pm 0.7	0.3 \pm 0.9	0.02	0.95	-1.2 \pm 0.5	-0.3 \pm 0.7	< 0.01	1.41
Iliacus	Flexion	34.0 \pm 3.2	35.2 \pm 2.6	0.27	0.41	31.6 \pm 3.5	31.3 \pm 3.1	0.80	0.09
	Adduction	2.0 \pm 3.3	6.5 \pm 3.6	< 0.01	1.30	-2.4 \pm 3.0	2.6 \pm 3.7	< 0.01	1.46
	Rotation	6.9 \pm 3.1	3.8 \pm 3.3	0.01	0.95	8.0 \pm 3.4	5.0 \pm 3.1	0.02	0.93
Tensor Fasciae Latae	Flexion	54.1 \pm 10.2	57.3 \pm 6.8	0.32	0.37	27.0 \pm 9.4	31.9 \pm 9.4	0.16	0.52
	Adduction	-38.4 \pm 8.4	-27.5 \pm 10.1	< 0.01	1.19	-47.1 \pm 8.6	-34.9 \pm 10.5	< 0.01	1.28
	Rotation	19.8 \pm 4.8	21.0 \pm 5.9	0.54	0.23	-0.9 \pm 3.6	2.0 \pm 4.9	0.07	0.68
Muscle LoA (%)		Healthy	DDH	<i>p</i> -value	Cohen's <i>d</i>	Healthy	DDH	<i>p</i> -value	Cohen's <i>d</i>
Gluteus Maximus (anterior section)	(+) AP (-)	-51.5 \pm 15.7	-41.7 \pm 10.5	0.09	0.73	-37.5 \pm 13.5	-29.8 \pm 8.0	0.17	0.70
	(+) SI (-)	80.4 \pm 10.1	84.2 \pm 4.6	0.57	0.49	78.1 \pm 6.1	78.8 \pm 4.8	0.72	0.13
	(+) ML (-)	22.1 \pm 12.0	31.5 \pm 7.9	0.02	0.92	47.1 \pm 8.6	52.8 \pm 6.2	0.05	0.75

Note: Positive values indicate hip flexion, adduction, or internal rotation MALs.

4.4.2 Hip Muscle MALs and LoAs

Compared to Healthy, DDH subjects had significantly different hip abduction-adduction and rotation MALs (Table 4.3, Figure 4.2). Specifically, abduction MALs were smaller for the primary hip abductors (e.g. gluteus medius, $p \leq 0.03$, $d \geq 0.83$), and flipped from abduction to adduction roles for the flexors (e.g. iliacus, $p < 0.01$, $d \geq 1.30$) throughout stance. Additionally, internal rotation MALs of the iliacus were significantly smaller in DDH ($p \leq 0.02$, $d \geq 0.93$). Hip flexion-extension MALs were not different between groups for any muscle.

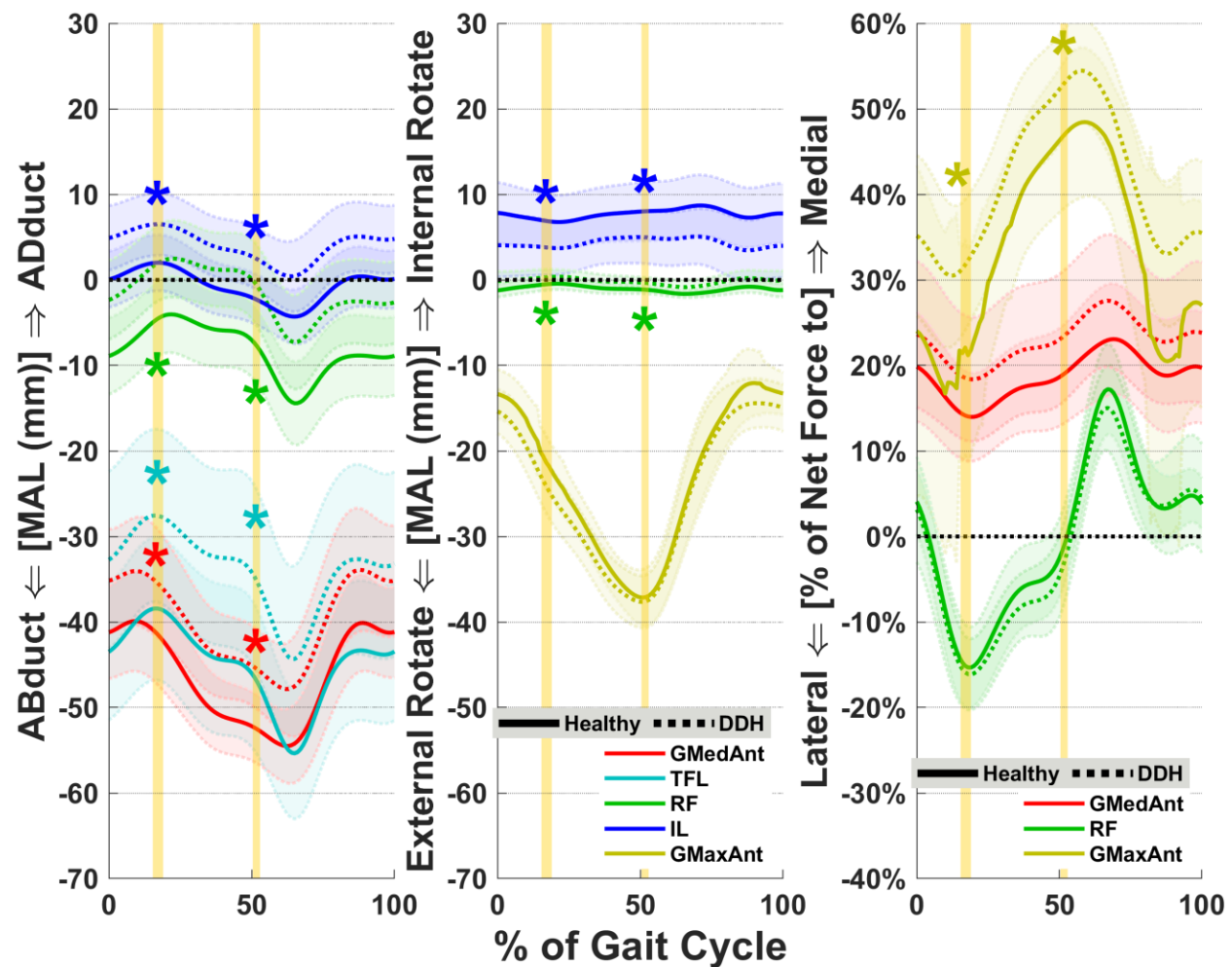


Figure 4.2. Average muscle MALs (left and center) and LoAs (right) for major hip abductors, flexors, and external rotators. Shades represent ± 1 SD. Vertical highlighted areas indicate the times of JRF peaks in early stance (JRF1) and late stance (JRF2). “*” indicates statistical inter-group significance. GMedAnt, anterior gluteus medius; TFL, tensor fasciae latae; RF, rectus femoris; IL, iliacus; GMaxAnt, anterior gluteus maximus.

For DDH subjects, muscle LoAs significantly differed for the gluteus maximus, which was directed more medially compared to Healthy ($p = 0.02$, $d = 0.92$ at JRF1; **Table 4.3**, **Figure 4.2**). No other LoAs were significantly different between DDH and Healthy groups, although the anterior section of gluteus medius also trended towards a more medial orientation in DDH at JRF1 ($p = 0.06$, $d = 0.71$; ¹*Supplemental Table 2*).

4.4.3 Hip Muscle Forces and JRFs

Resultant muscle forces differed between DDH and Healthy for the hip abductors and internal rotators. Abductor forces were significantly higher in the DDH group throughout stance ($p \leq 0.02$, $d \geq 0.88$; **Figure 4.3**). Internal rotator forces were also higher in DDH ($p \leq 0.04$, $d \geq 0.78$), as many concurrently served abductor roles (**Table 4.2**). Muscle force components were also higher in the DDH group for both abductors and internal rotators in the superior and medial directions ($p \leq 0.05$, $d \geq 0.76$), as well as for internal rotators in the anterior direction ($p = 0.02$, $d = 0.96$ at JRF2) (**Figure 4.3**). Additionally, the flexors and external rotators had higher medial forces at JRF1 ($p \leq 0.05$, $d \geq 0.52$). For individual hip muscles, the DDH group had higher forces (resultant and each component) from gluteus medius throughout stance ($p \leq 0.04$, $d \geq 0.77$; **Figure 4.4**), and tensor fasciae latae at JRF2 ($p < 0.01$, $d \geq 1.32$).

Finally, hip JRFs were different between the DDH and Healthy groups (**Figure 4.3**). The DDH group had significantly higher medial hip JRFs at JRF1 ($p = 0.03$, $d = 0.82$), and significantly higher resultant and superior JRFs at JRF2 ($p \leq 0.05$, $d \geq 0.76$).

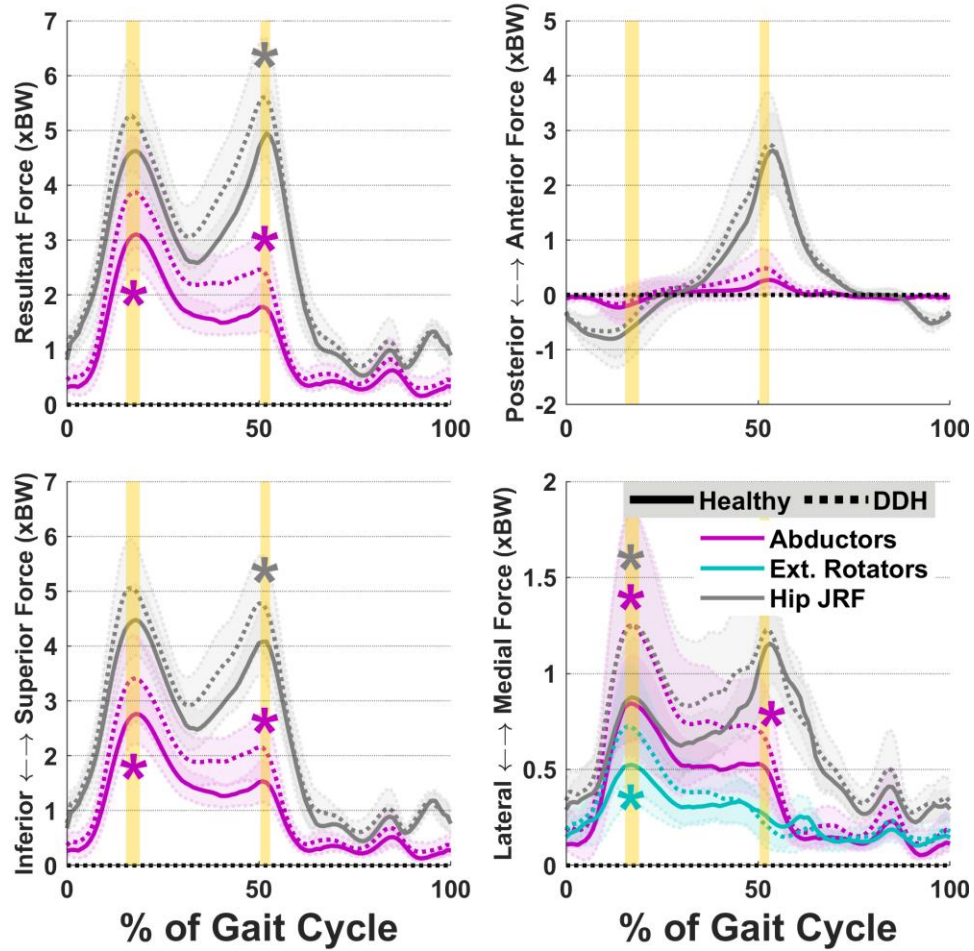


Figure 4.3. Average hip JRF components overlaid with abductor and external rotator muscle forces. Internal rotator forces (not shown) followed similar patterns to abductors. Shades represent ± 1 SD. Vertical highlighted areas indicate the times of hip JRF peaks. “*” indicates statistical inter-group significance.

4.4.4 Angles and Moments

During late stance (at JRF2), DDH subjects had a slightly adducted hip, instead of slightly abducted for Healthy ($1.2^\circ \pm 2.8^\circ$ vs. $-1.4^\circ \pm 2.6^\circ$, $p = 0.01$, $d = 0.95$). Also, the pelvis obliquity was towards the ipsilateral side for DDH subjects, rather than towards contralateral for Healthy ($1.2^\circ \pm 2.2^\circ$ vs. $-1.1^\circ \pm 1.8^\circ$, $p < 0.01$, $d = 1.15$). Other hip and pelvis angles, and hip moments were not different between groups.

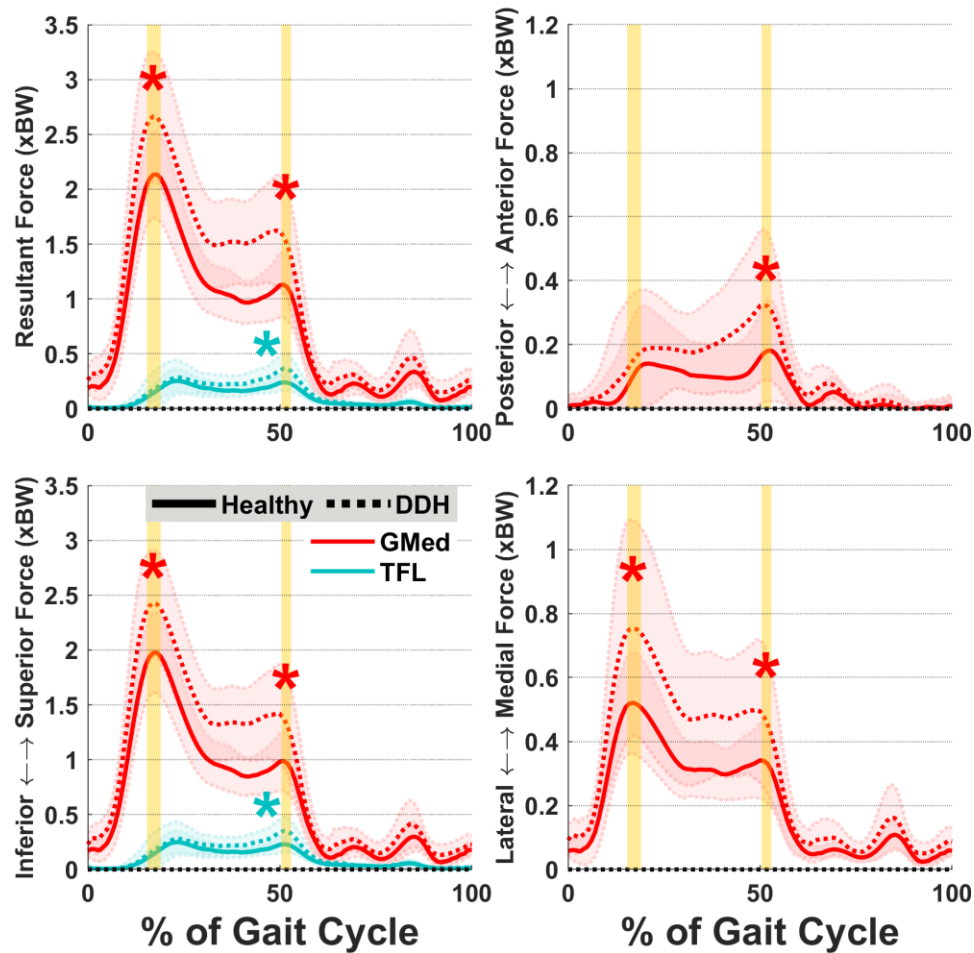


Figure 4.4. Average forces for the gluteus medius (GMed) and tensor fasciae latae (TFL) muscles. Three individual muscles had force differences between DDH and Healthy: gluteus medius, tensor fasciae latae (resultant and superior only), and gluteus minimus (similar patterns to gluteus medius). Shades represent ± 1 SD. Vertical highlighted areas indicate the times of hip JRF peaks. “*” indicates statistical inter-group significance.

4.5 Discussion

The objective of this study was to quantify how hip muscle MALs, LoAs, and their contributions to hip JRFs during gait are altered in patients with untreated DDH compared to healthy controls. Patients with DDH demonstrated differences in both muscle anatomy (MAL, LoA) and joint mechanics (muscle force, JRF). The differences were most substantial for the hip abductor muscles, where smaller MALs corresponded to higher forces and contributions to JRFs especially in the medial direction, which supported our hypothesis. Furthermore, the inter-group

differences for hip flexors and rotators exhibited how DDH alters their multi-planar functions, which suggested these muscles also contribute to atypical joint loading.

A prominent effect of the DDH bony anatomy was the shortening of dynamic MALs for the hip abductors. The abductor MALs in patients with DDH were smaller than healthy controls throughout the gait cycle, which suggest that static image-based measurements of gluteus medius MALs hold true during dynamic motions [12]. The primary cause of the shortened MALs was the significantly more lateral HJC locations in untreated DDH compared to healthy hips. Shorter MALs indicate a mechanical disadvantage for the abductors, which must produce higher forces to generate the joint moment needed for hip stabilization during stance [8,39], thereby elevating hip JRFs. Thus, to reduce hip loading in DDH, it is important to correct the shortened abductor MALs, which can be accomplished by medializing the HJC [40].

Higher abductor forces may also be due to the frontal-plane MALs of the surrounding hip muscles. Three-dimensional hip motions are dependent on all muscles that span the joint, including secondary muscle functions such as the abducting effects of rectus femoris [39]. For DDH subjects, almost all hip muscles had less abducting or more adducting MALs compared to healthy (e.g. iliacus and rectus femoris; **Table 4.3**). Such changes in MALs altered the relative demands on each muscle to collectively produce the hip-stabilizing abduction moment (which did not differ between groups) during single-leg support. For example, while the iliacus and rectus femoris produced high forces to propel the hip forward (¹*Supplemental Table 3*), they also had an abnormal adducting effect that was then balanced by elevated hip abductor forces.

The rotation MALs of large hip muscles may also indirectly influence force production by adjacent smaller muscles, especially those with multi-planar functions. For example, the force

from iliacus primarily contributes to hip flexion moments during gait. However, due to the shortened internal rotation MAL of iliacus, the tensor fasciae latae compensated with a higher-than-normal force to meet the net moment required for late-stance hip rotation [39]. Therefore, due to the 3D muscle paths and out-of-plane mechanics, relative contributions among adjacent muscles are integral to altered joint mechanics in the presence of DDH anatomy.

Hip muscle LoAs were less affected by the bony anatomy of untreated DDH compared to MALs. Patients with DDH had significantly more medial LoAs compared to healthy only for the gluteus maximus, although the LoAs of gluteus medius also trended towards a more medial orientation. We attribute these differences to the lateralized HJC and shape variability of the proximal femur where the gluteal muscles insert [41]. The altered LoAs of gluteal muscles meant a higher percentage of their forces were directed medially. Therefore, to lower the elevated medial hip JRFs, reducing the dynamic medial LoAs of these muscles (e.g. via HJC medialization) may be important for clinical interventions of DDH.

The dynamic force-generating ability of hip muscles may also be affected by joint positions [13]. For this cohort of patients with untreated DDH, there was a significant yet small ($\sim 2\text{-}3^\circ$) difference in hip adduction and pelvis obliquity during late stance. Hip adduction and opposite pelvis drop may be related to abductor muscle weakness [42,43], and may further influence their abduction MALs. However, it remains inconclusive whether such small kinematic differences are generalizable to the DDH population, or if they alter muscle mechanics in a clinically meaningful way.

Altered hip muscle anatomy or forces in DDH may not always propagate to JRF differences compared to healthy hips across the whole gait cycle. Our earlier modeling study of untreated

DDH also found higher medially-directed JRFs, along with higher hip abductor muscle forces, in late stance of barefoot over-ground gait [6]. Harris et al. speculated that abductor MALs were a cause of increased medial JRFs, which was confirmed by findings in the current study. In the current DDH cohort, increased abductor forces accompanied higher resultant hip JRFs only in late stance, and medial JRFs only in early stance. The contrast of hip JRF findings may be related to the gait mechanics during treadmill versus over-ground walking [25]. Nonetheless, both studies identified simultaneous elevations in hip abductor forces and medial JRFs, indicating such mechanical traits of DDH hold true while walking on flat surfaces.

Several limitations of this study must be considered. First, while we improved upon the generic model geometry by using MR-based bone-muscle anatomy, personalization of the muscle paths was limited to the static position within the MR images. Thus, inherent uncertainty exists in the model-estimated muscle paths through dynamic motions. Second, the models assumed the hip to be a rotation-only ball and socket joint. Hips with DDH may have increased instability [1], which could induce subtle translations that change dynamic MALs and LoAs. Since hips with untreated DDH primarily lack lateral femoral coverage [44], such instability would be most evident in the lateral direction, which would further reduce the abductor MALs. Third, we adopted and generically scaled muscle architecture parameters (e.g. fiber lengths) in our models, given that subject-specific data were unavailable. The altered muscle paths in presence of untreated DDH anatomy could potentially lead to architectural changes, which would further affect muscle force generation and contributions to joint loading. Likewise, the efficacy of treatments for DDH may also depend on their influence on hip muscle architecture. However, our findings suggest that hip muscle MALs can already be significantly altered by DDH anatomy even in the absence of architectural adaptation. Fourth, our study was limited to gait, which is primarily a sagittal motion.

It is possible that the dynamic muscle MALs, LoAs and forces in frontal and transverse planes, which were different in hips with DDH, would be further altered during multi-planar tasks such as squatting and pivoting. Lastly, while all of our DDH cohort had radiographically confirmed dysplasia, there was some heterogeneity in the severity of their bony deformities. Future research is needed to specify whether the mechanical roles of muscle MALs and LoAs change with DDH severity.

In conclusion, hip muscle MALs and contributions to JRFs were significantly altered by the abnormal bony anatomy of untreated DDH, while muscle LoAs were affected to a lesser extent. Patients with DDH demonstrated shorter hip abductor MALs than healthy controls, which corresponded to higher abductor forces. Such elevated forces are likely required to stabilize the hip in the presence of abnormal bony anatomy. Out-of-plane muscle MALs and medio-lateral LoAs also contributed to joint loading primarily in the medial direction. Thus, to better understand the mechanisms of joint degeneration and improve the efficacy of treatments for DDH, future research and interventions should collectively consider the dynamic anatomy-force relationships of the whole hip musculature and their multi-planar functions.

4.6 Acknowledgments

The authors do not have any financial or personal conflict of interest to disclose that could otherwise inappropriately influence or bias this work. This project was supported by the National Institutes of Health K01AR072072, P30AR074992 and the Lottie Caroline Charitable Trust. The research content herein is solely the responsibility of the authors and does not necessarily represent the official views of the National Institutes of Health. The authors thank Molly C. Shepherd for assistance with MR image data processing.

4.7 References

1. Wyles CC, Heidenreich MJ, Jeng J, Larson DR, Trousdale RT, Sierra RJ. The John Charnley Award: Redefining the natural history of osteoarthritis in patients with hip dysplasia and impingement. *Clin Orthop Relat Res*. 2017 Feb;475(2):336-50.
2. Groh MM, Herrera J. A comprehensive review of hip labral tears. *Curr Rev Musculoskelet Med*. 2009 Jun;2(2):105-17.
3. Lewis CL, Sahrman SA. Acetabular labral tears. *Phys Ther*. 2006 Jan;86(1):110-21.
4. Correa TA, Crossley KM, Kim HJ, Pandy MG. Contributions of individual muscles to hip joint contact force in normal walking. *J Biomech*. 2010 May 28;43(8):1618-22.
5. Skalskøi O, Iversen CH, Nielsen DB, Jacobsen J, Mechlenburg I, Søballe K, Sørensen H. Walking patterns and hip contact forces in patients with hip dysplasia. *Gait Posture*. 2015 Oct;42(4):529-33.
6. Harris MD, MacWilliams BA, Bo Foreman K, Peters CL, Weiss JA, Anderson AE. Higher medially-directed joint reaction forces are a characteristic of dysplastic hips: A comparative study using subject-specific musculoskeletal models. *J Biomech*. 2017 Mar 21;54:80-7.
7. Cheng R, Zhang H, Kernkamp WA, Zheng J, Dai K, Yao Y, Wang L, Tsai TY. Relations between the Crowe classification and the 3D femoral head displacement in patients with developmental dysplasia of the hip. *BMC Musculoskelet Disord*. 2019 Nov 11;20(1):530.
8. Maquet P. Biomechanics of hip dysplasia. *Acta Orthop Belg*. 1999 Sep;65(3):302-14.
9. Pandy MG. Moment arm of a muscle force. *Exerc Sport Sci Rev*. 1999;27:79-118.
10. Sherman MA, Seth A, Delp SL. What is a moment arm? Calculating muscle effectiveness in biomechanical models using generalized coordinates. *Proc ASME Des Eng Tech Conf*. 2013 Aug;2013:V07BT10A052.
11. Yanagawa T, Goodwin CJ, Shelburne KB, Giphart JE, Torry MR, Pandy MG. Contributions of the individual muscles of the shoulder to glenohumeral joint stability during abduction. *J Biomech Eng*. 2008 Apr;130(2):021024.
12. Liu R, Wen X, Tong Z, Wang K, Wang C. Changes of gluteus medius muscle in the adult patients with unilateral developmental dysplasia of the hip. *BMC Musculoskelet Disord*. 2012 Jun 15;13:101.
13. Delp SL, Hess WE, Hungerford DS, Jones LC. Variation of rotation moment arms with hip flexion. *J Biomech*. 1999 May;32(5):493-501.

14. Arnold AS, Salinas S, Asakawa DJ, Delp SL. Accuracy of muscle moment arms estimated from MRI-based musculoskeletal models of the lower extremity. *Comput Aided Surg.* 2000;5(2):108-19.
15. Blemker SS, Delp SL. Three-dimensional representation of complex muscle architectures and geometries. *Ann Biomed Eng.* 2005 May;33(5):661-73.
16. Scheys L, Van Campenhout A, Spaepen A, Suetens P, Jonkers I. Personalized MR-based musculoskeletal models compared to rescaled generic models in the presence of increased femoral anteversion: effect on hip moment arm lengths. *Gait Posture.* 2008 Oct;28(3):358-65.
17. van Arkel RJ, Modenese L, Phillips AT, Jeffers JR. Hip abduction can prevent posterior edge loading of hip replacements. *J Orthop Res.* 2013 Aug;31(8):1172-9.
18. Wesseling M, Meyer C, De Groote F, Corten K, Simon JP, Desloovere K, Jonkers I. Gait alterations can reduce the risk of edge loading. *J Orthop Res.* 2016 Jun;34(6):1069-76.
19. Song K, Anderson AE, Weiss JA, Harris MD. Musculoskeletal models with generic and subject-specific geometry estimate different joint biomechanics in dysplastic hips. *Comput Methods Biomech Biomed Engin.* 2019 Feb;22(3):259-70.
20. Faul F, Erdfelder E, Lang AG, Buchner A. G*Power 3: a flexible statistical power analysis program for the social, behavioral, and biomedical sciences. *Behav Res Methods.* 2007 May;39(2):175-91.
21. Wiberg G. Studies on dysplastic acetabula and congenital subluxation of the hip joint with special reference to the complication of osteoarthritis. *Acta Chir Scand.* 1939;83 Suppl 58:7-135.
22. MacDonald SJ, Garbuz D, Ganz R. Clinical evaluation of the symptomatic young adult hip. *Semin Arthroplasty.* 1997 Jan;8(1):3-9.
23. Zeni JA Jr, Higginson JS. Gait parameters and stride-to-stride variability during familiarization to walking on a split-belt treadmill. *Clin Biomech (Bristol, Avon).* 2010 May;25(4):383-6.
24. Winter DA. *Biomechanics and Motor Control of Human Movement.* 3rd ed. Hoboken, NJ: John Wiley & Sons; 2004.
25. Pickle NT, Grabowski AM, Auyang AG, Silverman AK. The functional roles of muscles during sloped walking. *J Biomech.* 2016 Oct 3;49(14):3244-51.

26. Lai AKM, Arnold AS, Wakeling JM. Why are antagonist muscles co-activated in my simulation? A musculoskeletal model for analysing human locomotor tasks. *Ann Biomed Eng.* 2017 Dec;45(12):2762-74.
27. Shelburne KB, Decker MJ, Krong J, Torry MR, Philippon MJ. Muscle forces at the hip during squatting exercise. Poster session presented at: 56th Annual Meeting of the Orthopaedic Research Society. 2010 March 6–9; New Orleans, LA.
28. Handsfield GG, Meyer CH, Hart JM, Abel MF, Blemker SS. Relationships of 35 lower limb muscles to height and body mass quantified using MRI. *J Biomech.* 2014 Feb 7;47(3):631-8.
29. Netter FH. *Atlas of Human Anatomy*. 6th ed. Philadelphia, PA: W.B. Saunders; 2014.
30. Wesseling M, De Groote F, Bosmans L, Bartels W, Meyer C, Desloovere K, Jonkers I. Subject-specific geometrical detail rather than cost function formulation affects hip loading calculation. *Comput Methods Biomech Biomed Engin.* 2016 Nov;19(14):1475-88.
31. Delp SL, Anderson FC, Arnold AS, Loan P, Habib A, John CT, Guendelman E, Thelen DG. OpenSim: open-source software to create and analyze dynamic simulations of movement. *IEEE Trans Biomed Eng.* 2007 Nov;54(11):1940-50.
32. Anderson FC, Pandy MG. Static and dynamic optimization solutions for gait are practically equivalent. *J Biomech.* 2001 Feb;34(2):153-61.
33. Steele KM, Demers MS, Schwartz MH, Delp SL. 2012. Compressive tibiofemoral force during crouch gait. *Gait Posture.* 35(4):556-60.
34. Hicks JL, Uchida TK, Seth A, Rajagopal A, Delp SL. Is my model good enough? Best practices for verification and validation of musculoskeletal models and simulations of movement. *J Biomech Eng.* 2015 Feb 1;137(2):020905.
35. Hermens HJ, Freriks B, Disselhorst-Klug C, Rau G. Development of recommendations for SEMG sensors and sensor placement procedures. *J Electromyogr Kinesiol.* 2000 Oct;10(5):361-74.
36. De Luca CJ, Gilmore LD, Kuznetsov M, Roy SH. Filtering the surface EMG signal: Movement artifact and baseline noise contamination. *J Biomech.* 2010 May 28;43(8):1573-9.
37. Moisio KC, Sumner DR, Shott S, Hurwitz DE. Normalization of joint moments during gait: a comparison of two techniques. *J Biomech.* 2003 Apr;36(4):599-603.

38. Cohen J. Statistical Power Analysis for the Behavioral Sciences. 2nd ed. Hillsdale, NJ: Lawrence Earlbaum Associates; 1988.
39. Neumann DA. Kinesiology of the hip: a focus on muscular actions. *J Orthop Sports Phys Ther.* 2010 Feb;40(2):82-94.
40. Gaffney BMM, Clohisy JC, Van Dillen LR, Harris MD. The association between periacetabular osteotomy reorientation and hip joint reaction forces in two subgroups of acetabular dysplasia. *J Biomech.* 2020 Jan 2;98:109464.
41. Gaffney BMM, Hillen TJ, Nepple JJ, Clohisy JC, Harris MD. Statistical shape modeling of femur shape variability in female patients with hip dysplasia. *J Orthop Res.* 2019 Mar;37(3):665-73.
42. Hardcastle P, Nade S. The significance of the Trendelenburg test. *J Bone Joint Surg Br.* 1985 Nov;67(5):741-6.
43. Harris-Hayes M, Mueller MJ, Sahrmann SA, Bloom NJ, Steger-May K, Clohisy JC, Salsich GB. Persons with chronic hip joint pain exhibit reduced hip muscle strength. *J Orthop Sports Phys Ther.* 2014 Nov;44(11):890-8.
44. Nepple JJ, Wells J, Ross JR, Bedi A, Schoenecker PL, Clohisy JC. Three patterns of acetabular deficiency are common in young adult patients with acetabular dysplasia. *Clin Orthop Relat Res.* 2017 Apr;475(4):1037-44.

Chapter 5: Acetabular Edge Loading during Gait is Elevated by the Anatomical Deformities of Hip Dysplasia

5.1 Abstract

Developmental dysplasia of the hip (DDH) is a known risk factor for articular tissue damage and secondary hip osteoarthritis. Acetabular labral tears are prevalent in hips with DDH and may result from excessive loading at the edge of the shallow acetabulum. Location-specific risks for labral tears may also depend on neuromuscular factors such as movement patterns and muscle-induced hip joint reaction forces (JRFs). To evaluate such mechanically-induced risks, we used subject-specific musculoskeletal models to compare acetabular edge loading (AEL) during gait between individuals with DDH (N=15) and healthy controls (N=15), and determined the associations between AEL and radiographic measures of DDH acetabular anatomy. The three-dimensional pelvis and femur anatomy of each DDH and control subject were reconstructed from magnetic resonance images and used to personalize hip joint center locations and muscle paths in each model. Model-estimated hip JRFs were projected onto the three-dimensional acetabular rim to predict instantaneous AEL forces and their accumulative impulses throughout a gait cycle. Compared to controls, subjects with DDH demonstrated significantly higher AEL in the antero-superior acetabulum during early stance (3.6 vs $2.8 \times BW$, $p \leq 0.01$), late stance (4.3 vs $3.3 \times BW$, $p \leq 0.05$), and throughout the gait cycle (1.8 vs $1.4 \times BW^*s$, $p \leq 0.02$), despite having similar hip movement patterns. Elevated AEL primarily occurred in regions where the shallow acetabular edge was in close proximity to the hip JRF direction, and was strongly correlated with the radiographic severity of acetabular deformities. The results suggest AEL is highly dependent on movement and muscle-induced joint loading, and significantly elevated by the DDH acetabular

deformities. Our findings can help refine our understanding of DDH-related pathomechanics, and inform clinical assessments of patient-specific risks for labral and chondral damage.

5.2 Introduction

Developmental dysplasia of the hip (DDH) is most commonly characterized by a shallow acetabulum and is a primary risk factor for premature development of hip osteoarthritis [1,2]. The main catalyst of hip osteoarthritis secondary to DDH is articular tissue damage resulting from aberrant loading [3], especially near the labrum on the lateral edge of acetabulum [4,5]. Tears to the acetabular labrum are highly prevalent in patients with DDH, often painful, and can limit joint function [1,4,6]. Such mechanically-induced tears, whether untreated or unresolved after surgery, may then induce detrimental mechano-biological changes that advance hip joint degeneration [2,5,7].

Effectively assessing or treating mechanically-induced labral tears requires first understanding the major contributors to acetabular edge loading (AEL). Because direct measurement of AEL is not possible, computer simulation of articular loading has been used to study both healthy and dysplastic hips. In DDH, contributions of abnormal or surgically-altered bones to chondro-labral mechanics have both been demonstrated by finite element models with detailed acetabular anatomy [8,9]. While these prior models provided valuable insights about intra-articular mechanics in hips with DDH, they were driven using generic loading conditions and omitted the influence of two major contributors to AEL, namely subject-specific movement patterns and muscle-induced joint reaction forces (JRFs) [10].

The influence of movement and JRFs on articular mechanics may be assessed using dynamic neuromusculoskeletal models [11]. Musculoskeletal modeling studies have previously

been used to estimate AEL following total-hip or resurfacing arthroplasty and have helped quantify the risks for implant wear with various movement patterns or implant positions [12-15]. Yet to date, musculoskeletal models have not been used to estimate AEL in native hips. A reason for the lack of such studies could be that the generic anatomy used in most models does not closely represent the bony deformities, and hence the joint pathomechanics, of dysplastic hips [16]. Recently, we showed that image-based musculoskeletal models can delineate joint and muscle mechanical differences between hips with and without DDH [17,18]. By combining subject-specific bony anatomy, movement patterns and muscle-induced JRFs, image-based models can provide refined AEL quantification and advance our understanding of how these factors collectively contribute to DDH pathomechanics and hip joint degeneration.

In addition to understanding the pathomechanics of DDH, it is important to know how mechanical variables such as AEL relate to clinically measurable variables. The clinical severity of DDH is most commonly assessed using radiographic measures of acetabular anatomy, namely the lateral center-edge angle (LCEA) and acetabular inclination (AI) [19,20]. For hips with DDH, an LCEA $< 20^\circ$ and AI $> 10^\circ$ are considered clinical indicators of structural instability [21]. However, without knowing a clear relationship between radiographic measures and pathomechanics, clinical risk assessment of DDH-related labral tears and articular cartilage damage remains a challenge. Identifying the associations between AEL and structural characteristics such as LCEA and AI can help bridge biomechanical and radiographic evaluation of patients to improve personalized risk assessments of mechanically-induced damage.

Accordingly, the objectives of this study were to (1) use image-based musculoskeletal models to estimate AEL in hips with DDH compared to healthy control hips during gait, and (2) determine the associations between AEL and radiographic measures of acetabular anatomy (LCEA

and AI). We hypothesized that AEL during gait would be higher in antero-superior regions of the acetabula with DDH compared to controls, and that AEL magnitude would be associated with the radiographic severity of DDH acetabular deformities.

5.3 Methods

5.3.1 Subjects and Data Collection

After Institutional Review Board approval and informed consent, 15 female patients with untreated DDH and 15 female healthy control subjects were included, as previously reported [18]. Patients were diagnosed by a single orthopaedic surgeon, had unilateral hip or groin pain lasting over 3 months, and radiographic evidence of an LCEA less than 20° [19]. Control subjects had no self-reported history of hip pathology, no history of groin or lateral hip pain, had no discomfort during a clinical exam of hip flexion-adduction-internal-rotation, and were confirmed to have no evidence of hip deformity visible on magnetic resonance images. Both groups had no past hip or lower extremity surgeries, or functional restraints that would limit gait movements.

The LCEA and AI angles were measured for each DDH subject on antero-posterior radiographs following established techniques [21]. The measurements were standardized with a customized Matlab image analysis tool (MathWorks; Natick, MA) (**Figure 5.1**) and made by a senior rater with 10 years of experience, using methods shown to have excellent intra- and inter-rater reliability [22].

With each DDH and control subject lying prone in a neutral hip position, magnetic resonance images were collected from the lumbar region to the knees using a 3T scanner (VIDA, Siemens AG; Munich, Germany) with T1-weighted VIBE gradient-echo sequences and SPAIR fat suppression ($1 \times 1 \times 1$ mm voxels) [18]. From the images, 3D bony anatomy of the whole pelvis and

femurs was reconstructed using Amira software (v2019a; Thermo Fisher Scientific; Houston, TX), including detailed acetabular anatomy.

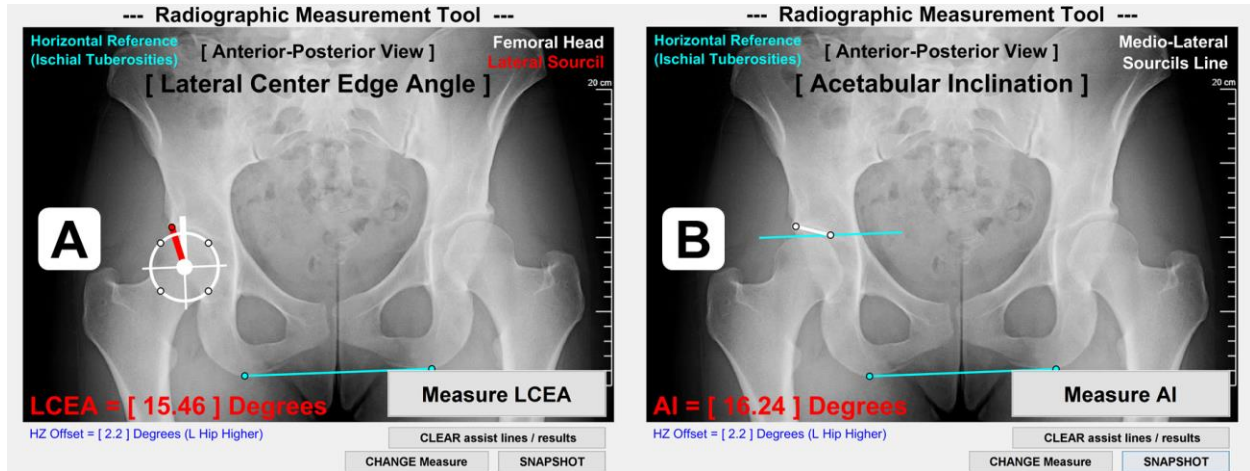


Figure 5.1. LCEA and AI measurement methods. (A) LCEA was measured as the angle between a first line (thick white) through the femoral head center and perpendicular to the inferior aspect of ischial tuberosities (light blue) and a second line connecting the femoral head center to the lateral aspect of acetabular sourcil (red). (B) AI was measured as the angle between a first line parallel to the inferior aspect of ischial tuberosities and a second line connecting the medial and lateral aspects of acetabular sourcils (thin white).

Motion data were collected at 100 Hz using 10 infrared cameras (Vicon; Centennial, CO) and 70 skin markers. All subjects walked at self-selected speed on an instrumented treadmill (Bertec; Columbus, OH). Ground reaction forces were recorded at 2000 Hz. Marker data were low-pass filtered with an 8 Hz cutoff frequency as determined with a residual analysis [23]. Force data were filtered at 6 Hz to minimize treadmill analog artifact noise [24].

5.3.2 Subject-Specific Musculoskeletal Models

Subject-specific musculoskeletal models were created in the OpenSim software [11] as recently described [18]. Briefly, a generic OpenSim model [25] was modified by adding image-based pelvis and femur bony anatomy, including landmark-based 3D alignment of the pelvis tilt, obliquity, and rotation. Aligned 3D bony anatomy was then used to update hip joint center (HJC)

locations, muscle anatomical paths, and muscle-tendon physiological parameters specific to each subject. These models were validated with electromyography as previously reported [18].

One representative gait cycle for each subject was simulated in OpenSim to estimate time-dependent hip biomechanics. Joint angles and net moments were calculated via inverse kinematics and inverse dynamics [23]. Hip resultant JRFs and antero-posterior, supero-inferior, and medio-lateral JRF components were computed using OpenSim Joint Reaction Analysis [26] from muscle forces estimated via static optimization [27]. Hip JRF components were expressed in the pelvis coordinate system to represent loading onto the acetabulum. JRFs, joint angles and moments on the symptomatic side of each DDH subject were chosen for subsequent analyses; for comparison, a random hip was chosen for each control subject.

5.3.3 Estimation of Acetabular Edge Loading (AEL)

AEL on the analyzed hip during each gait trial was computed by mathematically projecting hip JRFs onto the acetabular anatomy in each subject-specific model. First, the acetabular rim was delineated on each image-based 3D pelvis, using a principle curvature heat map (**Figure 5.2A**). Then, on each acetabular rim, nine clock-face points were designated within the anterior (2-4 o'clock), superior (11-1 o'clock), and posterior (8-10 o'clock) quadrants [28] (**Figure 5.2B**). A right-view clock-face convention was adopted for all hips regardless of side such that 3 o'clock represented anterior for both right and left hips [28].

The hip JRF was represented as a 3D force vector stemming from the femoral head, i.e. the HJC (**Figure 5.2C**). The direction of AEL was defined as the vector from HJC to a point on the acetabular rim. The AEL magnitude was then estimated via trigonometric projection of the JRF along the AEL direction towards each of the 9 clock-face points (**Figure 5.2C**). Additionally, a 'JRF-to-edge angle' was defined as the angle between the JRF direction and the AEL direction,

which represented how close the JRF was relative to the edge [13]. The JRF-to-edge angle was also computed at each clock-face point.

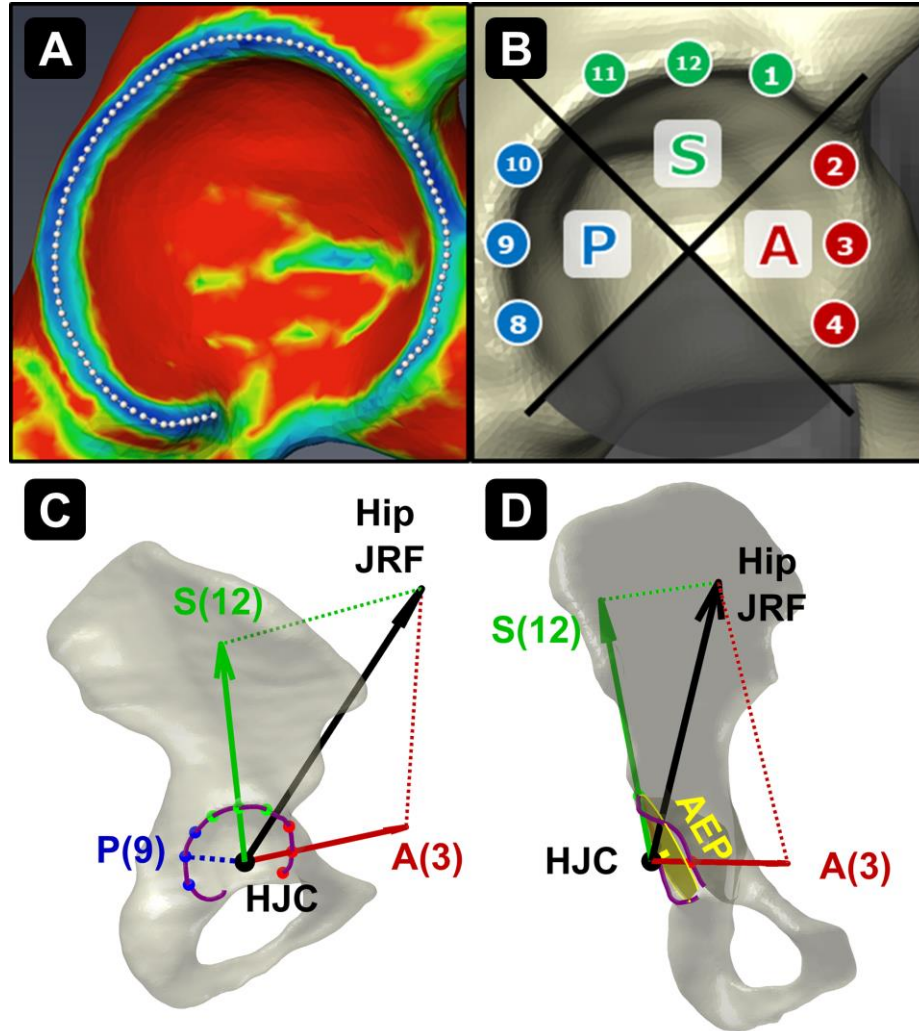


Figure 5.2. Estimation of acetabular edge loading (AEL). (A) The acetabular rim of each subject was delineated using a principal curvature heat map. (B) Nine clock-face points were designated on the anterior (“A”), superior (“S”), and posterior (“P”) quadrants of the rim. (C) AEL magnitudes were estimated via trigonometric projection of the hip JRF (black arrow) along the directions from HJC towards each clock-face point on the rim (red/green arrows). The JRF-to-edge angle was calculated as the angle between the JRF and the AEL directions (i.e. between black and red/green arrows). Note zero posterior AEL when JRF is directed anteriorly. (D) An ‘acetabular edge plane (AEP)’ was fit to the rim to measure the distance between the approximated acetabular border and the HJC.

Because the JRF magnitude and direction change during gait, the clock-face AEL magnitude and JRF-to-edge angle are both time-dependent, and were calculated at each time frame

throughout the gait trial. AEL was then numerically integrated over the duration of the whole gait cycle to calculate its accumulative impulse.

Finally, a 3D plane was fit to each delineated acetabular rim, termed the ‘acetabular edge plane (AEP)’ (**Figure 5.2D**). The distance from each HJC to AEP was calculated to approximate the relative position between the femoral head center and the acetabular border, as an additional measure of the DDH anatomical deformity.

5.3.4 Inter-Group Comparison and Correlations

Hip JRFs, clock-face AEL, and JRF-to-edge angles were time-normalized to 0-100 percent of a gait cycle. The forces were then normalized by body weight (unit: $\times BW$). To include the influence of the gait cycle duration, the accumulative impulses of AEL were not time-normalized, but magnitudes were normalized by BW (unit: $\times BW \cdot s$). Net hip moments were normalized by body mass (unit: Nm/kg). Timing of the two hip JRF peaks in early stance (termed ‘JRF1’) and late stance (‘JRF2’) in each gait cycle was identified. All instantaneous forces, angles, and moments at the times of JRF1 and JRF2 were extracted for statistical analyses, along with the accumulative impulses.

Each demographic, radiographic, and biomechanical variable was assessed for normality using the Shapiro-Wilk test. Normally distributed variables were compared between the DDH and control groups using independent *t*-tests, with corrections for heterogeneity of variance as needed. Variables violating data normality were compared using the non-parametric Mann-Whitney *U* tests. Statistical significance for all tests was $\alpha = 0.05$. Effect sizes were determined by Cohen’s *d*, with a large effect defined as $d \geq 0.8$ [29]. Within the DDH subjects, associations between biomechanical variables (JRFs, AEL, JRF-to-edge angles) and radiographic measures (LCEA and

AI) were assessed using Pearson's correlation (r), or Spearman's rank correlation (ρ) if data violated normality; a strong correlation was defined as $|r|$ or $|\rho| \geq 0.5$ [29].

5.4 Results

5.4.1 Subject Demographics and Anatomy

The DDH and control groups did not differ significantly in age, height, mass, body-mass index, or gait speed (**Table 5.1**). The average LCEA and AI values for the DDH group were within ranges of traditional DDH definitions [21]. Additionally, the HJC-to-AEP distance was significantly larger in hips with DDH compared to controls (**Table 5.1**), which strongly correlated with smaller LCEA ($\rho = -0.53$) and larger AI ($r = 0.58$) among the DDH subjects.

Table 5.1. Demographics, gait speed, radiographic measures, and the HJC-to-AEP distance (mean \pm SD) of DDH and control subjects.

	DDH (N = 15)	Control (N = 15)	<i>p</i> -value
Age (years)	26.5 \pm 7.9	24.6 \pm 6.3	0.62
Height (m)	1.66 \pm 0.07	1.67 \pm 0.06	0.85
Mass (kg)	62.7 \pm 9.3	61.9 \pm 7.8	0.79
Body-mass index (kg/m ²)	22.7 \pm 2.4	22.3 \pm 2.3	0.64
Gait speed (m/s)	1.37 \pm 0.15	1.39 \pm 0.15	0.59
Lateral Center-Edge Angle (degrees)	10.5 \pm 9.2	N/A	-
Acetabular Inclination (degrees)	18.0 \pm 8.4	N/A	-
HJC-to-AEP distance (mm)	9.3 \pm 2.5	5.9 \pm 1.4	<0.01

Note: Radiographic measurements of acetabular anatomy were only made for the DDH subjects. HJC, hip joint center; AEP, acetabular edge plane.

5.4.2 Hip JRFs

As reported in our previous study [18], DDH subjects had higher-than-control medial hip JRFs at JRF1 (1.3 \pm 0.6 vs 0.9 \pm 0.3 \times BW; $p = 0.03$, $d = 0.82$), as well as higher resultant (5.7 \pm 1.1 vs 5.0 \pm 0.8 \times BW) and superior JRFs (4.8 \pm 0.8 vs 4.1 \pm 0.7 \times BW) at JRF2 ($p \leq 0.05$, $d \geq 0.76$).

5.4.3 Clock-Face AEL and JRF-to-Edge Angles

At early-stance JRF1, DDH subjects had higher AEL than controls in the anterior and superior regions from 11 to 3 o'clock ($p \leq 0.01$, $d \geq 0.97$; **Figure 5.3AB**). Averaged AEL across the 11 to 3 o'clock points was $3.6 \times \text{BW}$ in DDH vs. $2.8 \times \text{BW}$ in controls. Higher AEL correlated with smaller LCEA ($\rho = -0.58$) and larger AI ($r = 0.53$) for DDH subjects at the 3 o'clock location, but not from 11-2 o'clock. Simultaneously, JRF-to-edge angles were smaller in hips with DDH in the anterior and superior regions (11-4 o'clock, **Figure 5.3AB**; $p \leq 0.01$, $d \geq 1.18$), which correlated with smaller LCEA ($\rho \geq 0.60$) and larger AI ($r \leq -0.45$) from 12-3 o'clock.

At late-stance JRF2, similar to early-stance, DDH subjects had higher AEL in the anterior and superior regions from 11-2 o'clock ($p \leq 0.05$, $d \geq 0.76$; **Figure 5.3AB**), which correlated with larger AI at 11 o'clock ($r = 0.60$). Averaged AEL across the 11 to 2 o'clock points was $4.3 \times \text{BW}$ in DDH vs. $3.3 \times \text{BW}$ in controls. The JRF-to-edge angles at JRF2 were again smaller in DDH subjects across the superior region (11-1 o'clock, **Figure 5.3B**; $p \leq 0.02$, $d \geq 0.92$). Posterior AEL magnitudes at JRF2 were minimal, but JRF-to-edge angles were significantly smaller in DDH subjects than controls in the posterior region (8-9 o'clock, **Figure 5.3C**; $p = 0.04$, $d \geq 0.79$). Smaller JRF-to-edge angles correlated with larger AI in all regions ($r \leq -0.52$), and with smaller LCEA at 1 o'clock ($\rho = 0.53$).

Over a whole gait cycle, DDH subjects had higher accumulative AEL (i.e. impulse) in a broad region from the anterior to postero-superior acetabulum (10-3 o'clock, **Figure 5.3**; $p \leq 0.02$, $d \geq 0.91$). Averaged AEL accumulative impulse across the 10 to 3 o'clock points was $1.8 \times \text{BW} \cdot \text{s}$ in DDH vs. $1.4 \times \text{BW} \cdot \text{s}$ in controls. Higher accumulative AEL correlated with smaller LCEA ($\rho = -0.54$) and larger AI ($r = 0.51$) at the 12 o'clock location.

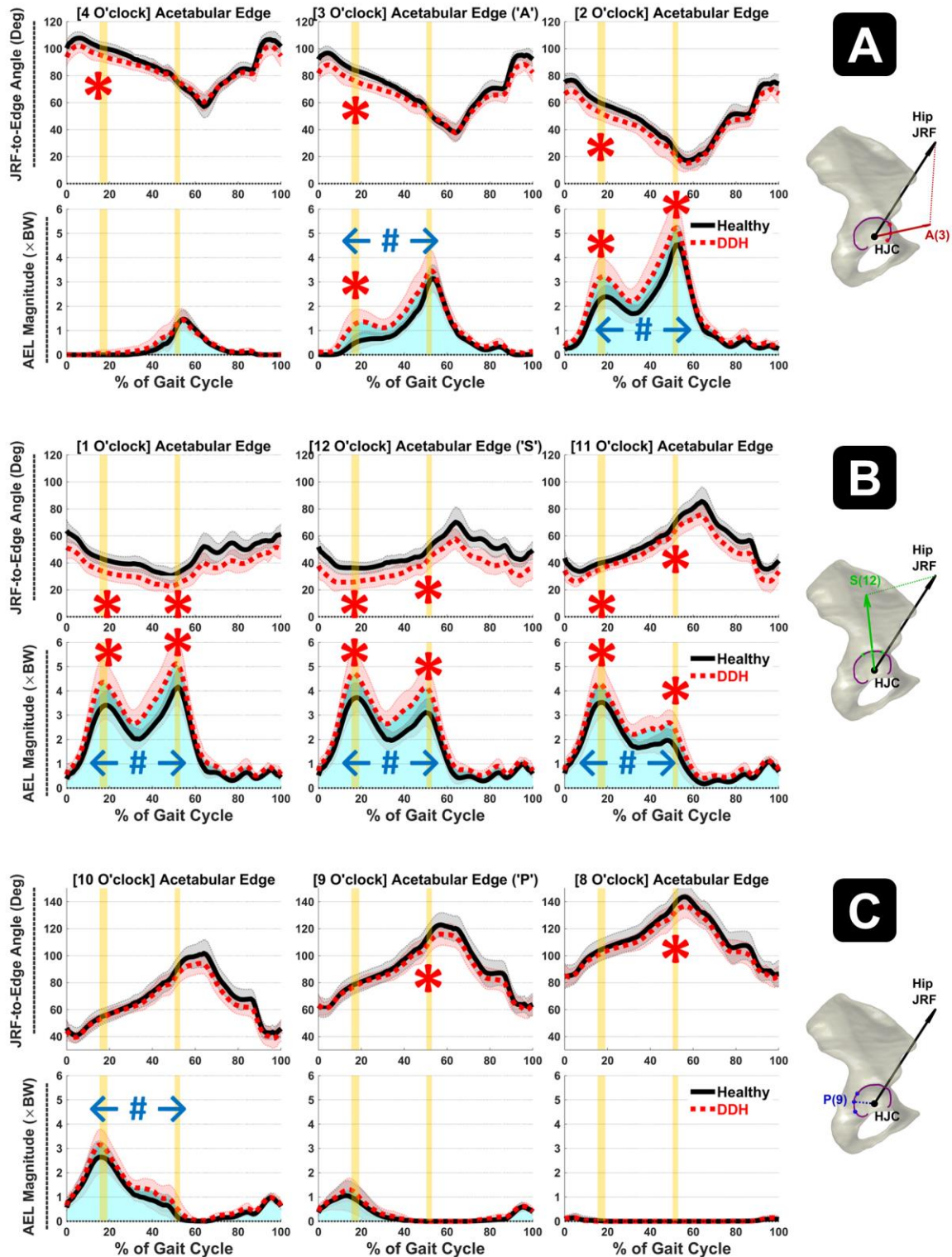


Figure 5.3. Average JRF-to-edge angles (top) and AEL (bottom) in (A) anterior (2-4 o'clock), (B) superior (11-1 o'clock), and (C) posterior (8-10 o'clock) regions throughout gait. Red/black shades = ± 1 SD. Vertical yellow bars indicate time of JRF peaks (JRF1 and JRF2). Blue shades illustrate accumulative impulses. Statistical significance: '*' instantaneous, '#' accumulative.

5.4.4 Joint Angles and Moments

Also as previously reported [18], DDH subjects had slightly larger hip adduction ($1.2^{\circ} \pm 2.8^{\circ}$ vs. $-1.4^{\circ} \pm 2.6^{\circ}$, $p = 0.01$, $d = 0.95$) and more pelvis obliquity towards the ipsilateral side than controls ($1.2^{\circ} \pm 2.2^{\circ}$ vs. $-1.1^{\circ} \pm 1.8^{\circ}$, $p < 0.01$, $d = 1.15$) in late stance (JRF2). Hip moments did not differ between groups.

5.5 Discussion

The objectives of this study were to estimate AEL in hips with DDH compared to healthy control hips during gait, and determine the associations between AEL and radiographic measures of acetabular anatomy. Results generally supported the hypothesized AEL elevation in hips with DDH. Our secondary hypothesis that AEL elevation was associated with the severity of acetabular deformities was also supported. Hips with DDH exhibited higher AEL both instantaneously when JRFs peaked, and accumulatively over the duration of gait. The specific location and timing of elevated AEL varied throughout different phases of gait, suggesting relationships among acetabular anatomy, movement, muscle-induced joint loading, and labral mechanics. Such dependencies support the need to comprehensively evaluate the whole hip biomechanical environment for a refined understanding of DDH pathomechanics, and patient-specific risk assessments of DDH-related labral tears and articular cartilage damage.

The location and severity of acetabular deformities were main contributors to AEL. First, elevated AEL almost always accompanied reduced JRF-to-edge angles, which meant that whenever hip loading acted in close proximity to the shallow acetabular edge, a large component of the JRF would be projected to the edge. This coupled phenomenon was consistent in the anterior and superior regions of the DDH acetabula, which matches well-established clinical descriptions of the locations where DDH-related labral tears frequently occur [4]. Prior models of articular

cartilage stress found that the bony deformities of DDH led to a disproportionately large amount of contact stresses on the superolateral labrum [8]. Our results support this edge loading phenomenon, and provide new evidence of how the shallow acetabulum of DDH also causes muscle-induced edge loading to be elevated. We also found that the shallower the acetabulum was, as shown by LCEA and AI, the higher JRF loading would be applied at the lateral edge in late stance and over a gait cycle. Additionally, a larger HJC-to-AEP distance demonstrated that the lateral edge of dysplastic hips was farther away from the femoral head center than controls [1,30], which further elevated AEL. Based on these associations, region-specific risks for labral tears or cartilage damage can vary according to radiographic metrics of acetabular deformity and in context with muscle-induced pathomechanics.

Labral tears can be caused by both acute and chronic mechanisms [5]. High acute hip loading during gait typically occurs in a transient phase of motion, such as weight acceptance during early stance (i.e., JRF1) and the late-stance transition to push-off (i.e., JRF2). Hip loading from JRFs is generally in the supero-medial direction throughout a gait cycle, and shifts from posterior to anterior over stance [31,32]. We found that instantaneous AEL was elevated in hips with DDH at both JRF1 and JRF2. Cyclic high instantaneous loading on the superior and anterior acetabulum when JRFs peak may be another risk factor that compounds with the shallow acetabulum to heighten the likelihood of labral tears and articular cartilage damage in those regions [1,5]. Although high instantaneous loads can occur during traumatic events, a large percentage of labral tears cannot be linked to known high-impact events [6,33]. Instead, most tears may be caused by accrued micro-damage from routine yet aberrant loading [34]. Muscle-induced AEL may contribute to such insidious damage not only at cyclic points when JRFs peak, but also through accumulative loads across the entire gait motion. Indeed, accumulative AEL during gait was not

only significantly increased in our patients with DDH, but also spanned a wide region around the acetabular rim. Because the duration of abnormal AEL could play a vital role in the development of labral tears, the assessments of labral mechanics in response to disease progression or treatments should be monitored over time.

It is notable that antero-superior AEL was elevated not just in late stance when anterior JRFs peaked, but also in early stance when the hip was flexed and the joint loading was less anterior. While JRFs were directed farther away from anterior edge in both groups during early stance (**Figure 5.3A**), the JRF-to-edge angles were *relatively* smaller in DDH subjects versus controls. Such inter-group differences may explain why AEL was *relatively* elevated and can be caused by the DDH subjects' higher medial JRFs during early stance. Although medial loading may be produced by the hip muscles to stabilize the femoral head in the shallow acetabulum [17], due to the dynamic nature of hip loading and 3D acetabular positions, a force component may still be projected towards the shallow anterior edge. This dynamic interaction may also explain why the lateral acetabular anatomy (LCEA and AI) was associated with an anterior AEL in early stance. Its potential contributions to labral and cartilage damage should not be overlooked, especially considering the accumulative impacts (**Figure 5.3**).

To our knowledge, this study was the first to quantify anatomy- and movement-specific loading at the native acetabular edge, either with or without anatomical deformity. Our findings were indirectly supported by edge loading evaluations of prosthetic hips [12,13]. Specifically, edge loading risks in prosthetic acetabular cups that poorly covered the femoral head were analogous to the elevated AEL we demonstrated in the shallow native acetabula. These prior studies also demonstrated how prosthetic cup positioning could reduce edge loading risks and implant wear. Likewise, surgical re-orientation of the native, pre-arthritic DDH acetabula have been shown (via

model simulations) to greatly influence muscle-induced JRFs [35], which may be further informed by model-based AEL analyses to minimize the risks for labral tears and joint degeneration.

Several limitations of this study should be considered. First, due to a small sample size, it was not feasible to statistically analyze the interactions between AEL and the different subgroups of posterior, anterior, and global acetabular deficiency [36]. DDH patients with poor anterior and posterior femoral coverage may possess different risks of edge loading and labral tears, and respond differently to peak or repetitive loading during movements. While we reported AEL for the DDH group as a whole, our methods were precise to individuals, which could be readily applied to subgroup analyses given a large enough sample. A second limitation was that HJC locations in the musculoskeletal models were assumed static within the acetabulum. Due to the potential instability of dysplastic hips [2], subtle translation of the femoral head during motion may occur and could affect projected AEL. However, by defining JRF and AEL directions both stemming from the HJC, their relative closeness (i.e. JRF-to-edge angle) should still robustly capture the mechanical influence of the acetabular deformities. Third, we used static optimization to estimate muscle forces, JRFs and AEL, which did not incorporate muscle co-contractions that could be altered in hips with DDH. We chose this method as it was able to estimate hip JRFs during gait close to benchmark data [27]. To study high-speed movements that involve significant muscle co-contractions, dynamic force estimation may be necessary.

In conclusion, AEL was significantly elevated in hips with DDH compared to healthy controls, both instantaneously when JRFs peaked and accumulatively over the duration of gait. The extent of high AEL was strongly correlated with the severity of DDH deformities, especially lateral acetabular deficiency. Our findings suggest that AEL magnitude and location are highly dependent on movement, muscle-induced joint loading, and the DDH acetabular deformities.

Because the anatomical, movement, and biomechanical factors are interrelated and patient-specific, clinical evaluations of DDH should consider the hip biomechanical environment in context with established anatomical measures as risk factors for labral tears and articular cartilage damage.

5.6 Acknowledgments

The studies involving human participants were reviewed and approved by Washington University Institutional Review Board. The patients/participants provided their written informed consent to participate in this study. Funding for this study was provided by the National Institutes of Health K01 AR072072, P30 AR074992 and the Lottie Caroline Charitable Trust. The authors declare that the research was conducted in the absence of any commercial or financial relationships that could be construed as a potential conflict of interest. The authors thank Molly Shepherd, Lauren Westen, Abby Matt, and Spencer Williams for assistance with magnetic resonance image and motion data processing.

5.7 References

1. Gala L, Clohisy JC, Beaulé PE. Hip dysplasia in the young adult. *J Bone Joint Surg Am*. 2016 Jan 6;98(1):63-73.
2. Beaulé PE, editor. *Hip Dysplasia: Understanding and Treating Instability of the Native Hip*. Cham, Switzerland: Springer Nature Switzerland AG; 2020.
3. Felson DT. Osteoarthritis as a disease of mechanics. *Osteoarthritis Cartilage*. 2013 Jan;21(1):10-5.
4. Hartig-Andreasen C, Søballe K, Troelsen A. The role of the acetabular labrum in hip dysplasia. A literature overview. *Acta Orthop*. 2013 Feb;84(1):60-4.
5. Lewis CL, Sahrman SA. Acetabular labral tears. *Phys Ther*. 2006 Jan;86(1):110-21.

6. Burnett RS, Della Rocca GJ, Prather H, Curry M, Maloney WJ, Clohisy JC. Clinical presentation of patients with tears of the acetabular labrum. *J Bone Joint Surg Am.* 2006 Jul;88(7):1448-57.
7. Cvetanovich GL, Heyworth BE, Murray K, Yen YM, Kocher MS, Millis MB. Hip arthroscopy in patients with recurrent pain following Bernese periacetabular osteotomy for acetabular dysplasia: operative findings and clinical outcomes. *J Hip Preserv Surg.* 2015 Jun 13;2(3):295-302.
8. Henak CR, Abraham CL, Anderson AE, Maas SA, Ellis BJ, Peters CL, Weiss JA. Patient-specific analysis of cartilage and labrum mechanics in human hips with acetabular dysplasia. *Osteoarthritis Cartilage.* 2014 Feb;22(2):210-7.
9. Abraham CL, Knight SJ, Peters CL, Weiss JA, Anderson AE. Patient-specific chondrolabral contact mechanics in patients with acetabular dysplasia following treatment with peri-acetabular osteotomy. *Osteoarthritis Cartilage.* 2017 May;25(5):676-84.
10. Thomas-Aitken HD, Willey MC, Goetz JE. Joint contact stresses calculated for acetabular dysplasia patients using discrete element analysis are significantly influenced by the applied gait pattern. *J Biomech.* 2018 Oct 5;79:45-53.
11. Delp SL, Anderson FC, Arnold AS, Loan P, Habib A, John CT, Guendelman E, Thelen DG. OpenSim: open-source software to create and analyze dynamic simulations of movement. *IEEE Trans Biomed Eng.* 2007 Nov;54(11):1940-50.
12. van Arkel RJ, Modenese L, Phillips AT, Jeffers JR. Hip abduction can prevent posterior edge loading of hip replacements. *J Orthop Res.* 2013 Aug;31(8):1172-9.
13. Wesseling M, Meyer C, De Groote F, Corten K, Simon JP, Desloovere K, Jonkers I. Gait alterations can reduce the risk of edge loading. *J Orthop Res.* 2016 Jun;34(6):1069-76.
14. Mellon SJ, Grammatopoulos G, Andersen MS, Pandit HG, Gill HS, Murray DW. Optimal acetabular component orientation estimated using edge-loading and impingement risk in patients with metal-on-metal hip resurfacing arthroplasty. *J Biomech.* 2015 Jan 21;48(2):318-23.
15. Mellon SJ, Grammatopoulos G, Andersen MS, Pegg EC, Pandit HG, Murray DW, Gill HS. Individual motion patterns during gait and sit-to-stand contribute to edge-loading risk in metal-on-metal hip resurfacing. *Proc Inst Mech Eng H.* 2013 Jul;227(7):799-810.
16. Song K, Anderson AE, Weiss JA, Harris MD. Musculoskeletal models with generic and subject-specific geometry estimate different joint biomechanics in dysplastic hips. *Comput Methods Biomech Biomed Engin.* 2019 Feb;22(3):259-70.

17. Harris MD, MacWilliams BA, Bo Foreman K, Peters CL, Weiss JA, Anderson AE. Higher medially-directed joint reaction forces are a characteristic of dysplastic hips: A comparative study using subject-specific musculoskeletal models. *J Biomech*. 2017 Mar 21;54:80-7.
18. Song K, Gaffney BMM, Shelburne KB, Pascual-Garrido C, Clohisy JC, Harris MD. Dysplastic hip anatomy alters muscle moment arm lengths, lines of action, and contributions to joint reaction forces during gait. *J Biomech*. 2020 Sep 18;110:109968.
19. Wiberg G. Studies on dysplastic acetabula and congenital subluxation of the hip joint with special reference to the complication of osteoarthritis. *Acta Chir Scand*. 1939;83 Suppl 58:7-135.
20. Tönnis D. Congenital Dysplasia and Dislocation of the Hip in Children and Adults. Berlin and Heidelberg, Germany: Springer-Verlag; 1987.
21. Clohisy JC, Carlisle JC, Beaulé PE, Kim YJ, Trousdale RT, Sierra RJ, Leunig M, Schoenecker PL, Millis MB. A systematic approach to the plain radiographic evaluation of the young adult hip. *J Bone Joint Surg Am*. 2008 Nov;90 Suppl 4:47-66.
22. Nepple JJ, Martell JM, Kim YJ, Zaltz I, Millis MB, Podeszwa DA, Sucato DJ, Sink EL, Clohisy JC; ANCHOR Study Group. Interobserver and intraobserver reliability of the radiographic analysis of femoroacetabular impingement and dysplasia using computer-assisted measurements. *Am J Sports Med*. 2014 Oct;42(10):2393-401.
23. Winter DA. Biomechanics and Motor Control of Human Movement. 3rd ed. Hoboken, NJ: John Wiley & Sons; 2004.
24. Pickle NT, Grabowski AM, Auyang AG, Silverman AK. The functional roles of muscles during sloped walking. *J Biomech*. 2016 Oct 3;49(14):3244-51.
25. Lai AKM, Arnold AS, Wakeling JM. Why are antagonist muscles co-activated in my simulation? A musculoskeletal model for analysing human locomotor tasks. *Ann Biomed Eng*. 2017 Dec;45(12):2762-74.
26. Steele KM, Demers MS, Schwartz MH, Delp SL. Compressive tibiofemoral force during crouch gait. *Gait Posture*. 2012 Apr;35(4):556-60.
27. Wesseling M, Derikx LC, de Groote F, Bartels W, Meyer C, Verdonschot N, Jonkers I. Muscle optimization techniques impact the magnitude of calculated hip joint contact forces. *J Orthop Res*. 2015 Mar;33(3):430-8.

28. Goronzy J, Blum S, Hartmann A, Plodeck V, Franken L, Günther KP, Thielemann F. Is MRI an adequate replacement for CT scans in the three-dimensional assessment of acetabular morphology? *Acta Radiol.* 2019 Jun;60(6):726-34.
29. Cohen J. *Statistical Power Analysis for the Behavioral Sciences.* 2nd ed. Hillsdale, NJ: Lawrence Earlbaum Associates; 1988.
30. Cheng R, Zhang H, Kernkamp WA, Zheng J, Dai K, Yao Y, Wang L, Tsai TY. Relations between the Crowe classification and the 3D femoral head displacement in patients with developmental dysplasia of the hip. *BMC Musculoskelet Disord.* 2019 Nov 11;20(1):530.
31. Bergmann G, Deuretzbacher G, Heller M, Graichen F, Rohlmann A, Strauss J, Duda GN. Hip contact forces and gait patterns from routine activities. *J Biomech.* 2001 Jul;34(7):859-71.
32. Lewis CL, Sahrman SA, Moran DW. Effect of hip angle on anterior hip joint force during gait. *Gait Posture.* 2010 Oct;32(4):603-7.
33. Santori N, Villar RN. Acetabular labral tears: result of arthroscopic partial limbectomy. *Arthroscopy.* 2000 Jan-Feb;16(1):11-5.
34. McCarthy JC, Noble PC, Schuck MR, Wright J, Lee J. The Otto E. Aufranc Award: The role of labral lesions to development of early degenerative hip disease. *Clin Orthop Relat Res.* 2001 Dec;(393):25-37.
35. Gaffney BMM, Clohisy JC, Van Dillen LR, Harris MD. The association between periacetabular osteotomy reorientation and hip joint reaction forces in two subgroups of acetabular dysplasia. *J Biomech.* 2020 Jan 2;98:109464.
36. Nepple JJ, Wells J, Ross JR, Bedi A, Schoenecker PL, Clohisy JC. Three patterns of acetabular deficiency are common in young adult patients with acetabular dysplasia. *Clin Orthop Relat Res.* 2017 Apr;475(4):1037-44.

Chapter 6: Hip Dysplasia Elevates Loading at the Posterior Acetabular Edge during Double-Legged Squat

6.1 Abstract

Hips with developmental dysplasia (DDH) are at a heightened risk of premature hip osteoarthritis, which is often expedited by mechanically-induced articular tissue damage. A prevalent form of damage in DDH is labral tears caused by abnormal loading at the shallow acetabular edge. Although the majority of DDH-related labral tears occur in the antero-superior acetabulum, posterior labral tears can be prevalent in individuals whose lifestyle involves frequent high hip flexion tasks such as squatting. To better understand the contributions of task-specific movements to acetabular edge loading (AEL), and the region-specific risks for labral tears, we used image-based musculoskeletal models to compare AEL during double-legged squat between hips with DDH (n=10) and healthy controls (n=10). Hips with DDH had higher-than-control posterior AEL at the lowest point of squat (2.6 vs $1.8 \times BW$, $p \leq 0.04$) and accumulatively throughout the duration of squatting motion (2.6 vs $1.9 \times BW^*s$, $p \leq 0.04$). Elevated posterior AEL coincided with increased net hip extension moments and posterior joint reaction forces, and was correlated with the severity of DDH acetabular deformity. Interestingly, the regions of peak and accumulative AEL corresponded to the intensity and duration of hip loading respectively. Our findings suggest AEL is highly dependent on specific movements such as squatting, and thus is unique to the lifestyles of individuals. Clinical evaluation of DDH should consider patient-specific anatomy, lifestyle, and time factors together to make personalized treatment decisions that reduce the risks of secondary labral and cartilage damage.

6.2 Introduction

Developmental dysplasia of the hip (DDH) is a major risk factor for premature development of hip osteoarthritis [1,2]. The onset of osteoarthritis secondary to DDH is often expedited by mechanically-induced articular tissue damage and the resulting detrimental mechano-biological changes [2,3]. For example, one of the most prevalent forms of damage in hips with DDH is labral tears and cartilage damage at the acetabular rim, which are thought to be caused by excessive loading near the labrum at the lateral acetabular edge [1,4,5]. Torn acetabular labrum compromises the normal loading environment of the hip, which may then lead to joint degeneration [6,7]. To better evaluate and accordingly reduce the risks for DDH-related labral tears and articular cartilage damage, reliable quantification of acetabular edge loading (AEL) and identification of its contributing factors are required.

A probable factor that contributes to excessive AEL is the anatomical deformity of DDH. DDH is clinically characterized by a shallow acetabulum that poorly covers the femoral head during movements [1,8]. Computational studies have shown that the shallow acetabulum causes a lateral shift of the articular contact area and increased contact stresses borne by the labrum at the supero-lateral acetabular edge [9]. Such study quantitatively described the altered labral mechanics unique to the DDH bony anatomy, and could partially explain why the supero-lateral region is among where labral tears were frequently observed [4].

However, acetabular anatomy alone cannot fully explain the region-specific risks for labral tears in DDH. Other than the supero-lateral region, the anterior acetabulum is another common site of labral tears [4,6]. US and England-based studies reported over two thirds of labral tears in the anterior region [7,10], which have been attributed to higher repetitive mechanical loading in the anterior hip during routine tasks such as gait [6,11]. For subjects with DDH, the task-specific

hip joint loading could compound with the existing anatomical deformity and complicate the region-specific risks for labral tears. Notably, in labral tear studies from Japan where daily tasks involve frequent high hip flexion such as squatting and sitting on the ground, posterior tears were found in at least 70% of the cases [12,13]. Despite this clinical observation, the mechanistic risk factors for posterior labral tears or AEL are unclear. It is worth noting that posterior acetabular deficiency can be as common as anterior or global deficiency among hips with DDH [14], while for a population like young adults with DDH, high hip flexion tasks can be prevalent due to their active lifestyles and involvement in sports. To reliably evaluate how likely these patients may suffer labral tears, and where in the acetabulum such tears are most likely to occur, quantification of AEL specific to dynamic movement tasks such as squatting is needed.

Although it is not possible to directly measure task-specific AEL in vivo, musculoskeletal models are capable of estimating joint reaction forces (JRFs) from subject-specific movements [15], which may be combined with medical image-based anatomy to predict articular-level mechanics. To our knowledge, no past study has reported how hip JRFs and the resulting AEL are altered in DDH during high flexion tasks such as double-legged squat. Thus, the objective of this study was to use image-based musculoskeletal models to estimate AEL during double-legged squat in hips with DDH compared to healthy controls. We hypothesized that AEL during squat would be higher in the posterior region of the acetabula with DDH, and the extent of AEL elevation would be correlated to the severity of DDH acetabular deformity.

6.3 Methods

6.3.1 Subjects and Experimental Data Collection

After Institutional Review Board approval and informed consent, 10 female patients with untreated DDH and 10 female healthy control subjects were included [16] as part of a larger case-

control study (Level of Evidence III). All subjects in the larger research had gait movement data collected for separate studies (Chapters 4 and 5) [16], among whom the 20 current subjects were a subset instructed to also perform double-legged squats at the time of data collection. Controls were age-matched to the DDH patients. Patients were diagnosed by a single orthopaedic surgeon and had radiographic evidence of a lateral center-edge angle (LCEA) $<20^\circ$ [8]. Control subjects had no self-reported history of hip pathology, no discomfort during a clinical exam of hip flexion-adduction-internal-rotation, and no hip anatomical deformity visible on magnetic resonance images. Both groups had no past hip surgeries or functional restraints that would limit their ability to perform double-legged squats. For each DDH subject, the LCEA and acetabular inclination (AI) angles (**Figure 6.1**) were measured on antero-posterior radiographs, following established clinical standards to evaluate the acetabular anatomy [17]. The measurements were standardized with a customized Matlab image analysis tool (MathWorks; Natick, MA).

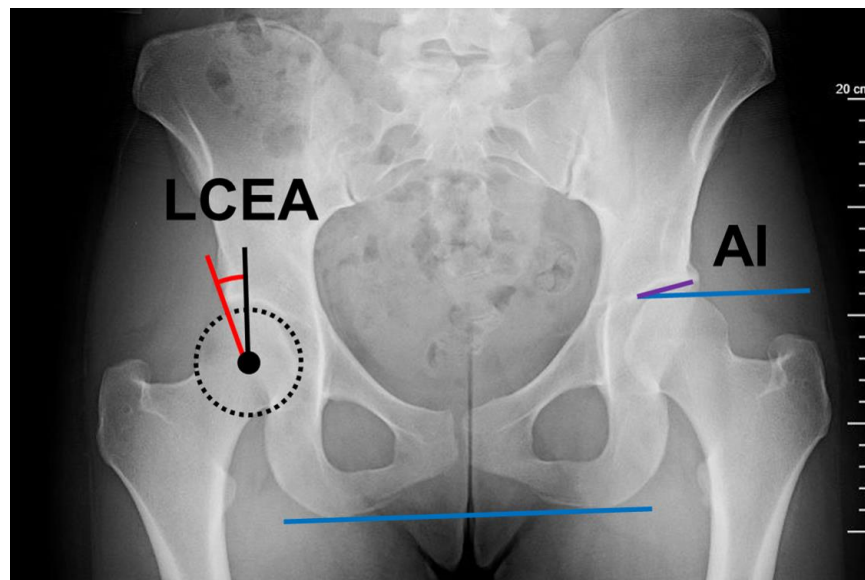


Figure 6.1. LCEA and AI measurements. LCEA was measured as the angle between a first line (black) through the femoral head center and perpendicular to the inferior aspect of ischial tuberosities (blue) and a second line connecting the femoral head center to the lateral aspect of acetabular source (red). AI was measured as the angle between a first line parallel to the inferior aspect of ischial tuberosities and a second line connecting the medial and lateral aspects of acetabular source (purple).

With each DDH and control subject lying prone in a neutral hip position, magnetic resonance (MR) images were collected from the lumbar region to the knees using a 3T scanner (VIDA, Siemens AG; Munich, Germany) with T1-weighted VIBE gradient-echo sequences and SPAIR fat suppression (1×1×1 mm voxels) [16]. From the MR images, 3D bony anatomy of the whole pelvis and both femurs was reconstructed using Amira software (v2019a; Thermo Fisher Scientific; Houston, TX), including detailed acetabular anatomy.

Squatting movement data were collected at 100 Hz using 10 infrared cameras (Vicon; Centennial, CO) and 70 skin-mounted markers placed on each subject. All subjects performed at least 3 successful double-legged squatting sequences (**Figure 6.2**) without interrupted motion or loss of balance, with each foot on separate in-ground force platforms (Bertec; Columbus, OH). Ground reaction forces on both feet were recorded at 2000 Hz. Marker trajectory and ground reaction force data were low-pass filtered with 8 Hz and 10 Hz cutoff frequencies respectively, as determined with a residual analysis [18].

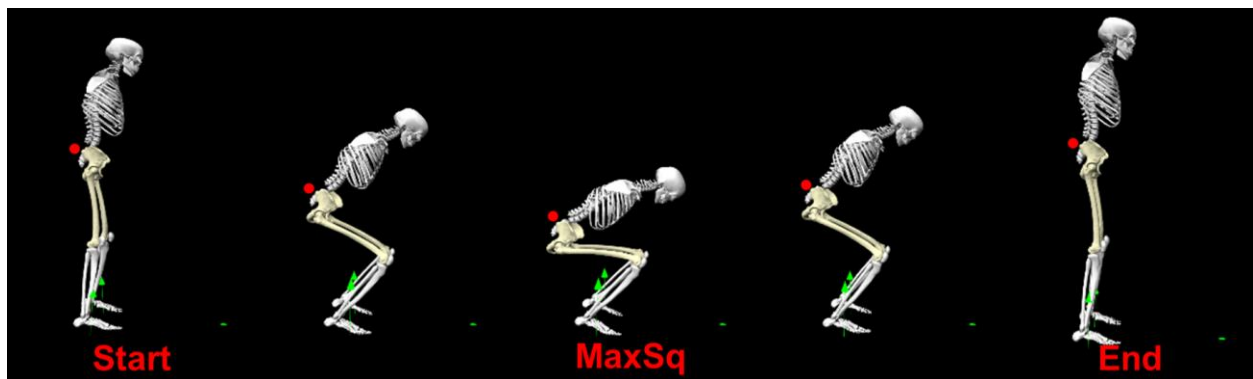


Figure 6.2. Example of a squatting sequence. Ground reaction forces (green arrows) on each foot were recorded by an in-ground force platform. The start, end, and lowest point of a squatting trial (MaxSq) were determined using the maximum and minimum vertical positions of a skin marker placed above the top of sacrum (red dot).

The start of each squatting trial was defined at the time point when the subject began descending, and ended when the subject finished ascending, based on the maximum vertical

position of a skin marker placed above the top of sacrum (**Figure 6.2**). The minimum vertical position of the sacral marker was used to define the time when the subject reached the lowest point of squat ('MaxSq'; **Figure 6.2**).

6.3.2 Image-based Musculoskeletal Models

Subject-specific musculoskeletal models were created in the OpenSim software [19] as recently described [16]. Briefly, a generic OpenSim model [20] was modified by adding MR-based pelvis and femur bony anatomy, including landmark-based 3D alignment of the pelvis tilt, obliquity, and rotation. Aligned 3D bony anatomy was then used to update hip joint center (HJC) locations, muscle anatomical paths, and muscle-tendon physiological parameters in the model specific to each subject. These models were validated with electromyography as previously reported [16].

One representative squatting trial for each subject was simulated in OpenSim to estimate hip biomechanics. Joint angles and net moments were calculated via inverse kinematics and inverse dynamics [18]. Resultant hip JRFs and their antero-posterior, supero-inferior, and medio-lateral components were computed using OpenSim Joint Reaction Analysis [15] from muscle forces estimated via static optimization [21]. Hip JRF components were expressed in the pelvis frame to represent loading onto the acetabulum. JRFs, joint angles and moments on the symptomatic side of each DDH subject were chosen for subsequent analyses; for comparison, a random hip was chosen for each control subject.

6.3.3 Acetabular Edge Loading (AEL) Estimation

AEL on the analyzed hip during each squatting trial was computed by mathematically projecting hip JRFs onto the acetabular anatomy in each subject-specific model. First, the acetabular rim was delineated on each MR-based 3D pelvis, using a principle curvature heat map

(**Figure 6.3A**). Then, on each acetabular rim, nine clock-face points were designated within the anterior (2-4 o'clock), superior (11-1 o'clock), and posterior (8-10 o'clock) quadrants (**Figure 6.3B**) [22]. A right-view clock-face convention was adopted for all hips regardless of side such that 3 o'clock represented anterior for both right and left hips [22].

The hip JRF was represented as a 3D force vector stemming from the center of femoral head, i.e. the HJC (**Figure 6.3C**). The direction of AEL was defined as the vector from HJC to a point on the acetabular rim. The AEL magnitude was then estimated via trigonometric projection of the JRF along the AEL direction towards each of the 9 clock-face points (**Figure 6.3C**). Next, a 'JRF-to-edge angle' was defined as the angle between the JRF direction and the AEL direction, which represented how close the JRF direction was relative to the edge [23]. The JRF-to-edge angle was also computed at each clock-face point.

The JRF magnitude and direction both change over the course of the squatting sequence. Therefore, the clock-face AEL magnitude and JRF-to-edge angle are both time-dependent, and were calculated at each time frame throughout every squatting trial. AEL was then numerically integrated over the duration of the whole trial to calculate its accumulative impulse throughout the squatting sequence.

Lastly, a 3D 'acetabular edge plane (AEP)' was fit to each delineated acetabular rim (**Figure 6.3D**). The distance from each HJC to AEP was calculated to approximate the relative position between the femoral head center and the acetabular border, as an additional mechanistic factor that could potentially alter hip JRFs [16] and the AEL during squat.

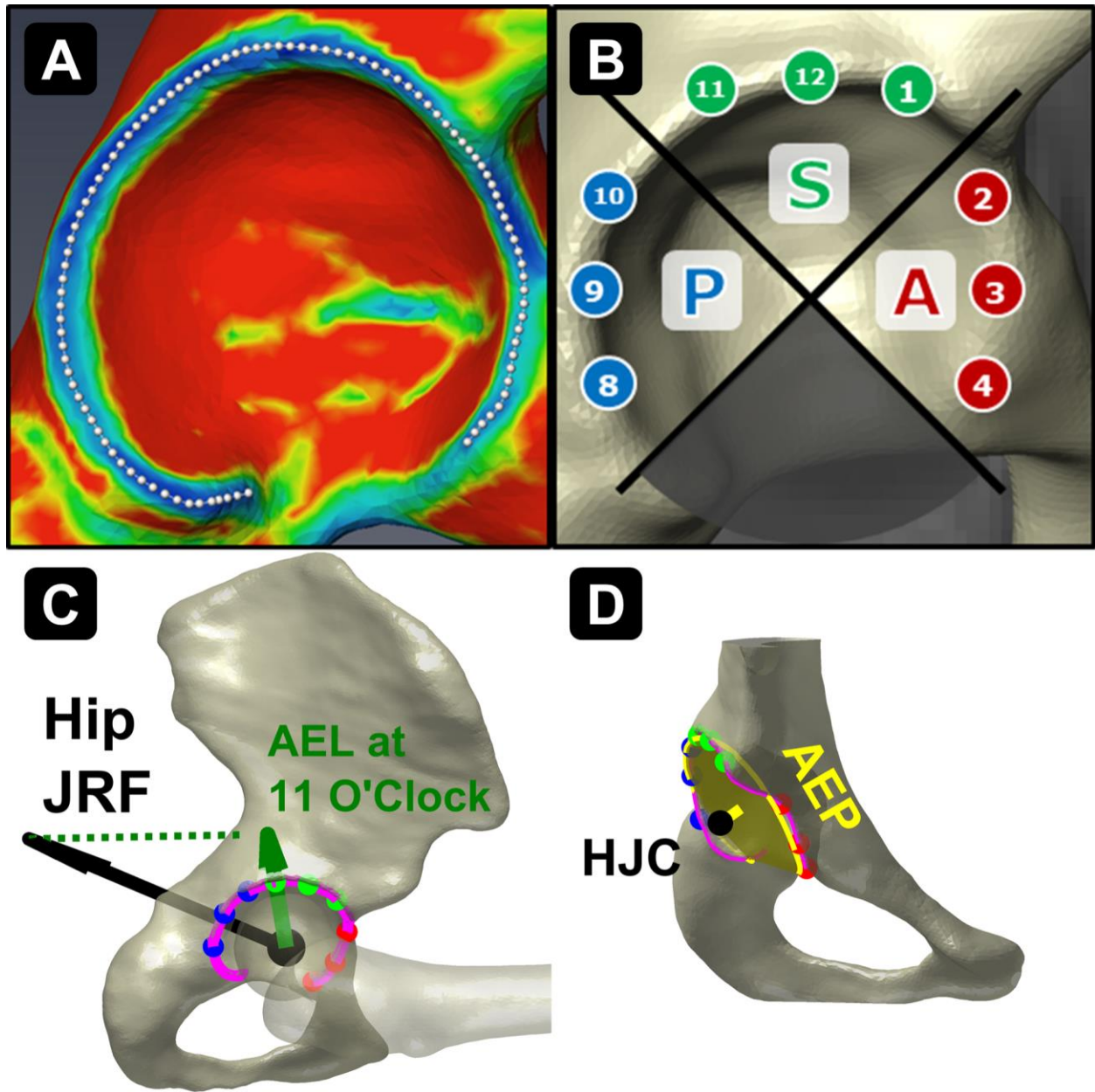


Figure 6.3. Estimation of acetabular edge loading (AEL) during squat. (A) The acetabular rim of each hip was delineated using a principal curvature heat map. (B) Nine clock-face points were designated on the anterior (“A”), superior (“S”), and posterior (“P”) quadrants of the rim. (C) AEL magnitudes were estimated via trigonometric projection of the hip JRF (black arrow) along the directions from HJC towards each clock-face point on the rim (e.g. green arrow for 11 o’clock). The JRF-to-edge angle was defined as the angle between the JRF and the AEL directions (e.g. between black and green arrows). Diagram depicts hip JRF near the lowest point of squat, which was in the posterior direction while AEL was projected to the posterior and superior acetabulum. (D) An ‘acetabular edge plane (AEP)’ was fit to the rim to measure the distance between the approximated acetabular border and the HJC (yellow line).

6.3.4 Data Analysis and Statistics

Hip JRFs, clock-face AEL, and JRF-to-edge angles were time-normalized to 0-100 percent of a squatting trial. The forces were then normalized by body weight (unit: $\times BW$). To include the influence of squatting duration, the accumulative impulses of AEL were not time-normalized, but magnitudes were normalized by BW (unit: $\times BW \cdot s$). Net hip moments were normalized by body mass (unit: Nm/kg). All time-dependent forces, angles, and moments were extracted at the time of MaxSq for subsequent statistical analyses, along with the integrated accumulative impulses.

Each demographic and biomechanical variable was assessed for normality using the Shapiro-Wilk test. Normally distributed variables were compared between the DDH and control groups using independent *t*-tests, with corrections for heterogeneity of variance as needed. Variables violating data normality were compared using the non-parametric Mann-Whitney *U* tests. Statistical significance for all tests was $\alpha = 0.05$. Effect sizes were determined by Cohen's *d*, with a large effect defined as $d \geq 0.8$ [24]. Within the DDH subjects, associations between biomechanical variables (JRFs, AEL, JRF-to-edge angles) and radiographic measures (LCEA and AI) were assessed using Pearson's correlation (*r*), or Spearman's rank correlation (ρ) if data violated normality; a strong correlation was defined as $|r|$ or $|\rho| \geq 0.5$ [24].

6.4 Results

6.4.1 Subject Demographics and Anatomy

The DDH and control groups did not differ significantly in age, height, mass, or body-mass index (**Table 6.1**). The average LCEA and AI values for the DDH subjects were within ranges of the clinical definitions of DDH [17]. HJC-to-AEP distance was significantly larger in hips with DDH compared to controls (**Table 6.1**), which strongly correlated with a smaller LCEA ($r = -0.56$) among the DDH subjects.

Table 6.1. Demographics, radiographic measures, and the HJC-to-AEP distance (mean \pm SD) of DDH and control subjects.

	DDH (n = 10)	Control (n = 10)	p-value
Age (years)	25.5 \pm 7.5	25.7 \pm 7.4	0.96
Height (m)	1.66 \pm 0.09	1.66 \pm 0.05	0.93
Mass (kg)	64.2 \pm 10.5	61.0 \pm 7.7	0.44
Body-mass index (kg/m ²)	23.3 \pm 2.3	22.1 \pm 2.5	0.30
Lateral Center-Edge Angle (degrees)	14.0 \pm 5.2	N/A	-
Acetabular Inclination (degrees)	16.3 \pm 6.1	N/A	-
HJC-to-AEP distance (mm)	8.8 \pm 1.9	6.0 \pm 1.6	<0.01

Note: Radiographic measurements were only made for the DDH subjects. HJC, hip joint center; AEP, acetabular edge plane.

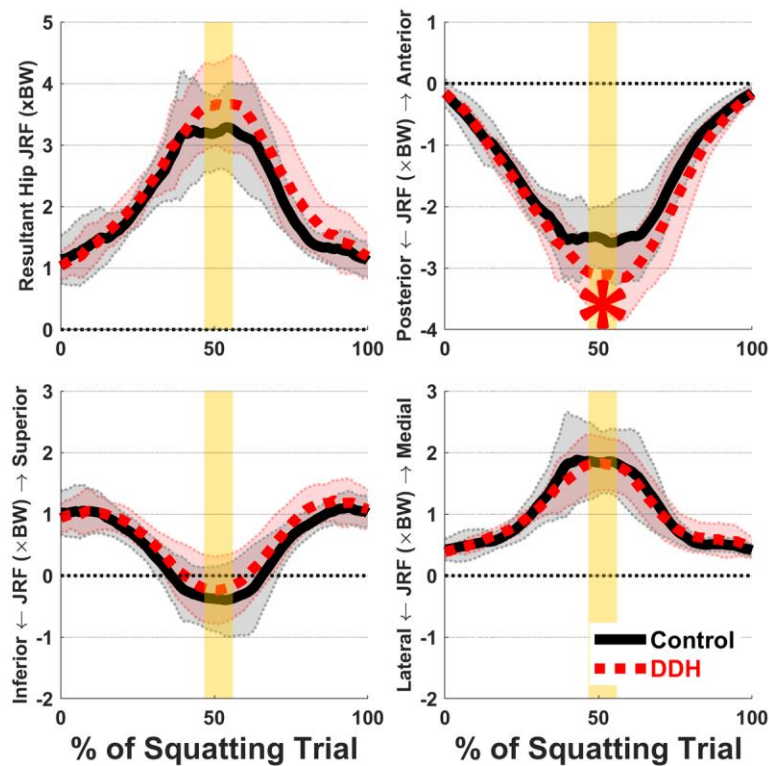


Figure 6.4. Hip JRF resultant and antero-posterior, supero-inferior, medio-lateral components throughout a squatting trial, averaged among DDH and control subjects. Red/black shades = \pm 1 SD. Vertical yellow bars indicate time of lowest point of squat (MaxSq). ‘*’ Indicates inter-group statistical significance.

6.4.2 Hip JRFs

At MaxSq, DDH subjects had significantly higher posterior hip JRFs compared to healthy controls (3.4 ± 0.6 vs $2.7 \pm 0.7 \times \text{BW}$, **Figure 6.4**; $p = 0.03$, $d = 1.05$). Higher posterior JRFs also correlated with smaller LCEA for the DDH subjects ($r = 0.52$).

6.4.3 Clock-Face AEL and JRF-to-Edge Angles

At MaxSq, DDH subjects had higher AEL in the posterior acetabular region compared to controls, which extended to the posterior end of the superior region (8-11 o'clock, **Figure 6.5**; $p \leq 0.04$, $d \geq 0.99$) and correlated with smaller LCEA from 9-11 o'clock ($r \leq -0.63$). Averaged AEL at MaxSq across 8-11 o'clock points was $2.6 \times \text{BW}$ in DDH vs. $1.8 \times \text{BW}$ in controls. Elevated AEL accompanied reduced JRF-to-edge angles across the entire posterior and superior regions (8-1 o'clock, **Figure 6.5**; $p \leq 0.03$, $d \geq 1.17$), which correlated with smaller LCEA from 9-12 o'clock ($r \geq 0.56$).

Over the whole squatting sequence, DDH subjects had higher AEL accumulative impulses from the superior end of the posterior acetabulum to the most superior region (10-12 o'clock, **Figure 6.5**; $p \leq 0.04$, $d \geq 0.97$), which were slightly less posterior and more superior compared to the high-AEL regions at MaxSq. Averaged AEL accumulative impulse across 10-12 o'clock points was $2.6 \times \text{BW} \cdot \text{s}$ in DDH vs. $1.9 \times \text{BW} \cdot \text{s}$ in controls. Higher accumulative AEL correlated with smaller LCEA ($\rho = -0.54$) at 12 o'clock.

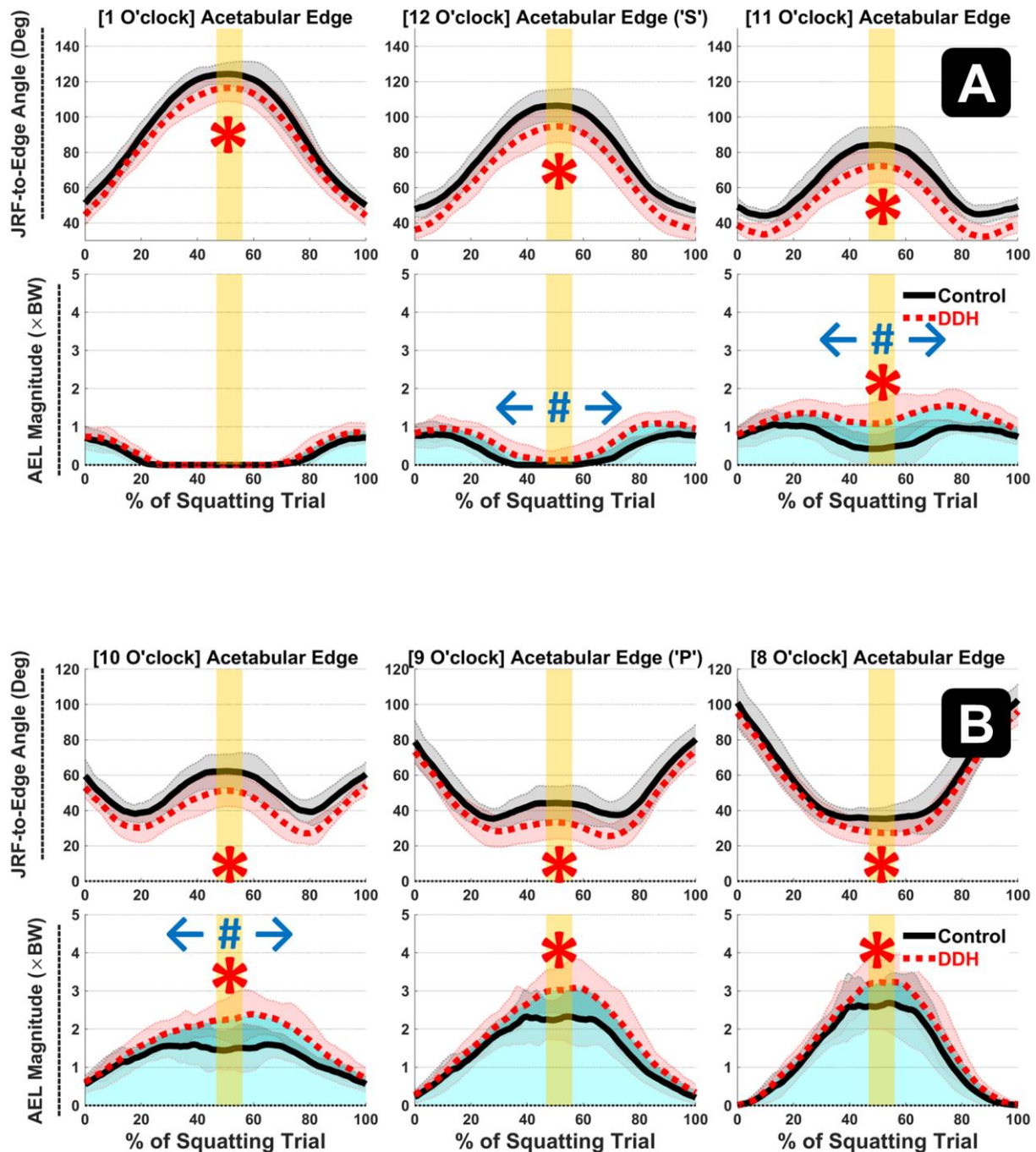


Figure 6.5. Average JRF-to-edge angles (top) and AEL (bottom) in (A) superior (11-1 o'clock) and (B) posterior (8-10 o'clock) regions throughout a squatting trial. Note AEL in the anterior region (2-4 o'clock) was minimal, where no inter-group differences were found, thus were not shown. Red/black shades = ± 1 SD. Vertical yellow bars indicate time of MaxSq. Blue shades illustrate accumulative impulses over the duration of a whole squatting trial. Inter-group statistical significance: '*' instantaneous, '#' accumulative.

6.4.4 Joint Angles and Moments

At MaxSq, DDH subjects had a small pelvis obliquity towards contralateral, instead of towards ipsilateral for controls ($-1.1^{\circ} \pm 2.4^{\circ}$ vs. $1.4^{\circ} \pm 1.8^{\circ}$, $p = 0.01$, $d = 1.20$). Hip moments significantly differed between the groups, as DDH subjects had larger hip extension moments (0.82 ± 0.21 vs. 0.65 ± 0.14 Nm/kg, $p = 0.04$, $d = 0.97$) and smaller external rotation moments (0.06 ± 0.11 vs. 0.17 ± 0.09 Nm/kg, $p = 0.02$, $d = 1.18$) than controls at MaxSq.

6.5 Discussion

The objective of this study was to use image-based musculoskeletal models to estimate AEL during double-legged squat in hips with DDH compared to healthy controls. Our models demonstrated that AEL during squat was higher in the posterior-to-superior regions of the acetabula with DDH, and the extent of elevated AEL was correlated with the severity of DDH acetabular deformity (as quantified by the LCEA and AI radiographic measures), which generally supported our hypothesis. Elevated posterior AEL coincided with increased hip JRFs and net hip extension moments, which suggested that labral loading is directly dependent on task-specific movements and muscle-induced joint loading. A particularly interesting finding was that the regions of elevated peak and accumulative AEL corresponded to the intensity and duration of hip JRFs respectively, which supported the distinctive contributions of acute and chronic joint loading and the multiple pathways to region-specific labral pathomechanics. The convoluted influences of abnormal anatomy, task-specific movements, and duration of loading suggest that the risks for DDH-related labral tears may be highly subject-specific, thus the anatomical, lifestyle, and time factors for unique patient individuals should all be considered during clinical evaluation and the corresponding treatment decision making.

The anatomical deformity of the dysplastic acetabulum likely contributed to elevated AEL during double-legged squat. We found that AEL in the superior region of the acetabula with DDH was not only higher than controls, but also associated with smaller LCEA, a standard clinical measure of shallow lateral acetabulum [8,17]. Namely, the severity of supero-lateral deficiency directly linked to the extent of AEL elevation at the superior acetabular edge, which agreed with prior finite element models that showed higher contact stresses on the supero-lateral labrum during simulated gait [9]. Even as hip joint motions and loading patterns were entirely different between a gait cycle and a squatting sequence, elevated loading on the shallow supero-lateral edge was common for both movement tasks. Considering supero-lateral deficiency is almost universal in hips with DDH [14], this region may be prone to mechanically-induced labral tears for most patients.

The elevation of posterior AEL is unique to high hip flexion tasks such as double-legged squat, and may be caused by a combination of mechanical and anatomical factors. Because most clinical reports from Western countries found antero-superior labral tears to be more common [7,10], the importance of posterior labral mechanics has not been emphasized. Yet, other than Japanese studies that found over 70% of the tears posteriorly [12,13], in some reports from Western countries, there were also tears or fraying of the posterior labrum in more than 25% of the patients [7,10]. These studies have associated the posterior tears with traumatic high-impact events. Such association is supported by our finding of higher-than-control posterior JRFs in DDH at MaxSq, a time point when high impact loading was exerted to the posterior acetabulum and possibly near the labrum at the edge. The higher posterior JRFs may in turn be a result of the abnormal DDH anatomy, including an increased HJC-to-AEP distance that alters force production from the surrounding hip muscles [16]. Indeed, the total muscle force demand to maintain the squatted

position may be higher in DDH subjects, as suggested by the higher net hip extension moments at MaxSq. It should be noted that the inter-group differences in hip moments, JRFs and AEL all existed without a substantial difference in hip angles at MaxSq. The contrast of similar kinematics and altered mechanics indicates that abnormal anatomy can combine with possibly normal motions and still results in abnormal articular forces. Hence for individuals with DDH whose routine or lifestyle demands frequent high hip flexion tasks, extra attention should be paid to the risks of posterior labral pathomechanics, even if there is no visible movement deficiency.

Although generally posterior, the regions of higher-than-control peak and accumulative AEL due to DDH slightly differed, which may indicate the multiple mechanical pathways that could lead to DDH-related labral tears. The instantaneous AEL peaked near MaxSq along with the resultant and posterior hip JRFs. Accordingly, the regions of elevated peak AEL were most posterior (8-11 o'clock) where the peak JRF was directed (**Figure 6.3C**). However, when integrated over the full squatting sequence, the accumulative effect of elevated AEL was most evident in a postero-superior region (10-12 o'clock) that did not include the very posterior end. It is notable that although the posterior-most region was bearing the peak hip loading mid-squat, the postero-superior region was loaded for a longer duration throughout the squatting sequence. The time-dependent effect may be best seen at 11 o'clock, where AEL during the descending and ascending phases of squat exceeded that near MaxSq (**Figure 6.5A**, right). These findings support clinical reports of the postero-superior labral tear locations [13], and highlight the potential roles of repetitive loading on mechanically-induced damage. Collectively, these results indicate that acute high impact and insidious repetitive overloading during high hip flexion tasks could both contribute to posterior labral damage, with each affecting potentially different locales. Vice versa, evaluating the patterns of DDH-related labral damage in context with quantitative hip mechanics

such as the task-specific AEL may help clinicians identify patient-specific etiology and possibly a better-informed decision for treatments.

Our study was the first to estimate in-vivo loading at the native hip acetabular edge during double-legged squat. A few past studies also used musculoskeletal models to predict edge loading risks in prosthetic hip acetabular cups during tasks ranging from routine gait [23] to high hip flexion sit-to-stand [25]. These prior studies showed that movement alterations such as increased hip abduction could effectively lower the risks of edge loading. Analogously, movement alterations could also potentially reduce edge loading in the pre-arthritis hips with DDH. Indeed, recent musculoskeletal models demonstrated that movement retraining can lower JRFs in dysplastic hips during single-legged squat [26]. While surgical correction of anatomy remains the most common treatment for DDH, new interventions that involve movement retraining should be considered to further reduce the risks of edge loading.

The results of this study and our interpretations should be considered with several limitations. First, our results do not necessarily capture the precise effects of posterior acetabular deformity on AEL. The LCEA and AI angles primarily quantify lateral acetabular deficiency, while standardized radiographic measures such as the crossover and posterior wall signs only qualitatively (and often poorly) describe posterior deficiency [14,17]. Some 3D-based measures on posterior coverage exist such as the acetabular sector angle [27], but their reliability on MR images has not been verified. Recent research have combined 3D acetabular and femur anatomy from MR to quantify region-specific coverage [28], which may be used to characterize the relationships between posterior deficiency and task-specific AEL. Second, the relatively small sample size could not empower us to reliably detect the underlying mechanistic factors that could contribute to the altered muscle demand (i.e. net hip moments) and induced hip loading (i.e. JRFs).

For example, the smaller-than-control hip external rotation moments may indicate subtle kinetic strategies adapted by the DDH subjects to compensate for increased hip extension moments. Altered hip kinetics and muscle activity during squat have been observed in subjects with femoroacetabular deformity [29], and could likewise occur in those with DDH. With a larger cohort, future studies may further delineate the neuromuscular risk factors that ultimately lead to abnormal articular or labral loading. Lastly, the static optimization criterion we used to estimate muscle forces may underestimate hip muscle co-contractions during squat, and thus the muscle-induced JRFs and AEL. We chose this method to better match the benchmark hip JRF data and other recent hip musculoskeletal models used to simulate double-legged squats [21].

In conclusion, AEL during double-legged squat was significantly elevated in the posterior-to-superior regions of the acetabula with DDH, which was correlated with the severity of anatomical deformity. Elevated posterior AEL coincided with increased hip JRFs and net hip extension moments, indicating altered kinetics and muscle demand that were unique to squatting motion and also contributed by the abnormal anatomy. Regions of AEL elevation corresponded to the intensity and duration of hip loading, which supported time-dependent effects and the multiple distinctive pathways to region-specific labral pathomechanics in DDH. These findings collectively suggest that AEL is highly dependent on task-specific movements and muscle-induced joint loading, thus unique to the routine lifestyles of patient individuals. For this reason, we recommend future clinical evaluation of DDH to consider the anatomical, lifestyle, and time factors together and specifically for each patient, in order to make personalized treatment decisions that better reduce the risks of secondary labral and articular damage.

6.6 Acknowledgments

This project was funded by the National Institutes of Health K01 AR072072, P30 AR074992 and the Lottie Caroline Charitable Trust. The authors thank Molly Shepherd, Lauren Westen, Abby Matt, and Spencer Williams for assistance with MR image and motion data processing.

6.7 References

1. Gala L, Clohisy JC, Beaulé PE. Hip dysplasia in the young adult. *J Bone Joint Surg Am* 2016 Jan 6;98(1):63-73.
2. Beaulé PE, editor. Hip dysplasia: understanding and treating instability of the native hip. Cham, Switzerland: Springer Nature Switzerland AG; 2020.
3. Felson DT. Osteoarthritis as a disease of mechanics. *Osteoarthritis Cartilage* 2013 Jan;21(1):10-5.
4. Hartig-Andreasen C, Søballe K, Troelsen A. The role of the acetabular labrum in hip dysplasia. A literature overview. *Acta Orthop* 2013 Feb;84(1):60-4.
5. Maquet P. Biomechanics of hip dysplasia. *Acta Orthop Belg* 1999 Sep;65(3):302-14.
6. Lewis CL, Sahrman SA. Acetabular labral tears. *Phys Ther* 2006 Jan;86(1):110-21.
7. McCarthy JC, Noble PC, Schuck MR, Wright J, Lee J. The Otto E. Aufranc Award: the role of labral lesions to development of early degenerative hip disease. *Clin Orthop Relat Res* 2001 Dec;(393):25-37.
8. Wiberg G. Studies on dysplastic acetabula and congenital subluxation of the hip joint with special reference to the complication of osteoarthritis. *Acta Chir Scand*. 1939;83 Suppl 58:7-135.
9. Henak CR, Abraham CL, Anderson AE, Maas SA, Ellis BJ, Peters CL, Weiss JA. Patient-specific analysis of cartilage and labrum mechanics in human hips with acetabular dysplasia. *Osteoarthritis Cartilage*. 2014 Feb;22(2):210-7.
10. Santori N, Villar RN. Acetabular labral tears: result of arthroscopic partial limbectomy. *Arthroscopy*. 2000 Jan-Feb;16(1):11-5.
11. Lewis CL, Sahrman SA, Moran DW. Effect of hip angle on anterior hip joint force during gait. *Gait Posture*. 2010 Oct;32(4):603-7.

12. Hase T, Ueo T. Acetabular labral tear: arthroscopic diagnosis and treatment. *Arthroscopy*. 1999 Mar;15(2):138-41.
13. Ikeda T, Awaya G, Suzuki S, Okada Y, Tada H. Torn acetabular labrum in young patients. Arthroscopic diagnosis and management. *J Bone Joint Surg Br*. 1988 Jan;70(1):13-6.
14. Nepple JJ, Wells J, Ross JR, Bedi A, Schoenecker PL, Clohisy JC. Three patterns of acetabular deficiency are common in young adult patients with acetabular dysplasia. *Clin Orthop Relat Res*. 2017 Apr;475(4):1037-44.
15. Steele KM, Demers MS, Schwartz MH, Delp SL. Compressive tibiofemoral force during crouch gait. *Gait Posture*. 2012 Apr;35(4):556-60.
16. Song K, Gaffney BMM, Shelburne KB, Pascual-Garrido C, Clohisy JC, Harris MD. Dysplastic hip anatomy alters muscle moment arm lengths, lines of action, and contributions to joint reaction forces during gait. *J Biomech*. 2020 Sep 18;110:109968.
17. Clohisy JC, Carlisle JC, Beaulé PE, Kim YJ, Trousdale RT, Sierra RJ, Leunig M, Schoenecker PL, Millis MB. A systematic approach to the plain radiographic evaluation of the young adult hip. *J Bone Joint Surg Am*. 2008 Nov;90 Suppl 4:47-66.
18. Winter DA. *Biomechanics and Motor Control of Human Movement*. 3rd ed. Hoboken, NJ: John Wiley & Sons; 2004.
19. Delp SL, Anderson FC, Arnold AS, Loan P, Habib A, John CT, Guendelman E, Thelen DG. OpenSim: open-source software to create and analyze dynamic simulations of movement. *IEEE Trans Biomed Eng*. 2007 Nov;54(11):1940-50.
20. Lai AKM, Arnold AS, Wakeling JM. Why are antagonist muscles co-activated in my simulation? A musculoskeletal model for analysing human locomotor tasks. *Ann Biomed Eng*. 2017 Dec;45(12):2762-74.
21. Catelli DS, Ng KCG, Wesseling M, Kowalski E, Jonkers I, Beaulé PE, Lamontagne M. Hip muscle forces and contact loading during squatting after cam-type FAI surgery. *J Bone Joint Surg Am*. 2020 Nov 4;102(Suppl 2):34-42.
22. Goronzy J, Blum S, Hartmann A, Plodeck V, Franken L, Günther KP, Thielemann F. Is MRI an adequate replacement for CT scans in the three-dimensional assessment of acetabular morphology? *Acta Radiol*. 2019 Jun;60(6):726-734.
23. Wesseling M, Meyer C, De Groote F, Corten K, Simon JP, Desloovere K, Jonkers I. Gait alterations can reduce the risk of edge loading. *J Orthop Res*. 2016 Jun;34(6):1069-76.

24. Cohen J. Statistical Power Analysis for the Behavioral Sciences. 2nd ed. Hillsdale, NJ: Lawrence Earlbaum Associates; 1988.
25. van Arkel RJ, Modenese L, Phillips AT, Jeffers JR. Hip abduction can prevent posterior edge loading of hip replacements. *J Orthop Res*. 2013 Aug;31(8):1172-9.
26. Gaffney BMM, Harris-Hayes M, Clohisy JC, Harris MD. Effect of simulated rehabilitation on hip joint loading during single limb squat in patients with hip dysplasia. *J Biomech*. 2021 Feb 12;116:110183.
27. Anda S, Terjesen T, Kvistad KA, Svenningsen S. Acetabular angles and femoral anteversion in dysplastic hips in adults: CT investigation. *J Comput Assist Tomogr*. 1991 Jan-Feb;15(1):115-20.
28. Gaffney BMM, Clohisy JC, Van Dillen LR, Harris MD. The association between periacetabular osteotomy reorientation and hip joint reaction forces in two subgroups of acetabular dysplasia. *J Biomech*. 2020 Jan 2;98:109464.
29. Catelli DS, Kowalski E, Beaulé PE, Smit K, Lamontagne M. Asymptomatic participants with a femoroacetabular deformity demonstrate stronger hip extensors and greater pelvis mobility during the deep squat task. *Orthop J Sports Med*. 2018 Jul 17;6(7):2325967118782484.

Chapter 7: Summary and Future Directions

7.1 Conclusions, Significance, and Novelty

This research aimed to (1) establish and standardize the creation of image-based MSMs for estimation of hip biomechanics in DDH, and then to (2) use subject-specific MSMs to estimate hip biomechanics in DDH compared to healthy controls, and analyze their relationships with the hip anatomical abnormalities of DDH. To address these aims, image-based MSMs with detailed anatomy were first compared against conventional MSMs with generic anatomy, to identify the influences of model anatomy on estimated hip biomechanics, on both DDH and healthy control subjects (Chapter 3). Findings from Chapter 3 helped determine the level of anatomical details in MSMs needed for reliable and feasible estimation of DDH biomechanics. Then, using MSMs with the appropriate level of specificity, key biomechanical estimates such as hip joint reaction forces (JRFs) and muscle forces during gait were compared between DDH and control groups along with hip muscle moment arm lengths (MALs) and lines of action (LoAs), to clarify the relationships between DDH hip anatomy, dynamic muscle force production, and contributions to joint loading (Chapter 4). Next, muscle-induced hip JRF estimates from the MSMs were projected to image-based 3D pelvis to predict how DDH bony anatomy affects dynamic loading at the shallow acetabular edge (Chapter 5). In addition to DDH-to-control comparisons, acetabular edge loading (AEL) during gait was also analyzed against clinical radiographic measures to determine its associations with the anatomical characteristics. Finally, MSM-based AEL methods in Chapter 5 were extended to analyze double-legged squat (Chapter 6), to more comprehensively identify the contributors to task-specific articular-level hip biomechanics in DDH. Outcomes from Chapters 4 through 6 helped clarify both the mechanistic sources and influences of abnormal joint loading in hips with DDH during dynamic movements, which improved our knowledge how mechanically-

induced joint damage may be developed in those structurally abnormal hips. Such new knowledge can potentially inform personalized clinical evaluation and treatments of DDH to better correct the hip biomechanical environment and improve long-term hip joint health.

Despite their significant clinical meanings, hip joint and muscle forces in DDH during dynamic activities have rarely been quantified, partly due to the difficulties with direct measurements. Even as MSMs can estimate such quantities via simulation, the few MSM studies on DDH prior to this dissertation [1,2] did not reach consensus on the biomechanical findings, potentially due to the different levels of model anatomy used. To determine whether detailed model anatomy is a prerequisite for MSMs to delineate hip pathomechanics unique to DDH, direct model-to-model comparisons on the same subjects were needed [3]. Chapter 3 was the first study to make such comparisons on both DDH and healthy subjects, which found estimates from CT-based subject-specific MSMs and scaled generic MSMs to be significantly different, and differences among the models on DDH subjects were larger than those on the controls. Especially, higher hip JRFs as a result of dysplastic bony anatomy supported past mechanical theories of DDH [4], which indicated a relative improvement in model accuracy. Among potential contributors to the altered JRFs, a more accurate representation of the lateralized hip joint center (HJC) [5] was speculated as a major factor. These findings suggest that a high level of patient-specific anatomical detail that captures the unique deformity traits of DDH is necessary for MSMs to identify potentially detrimental hip mechanics during dynamic movements. A notable finding was that the moderately-specific models with CT-based pelvis scaling estimated very similar JRFs and muscle forces to the generic MSMs. These “semi-specific” MSMs were still more specific than generic, but much simpler (and cost-friendly) than models using full CT-based 3D anatomy, because the nonuniform scaling would be replicable with multi-view 2D radiographs readily available in the clinics.

However, the non-difference versus generic suggests such approach was not enough to identify the unique hip mechanics of DDH. Therefore, even as their creation remains an challenging task, image-based MSMs were recommended as the most appropriate for estimating hip biomechanics in DDH. This conclusion from Chapter 3 provide valuable references on how MSMs may be used in DDH and other hip-related biomechanical studies, while laying the methodological framework for the subsequent studies in this dissertation.

Past theories [4] and model studies [5] including MSMs [2] have all agreed that abnormal bony anatomy is a major contributor to pathological hip joint loading in DDH. However, the mechanistic relationships between anatomy (deformity of the bones) and dynamic forces (altered joint loading during movements) were not fully clarified. For example, it was unclear *how* lateralized HJC [6] contributed to higher hip JRFs compared to controls [2] and in DDH-specific models (Chapter 3) [7]. Because dynamic hip loading was known to be primarily contributed from hip muscles [8], Chapter 4 was dedicated to the analyses of two muscle parameters directly linked to both anatomical path and dynamic force production, the MAL and the LoA. The primary finding was that the lateralized HJC became closer to the hip abductor muscle paths (e.g. gluteus medius), which reduced its MALs and effectiveness at generating hip-stabilizing torques during gait stance, resulting in an elevated force demand. This result was consistent with the very limited past finding on hip muscle MALs in DDH [9], yet novel as it described the muscles' mechanical effectiveness true to the joint dynamic positions. Another new finding was the roles of secondary muscle actions and out-of-plane contributions, such as the potential adduction and internal rotation effects of the iliopsoas [10]. Because many hip muscles produce high forces during routine tasks, their 3D coordination and force contribution can alter hip joint loading significantly. Such 3D contributions were further affirmed by the higher gluteal muscle medial LoAs in DDH and concurrently higher

medially-directed JRFs [2]. To summarize, results of Chapter 4 showed how DDH bony anatomy directly alters muscle dynamic force production and 3D action, which had significant contributions to hip joint loading. These findings can help update the current theoretical paradigm on how DDH anatomy leads to abnormal biomechanics, by demonstrating the roles of hip muscles that may be previously overlooked. This new knowledge on the hip anatomy-force relationships can also potentially help clinical treatments, including movement retraining, to optimize the dynamic hip biomechanical environment specific to patients' activity demands during daily living.

Although past MSMs [1,2] and Chapter 4 [10] both showed that muscle-induced hip JRFs are altered in DDH, it was a challenge to understand how the model-based JRFs are related to mechanically-induced pathology, and how it should be interpreted in context with the clinical characteristics of the disease. As a clinically important example, acetabular labral tears are among the most prevalent forms of damage in DDH and may be caused by abnormal dynamic loading at the shallow acetabular edge [11,12]. MSM studies have analyzed acetabular edge loading (AEL) in prosthetic hips [13,14], but extension of such analyses to native hips was limited by the model representation of subject-specific anatomy, which was found to be essential for DDH research (Chapter 3) [7]. In Chapter 5, the subject-specific MSMs established from Chapter 3 and refined through Chapter 4 enabled dynamic prediction of muscle-induced AEL in DDH, both compared with controls and analyzed by correlations with clinical radiographic measures such as the LCEA and AI angles. The primary result was that the characteristic shallow acetabulum caused its edge to be in close proximity with the hip JRF direction, which directly led to a larger force component (AEL) projected towards the edge. Elevated AEL during gait occurred in the anterior and superior acetabulum, which matched the regions bearing high repetitive forces during gait [8] and where labral tears were most frequently found [11,12]. Elevated AEL was also strongly correlated with

standard clinical metrics of DDH acetabular anatomy (LCEA and AI), suggesting the risks for labral and chondral damage may increase with the severity of the deformity. An important finding was that when integrated over time, the accumulative impulse of AEL was elevated over a wide region of the acetabular rim, which affirmed the roles of chronic overloading on the insidious developments of labral tears [15,16]. Overall, findings from Chapter 5 supported past models of labral pathomechanics in DDH [5] and were analogous to AEL in prosthetic hips [13,14], yet was the very first to quantify muscle-induced dynamic AEL in native hips, either with or without abnormal anatomy. The novel methods enabled by image-based MSMs provide new insights into the mechanical causes of labral and chondral damage in DDH, and support the needs for clinical evaluations to consider patient-specific hip biomechanics in context with anatomical traits.

It should be noted that although anatomical deformity is the best-known characteristic of DDH, anatomy alone may not fully explain the patient-specific risks for all types of DDH-related joint damage. Regarding labral tears, a unique clinical observation is the prevalence of posterior tear location for some patients, which were thought to be related to high hip flexion relevant to certain routine lifestyles [17,18] or sports [15]. Despite a potential dependency between posterior labral tears and dynamic AEL during high hip flexion tasks such as double-legged squat, no past study has quantified hip biomechanics during such dynamic tasks in hips with DDH. As the first study to do so, Chapter 6 found increased posterior AEL in hips with DDH compared to controls, which accompanied simultaneous increase in peak posterior JRFs and net hip extension moments near the lowest point of squat. These differences indicate hips with DDH may have altered kinetics and muscle demand unique to squatting motion, even as movement patterns were not substantially different from controls. Similar to Chapter 5, the effects of loading duration was also substantial, as the region of elevated accumulative AEL differed from that of the peak AEL, which supported

the multiple mechanical pathways that could lead to both acute and chronic damage. Overall, AEL during gait (Chapter 5) and double-legged squat (Chapter 6) were both elevated by the acetabular deformity of DDH, but in distinct regions that matched the task-specific hip loading. Chapters 5 and 6 collectively support the importance for clinical evaluations of DDH to consider anatomy, lifestyle, and time factors together in order to make patient-specific treatment decisions, including targeted surgical correction and movement retraining, to optimize hip biomechanics during various tasks of daily living and minimize the risks for joint damage and degeneration.

7.2 Limitations and Future Directions

Although the limitations of each specific study have been described in the discussions of Chapters 3 through 6, the MSMs created and used throughout this dissertation shared some common general limitations, which are reviewed here to clearly define the scope of this research and the findings summarized above in Section 7.1. Each limitation may warrant future studies or method developments; such potential directions are described along with each limitation, followed by other future work that is otherwise outside the scope of this dissertation but can be valuable to further advance our knowledge of the biomechanics of DDH.

As with any MSM-based studies of the hip, the lack of direct force measurement data for model validation remains a major challenge. Even as increased hip JRFs due to patient-specific model anatomy [7] were consistent with mechanical theories of DDH [4], without knowing the in-vivo hip JRFs in the same subjects, the absolute accuracy of the MSM-based estimates cannot be directly validated. Compared to hip contact forces recorded from instrumented prosthetics in older individuals [19], MSM-estimated JRFs tended to be higher in magnitude. A recent study found MR-based MSMs to estimate JRFs lower than generic models while closer to the benchmark data, although such findings were based on models of healthy middle-aged subjects [3]. The reliability

of the subject-specific MSMs for DDH was partly supported by their ability to demonstrate altered muscle MALs [10] that were consistent with imaging studies [9] and theoretically contribute to higher JRFs [4]. The MSMs in this dissertation were validated with muscle activation experimental data recorded using electromyography [20], and experimental activation patterns of major hip muscles qualitatively agreed with model estimation [2,10]. Hip JRF and muscle force estimates were also compared among recent MSM studies to ensure general agreements in force magnitudes [2,3,7,10]. Future biomechanics research of DDH and other hip diseases should continue to verify and validate the MSMs following established best practices for simulation [20].

Although the anatomy is improved in image-based MSMs, many other model elements still followed conventional methods. For example, the hip joint center (HJC) was assumed static within the pelvis frame, with only the rotational degrees of freedom allowed (i.e. ideal ball-and-socket joint). Hips with DDH are known to exhibit instability [21,22], which could lead to subtle migrations of the femoral head center (i.e. HJC) inside the acetabulum during motion. Relative HJC translations could influence hip muscle MALs and their force contributions to the JRFs [10], while uncertainties in the HJC-to-acetabulum relative position could further affect dynamic AEL projection. As speculated in Chapters 4, such HJC translations would most likely be lateral due to the deficient femoral coverage [23], which could further elevate the abductor force demand and muscle-induced JRFs. Then in the AEL analyses, because the relative closeness between JRF and the shallow edge would still be captured by the models, projected AEL could be even higher. Thus, the mechanical phenomena found in Chapters 4 through 6 that depicted the causes and effects of dynamic hip loading are expected to be robust to the dysplastic HJC instability, although the extent of biomechanical influences could be underestimated. While HJCs in the current MSMs were updated using CT or MR data, the standard MSM workflow did not facilitate dynamic perturbation

of the HJC mid-simulation. One useful method to potentially address this challenge is probabilistic analyses of the MSM simulations, such as Monte-Carlo methods to determine the sensitivity of biomechanical estimates to uncertainties in model parameters [24,25]. Probabilistic MSMs have recently been used to simulate DDH hip mechanics under treatment scenarios [26,27], and may be applied to analyze the effects of femoral head instability on estimated forces.

As with hip joint position, muscle paths were also personalized in the models using imaging data, but other muscle properties that influence force production were processed generically. For example, the optimal fiber length and tendon slack length of each muscle was linearly scaled according to the updated full anatomical path [3], while maximum isometric force (i.e. strength) was matched to the generic models. Although outside the scope of this dissertation, muscle weakness [28] or muscle-tendon abnormalities [29] in hips with DDH could affect their force production during dynamic movements, and in turn further alter muscle-induced JRFs, AEL, etc. Recent work [27] has used probabilistic MSMs to demonstrate the influences of muscle strength on DDH hip mechanics; future studies can likewise simulate the mechanical effects of muscle fiber or tendon abnormalities. Biomechanics of the hip muscles can also be analyzed along with other muscle properties such as physical size [9,30] to further update our understanding on the roles of hip muscles in the developments of DDH pathology.

Estimating the forces in each hip muscle required solving the underdetermined mechanical system equations, using a static or dynamic optimization criterion (Section 2.3.1) [31,32]. The MSMs in this research used static optimization [31], which was suggested as appropriate for gait simulation while computationally more efficient than dynamic methods [32]. Hip-specific studies also found that static optimization estimated hip contact forces closest to benchmark experimental data during both gait and sit-to-stand [33]. However, static optimization does not consider the time-

dependent effects of muscle physiology, activation, or coordination that could be important in highly dynamic movements such as running or sport-specific tasks [20,32]. Gait and double-legged squat (which involves high hip flexion similar to sit-to-stand) were studied in this dissertation due to their importance in routine mobility and potential links to DDH-specific joint damages. Yet for young adults with DDH, highly dynamic and sport-specific tasks can be relevant, thus future studies should simulate such tasks with MSMs using dynamic characterization of muscle activation and forces. Computed muscle control [34], electromyography-driven muscle activation [35], and synergies-based analysis [36] are some options to predict highly dynamic muscle functions. Future MSMs to study DDH biomechanics during such movements should also verify and validate the chosen approach according to recommended best practices [20].

The mechanical estimates from MSMs are specific to prescribed motion kinematics, and incorporate the effects due to muscle function, making them uniquely useful for understanding the relationships among multiple factors that contribute to joint biomechanics dynamically. However, joint and articular-level mechanics such as JRFs and AEL are only part of the mechanical factors toward joint damage. A common understanding is that tissue damage and degeneration are resulted from abnormal acute or chronic mechanical stresses [37], which have been demonstrated in hips with DDH using finite element (FE) models driven by generic hip joint loading [5]. Because MSMs can quantify subject-specific hip loading, opportunities exist to use MSM-based JRFs (as determined for DDH in this research) to drive FE or discrete element (DE) models for improved estimation of dysplastic hip articular contact stresses [38,39]. Articular stresses estimated from MSM-FE/DE hybrid models may then be compared against medical imaging-based quantifications of cartilage composition [40] to help further clarify the mechanistic connections between altered hip biomechanics and tissue damage in DDH.

It was concluded from Chapter 3 that for reliable estimation of DDH biomechanics, a high level of image-based anatomical detail is required in the MSMs. Although the model creation workflow used throughout this research was standardized in Chapter 3, it remains painstaking and requires many manual geometrical processing steps, which could induce uncertainties to the mechanical estimates [24]. An arduous process also potentially limits the sample size and thus the statistical power for significant findings in future studies. Although the robustness of the MSMs in this dissertation was verified with a sensitivity analysis (Chapter 3) [7], to benefit future DDH biomechanics research in larger scales, automated creation of image-based MSMs will be helpful. Recent publications have introduced several modalities to automatically update joint positions and muscle paths using segmented 3D bony anatomy [41,42]. While these tools provide promising frameworks to create image-based MSMs for DDH, cautions should be taken regarding accurate representation of the unique abnormal anatomy, with manual refinements to be made as needed.

Other than MSM-related limitations, another topic not exhaustively investigated in this research was the associations of DDH biomechanics with the 3D anatomical traits of the hip. Chapters 5 and 6 only analyzed the correlations between biomechanical estimates (JRFs, AEL) with the LCEA and AI angles, which were common clinical metrics of the acetabular anatomy but limited to characterization of the lateral deficiency. Even as LCEA and AI were strongly correlated with antero-superior AEL during gait (Chapter 5) and posterior AEL during squat (Chapter 6), these findings do not necessarily suggest the relative risks for tissue damage in subgroups of DDH who have anterior, posterior, or global acetabular deficiency [23]. Without subgroup mechanical analyses or correlations to 3D metrics of anatomical deformity, it remains undetermined which anatomical traits may be more indicative of damage risks. Furthermore, the mechanical influences of 3D femoral deformities in DDH [43] could also be important, but were beyond the scope of this

dissertation. Such extended analyses were partly limited by the relatively small sample sizes due to the model creation burdens aforementioned. In future studies empowered with automated MSM creation, dynamic muscle MAL, LoA, and AEL methods established in Chapters 4 through 6 may be replicated in subgroups of DDH, and correlations with the 3D anatomy of acetabulum and femurs [23,43] can both be analyzed. These extension studies will help us more comprehensively identify the anatomical factors that contribute to patient-specific pathology.

To truly understand which biomechanical traits of DDH are indicative of joint damage and symptoms, thus can be key modifiable factors for clinical evaluation and intervention to target, we need to establish the relationships between laboratory-based biomechanics and clinical parameters of the DDH presentation or prognosis. Questionnaire-based patient-reported outcomes (PROs) are the most common clinical tools to evaluate DDH patients' pain, functional limitations, and quality of life [44]. Therefore, future studies can analyze the associations between PRO responses and MSM-based biomechanics to determine which variables are most closely linked with symptoms. For example, we may better understand whether elevated posterior AEL during squat is correlated with posterior pain felt by the patients, or their perceived difficulties to perform high hip flexion tasks. Such knowledge may help explain the mismatch between symptom severity and anatomical traits in some patients [44]. Longitudinal analyses will also be highly valuable to determine the associations between biomechanics and the development of joint damage, such as whether hips with elevated AEL would indeed more likely develop labral tears or chondral lesions later. Such research requires a much larger cohort and continued commitment, but will complement clinical studies of hip anatomical and biological changes over time [22] and significantly improve our understanding on how the chronic pathology of DDH is developed.

The ultimate purpose of quantifying hip biomechanics in DDH, along with its relationships with anatomical and clinical parameters, is to help future clinical intervention improve efficacy, preserve hip joint health, minimize the risks for tissue damage, and delay the development of OA. Therefore, an important future extension of this dissertation is to use MSMs to estimate or simulate hip biomechanics in response to the treatments of DDH. As introduced in Chapter 2, Bernese PAO surgery is the most common treatment to correct anatomy in pre-arthritis hips with DDH, which aims to preserve the joint by restoring a normal hip biomechanical environment [45]. Considering the long-term hip joint survival rate after PAO was suboptimal for many [46], quantification of post-PAO, patient-specific hip biomechanics may be a missing piece to explain why some patients had worse surgical outcomes than others. Image-based MSMs for DDH established in this research provide a framework for such analyses, including how modified femoral coverage or medialized HJC could lower hip JRFs [26] and the AEL to help reduce the risks for labral tears. MSM-based dynamic estimates could complement motion analyses [47] and finite element models [48] to refine our understanding of the hip biomechanics after PAO. Likewise, because post-PAO or non-PAO rehabilitation has often lacked quantitative evidences, MSM-based simulations [27] may be combined with muscle-related analyses (e.g. dynamic MALs and LoAs, as in Chapter 4) to predict how rehabilitation could be designed to optimize muscle mechanical functions. Furthermore, as with longitudinal follow-ups of natural disease progression, associations between post-treatment hip mechanics, PROs, and joint biological status may be tracked over time to verify which biomechanical parameters are predictive of favorable clinical outcomes, thus may be emphasized in future intervention. Overall, using subject-specific MSMs in longitudinal studies can yield valuable biomechanical data that fills the knowledge gap between clinical metrics of DDH, thus inform personalized treatments for improved long-term efficacy.

Finally, subject-specific MSMs for DDH may benefit from state-of-the-art technology for research in larger scales and wider scopes. Other than model automation to allow larger cohorts [41,42], the abundance of data can also be analyzed in novel ways to thoroughly explore the roles of biomechanics within the spectrum of DDH etiology. For example, machine learning algorithm is useful for establishing associations between source and outcome variables, and has recently been applied to predict the clinical outcomes of hip arthroscopy [49]. Such approach may be adapted in DDH research, with the addition of MSM-based biomechanical data, to develop predictive models of favorable effects based on clinical evaluation, thereby assist patient-specific treatment decision making. Another promising methodological development is the use of wearable sensors to assess natural dynamic movements outside of laboratory, which could be used to drive MSMs [50] and quantify DDH biomechanics in real-world scenarios for a longer duration, yielding more data representative of unique patient individual's daily living. These modern technologies provide great potentials for scientists to better understand the biomechanics of DDH, for clinicians to improve personalized treatments, and ultimately for more patients to achieve desirable hip joint health.

7.3 References

1. Skalsjø O, Iversen CH, Nielsen DB, Jacobsen J, Mechlenburg I, Søballe K, Sørensen H. Walking patterns and hip contact forces in patients with hip dysplasia. *Gait Posture*. 2015 Oct;42(4):529-33.
2. Harris MD, MacWilliams BA, Bo Foreman K, Peters CL, Weiss JA, Anderson AE. Higher medially-directed joint reaction forces are a characteristic of dysplastic hips: A comparative study using subject-specific musculoskeletal models. *J Biomech*. 2017 Mar 21;54:80-7.
3. Wesseling M, De Groote F, Bosmans L, Bartels W, Meyer C, Desloovere K, Jonkers I. Subject-specific geometrical detail rather than cost function formulation affects hip loading calculation. *Comput Methods Biomech Biomed Engin*. 2016 Nov;19(14):1475-88.
4. Maquet P. Biomechanics of hip dysplasia. *Acta Orthop Belg*. 1999 Sep;65(3):302-14.

5. Henak CR, Abraham CL, Anderson AE, Maas SA, Ellis BJ, Peters CL, Weiss JA. Patient-specific analysis of cartilage and labrum mechanics in human hips with acetabular dysplasia. *Osteoarthritis Cartilage*. 2014 Feb;22(2):210-7.
6. Cheng R, Zhang H, Kernkamp WA, Zheng J, Dai K, Yao Y, Wang L, Tsai TY. Relations between the Crowe classification and the 3D femoral head displacement in patients with developmental dysplasia of the hip. *BMC Musculoskelet Disord*. 2019 Nov 11;20(1):530.
7. Song K, Anderson AE, Weiss JA, Harris MD. Musculoskeletal models with generic and subject-specific geometry estimate different joint biomechanics in dysplastic hips. *Comput Methods Biomech Biomed Engin*. 2019 Feb;22(3):259-70.
8. Lewis CL, Sahrman SA, Moran DW. Effect of hip angle on anterior hip joint force during gait. *Gait Posture*. 2010 Oct;32(4):603-7.
9. Liu R, Wen X, Tong Z, Wang K, Wang C. Changes of gluteus medius muscle in the adult patients with unilateral developmental dysplasia of the hip. *BMC Musculoskelet Disord*. 2012 Jun 15;13:101.
10. Song K, Gaffney BMM, Shelburne KB, Pascual-Garrido C, Clohisy JC, Harris MD. Dysplastic hip anatomy alters muscle moment arm lengths, lines of action, and contributions to joint reaction forces during gait. *J Biomech*. 2020 Sep 18;110:109968.
11. Lewis CL, Sahrman SA. Acetabular labral tears. *Phys Ther*. 2006 Jan;86(1):110-21.
12. Hartig-Andreasen C, Søballe K, Troelsen A. The role of the acetabular labrum in hip dysplasia. A literature overview. *Acta Orthop*. 2013 Feb;84(1):60-4.
13. van Arkel RJ, Modenese L, Phillips AT, Jeffers JR. Hip abduction can prevent posterior edge loading of hip replacements. *J Orthop Res*. 2013 Aug;31(8):1172-9.
14. Wesseling M, Meyer C, De Groote F, Corten K, Simon JP, Desloovere K, Jonkers I. Gait alterations can reduce the risk of edge loading. *J Orthop Res*. 2016 Jun;34(6):1069-76.
15. McCarthy JC, Noble PC, Schuck MR, Wright J, Lee J. The Otto E. Aufranc Award: The role of labral lesions to development of early degenerative hip disease. *Clin Orthop Relat Res*. 2001 Dec;(393):25-37.
16. Klaue K, Durnin CW, Ganz R. The acetabular rim syndrome. A clinical presentation of dysplasia of the hip. *J Bone Joint Surg Br*. 1991 May;73(3):423-9.
17. Hase T, Ueo T. Acetabular labral tear: arthroscopic diagnosis and treatment. *Arthroscopy*. 1999 Mar;15(2):138-41.

18. Ikeda T, Awaya G, Suzuki S, Okada Y, Tada H. Torn acetabular labrum in young patients. Arthroscopic diagnosis and management. *J Bone Joint Surg Br.* 1988 Jan;70(1):13-6.
19. Bergmann G, Deuretzbacher G, Heller M, Graichen F, Rohlmann A, Strauss J, Duda GN. Hip contact forces and gait patterns from routine activities. *J Biomech.* 2001 Jul;34(7):859-71.
20. Hicks JL, Uchida TK, Seth A, Rajagopal A, Delp SL. Is my model good enough? Best practices for verification and validation of musculoskeletal models and simulations of movement. *J Biomech Eng.* 2015 Feb 1;137(2):020905.
21. Beaulé PE, editor. *Hip Dysplasia: Understanding and Treating Instability of the Native Hip.* Cham, Switzerland: Springer Nature Switzerland AG; 2020.
22. Wyles CC, Heidenreich MJ, Jeng J, Larson DR, Trousdale RT, Sierra RJ. The John Charnley Award: Redefining the natural history of osteoarthritis in patients with hip dysplasia and impingement. *Clin Orthop Relat Res.* 2017 Feb;475(2):336-50.
23. Nepple JJ, Wells J, Ross JR, Bedi A, Schoenecker PL, Clohisy JC. Three patterns of acetabular deficiency are common in young adult patients with acetabular dysplasia. *Clin Orthop Relat Res.* 2017 Apr;475(4):1037-44.
24. Valente G, Pitto L, Testi D, Seth A, Delp SL, Stagni R, Viceconti M, Taddei F. Are subject-specific musculoskeletal models robust to the uncertainties in parameter identification? *PLoS One.* 2014 Nov 12;9(11):e112625.
25. Myers CA, Laz PJ, Shelburne KB, Davidson BS. A probabilistic approach to quantify the impact of uncertainty propagation in musculoskeletal simulations. *Ann Biomed Eng.* 2015 May;43(5):1098-111.
26. Gaffney BMM, Clohisy JC, Van Dillen LR, Harris MD. The association between periacetabular osteotomy reorientation and hip joint reaction forces in two subgroups of acetabular dysplasia. *J Biomech.* 2020 Jan 2;98:109464.
27. Gaffney BMM, Harris-Hayes M, Clohisy JC, Harris MD. Effect of simulated rehabilitation on hip joint loading during single limb squat in patients with hip dysplasia. *J Biomech.* 2021 Feb 12;116:110183.
28. Sørensen H, Nielsen DB, Jacobsen JS, Søballe K, Mechlenburg I. Isokinetic dynamometry and gait analysis reveal different hip joint status in patients with hip dysplasia. *Hip Int.* 2019 Mar;29(2):215-21.

29. Jacobsen JS, Bolvig L, Hölmich P, Thorborg K, Jakobsen SS, Søballe K, Mechlenburg I. Muscle-tendon-related abnormalities detected by ultrasonography are common in symptomatic hip dysplasia. *Arch Orthop Trauma Surg.* 2018 Aug;138(8):1059-67.
30. Chalian M, Schauwecker N, Cai A, Dessouky R, Fey N, Xi Y, Chhabra A, Wells J. Regional muscle changes in adult dysfunctional hip conditions of femoroacetabular impingement and hip dysplasia. *Skeletal Radiol.* 2020 Jan;49(1):101-8.
31. Crowninshield RD, Brand RA. A physiologically based criterion of muscle force prediction in locomotion. *J Biomech.* 1981;14(11):793-801.
32. Anderson FC, Pandy MG. Static and dynamic optimization solutions for gait are practically equivalent. *J Biomech.* 2001 Feb;34(2):153-61.
33. Wesseling M, Derikx LC, de Groote F, Bartels W, Meyer C, Verdonchot N, Jonkers I. Muscle optimization techniques impact the magnitude of calculated hip joint contact forces. *J Orthop Res.* 2015 Mar;33(3):430-8.
34. Thelen DG, Anderson FC, Delp SL. Generating dynamic simulations of movement using computed muscle control. *J Biomech.* 2003 Mar;36(3):321-8.
35. Lloyd DG, Besier TF. An EMG-driven musculoskeletal model to estimate muscle forces and knee joint moments in vivo. *J Biomech.* 2003 Jun;36(6):765-76.
36. Ting LH, McKay JL. Neuromechanics of muscle synergies for posture and movement. *Curr Opin Neurobiol.* 2007 Dec;17(6):622-8.
37. Felson DT. Osteoarthritis as a disease of mechanics. *Osteoarthritis Cartilage.* 2013 Jan;21(1):10-5.
38. Hume DR, Navacchia A, Rullkoetter PJ, Shelburne KB. A lower extremity model for muscle-driven simulation of activity using explicit finite element modeling. *J Biomech.* 2019 Feb 14;84:153-60.
39. Thomas-Aitken HD, Willey MC, Goetz JE. Joint contact stresses calculated for acetabular dysplasia patients using discrete element analysis are significantly influenced by the applied gait pattern. *J Biomech.* 2018 Oct 5;79:45-53.
40. Anwender H, Rakhra KS, Melkus G, Beaulé PE. T1p hip cartilage mapping in assessing patients with cam morphology: How can we optimize the regions of interest? *Clin Orthop Relat Res.* 2017 Apr;475(4):1066-75.

41. Valente G, Crimi G, Vanella N, Schileo E, Taddei F. nmsBuilder: Freeware to create subject-specific musculoskeletal models for OpenSim. *Comput Methods Programs Biomed.* 2017 Dec;152:85-92.
42. Modenese L, Renault JB. Automatic generation of personalised skeletal models of the lower limb from three-dimensional bone geometries. *J Biomech.* 2021 Feb 12;116:110186.
43. Gaffney BMM, Hillen TJ, Nepple JJ, Clohisy JC, Harris MD. Statistical shape modeling of femur shape variability in female patients with hip dysplasia. *J Orthop Res.* 2019 Mar;37(3):665-73.
44. Nunley RM, Prather H, Hunt D, Schoenecker PL, Clohisy JC. Clinical presentation of symptomatic acetabular dysplasia in skeletally mature patients. *J Bone Joint Surg Am.* 2011 May;93 Suppl 2:17-21.
45. Leunig M, Siebenrock KA, Ganz R. Rationale of periacetabular osteotomy and background work. *Instr Course Lect.* 2001;50:229-38.
46. Lerch TD, Steppacher SD, Liechti EF, Tannast M, Siebenrock KA. One-third of hips after periacetabular osteotomy survive 30 years with good clinical results, no progression of arthritis, or conversion to THA. *Clin Orthop Relat Res.* 2017 Apr;475(4):1154-68.
47. Sucato DJ, Tulchin K, Shrader MW, DeLaRocha A, Gist T, Sheu G. Gait, hip strength and functional outcomes after a Ganz periacetabular osteotomy for adolescent hip dysplasia. *J Pediatr Orthop.* 2010 Jun;30(4):344-50.
48. Abraham CL, Knight SJ, Peters CL, Weiss JA, Anderson AE. Patient-specific chondrolabral contact mechanics in patients with acetabular dysplasia following treatment with peri-acetabular osteotomy. *Osteoarthritis Cartilage.* 2017 May;25(5):676-84.
49. Nwachukwu BU, Beck EC, Lee EK, Cancienne JM, Waterman BR, Paul K, Nho SJ. Application of machine learning for predicting clinically meaningful outcome after arthroscopic femoroacetabular impingement surgery. *Am J Sports Med.* 2020 Feb;48(2):415-23.
50. Koning BH, van der Krogt MM, Baten CT, Koopman BF. Driving a musculoskeletal model with inertial and magnetic measurement units. *Comput Methods Biomech Biomed Engin.* 2015 Jul;18(9):1003-13.